

STATUS OF THESIS

Title of thesis Chemical-looping combustion investigation of copper metal oxide with praseodymium modified gamma-alumina support oxygen carrier.

I MUHAMMAD QASIM

hereby allow my thesis to be placed at the Information Resource Center (IRC) of Universiti Teknologi PETRONAS (UTP) with the following conditions:

1. The thesis becomes the property of UTP
2. The IRC of UTP may make copies of the thesis for academic purposes only.
3. This thesis is classified as

Confidential

Non-confidential

If this thesis is confidential, please state the reason:

The contents of the thesis will remain confidential for 2022 years.

Remarks on disclosure:

Signature of Author

Permanent address: Village Khokhar
Gharbi, Post office khas, Tehsil and
district of Gujrat, 50700, Pakistan

Date: 17-03-2022

Endorsed by

DR MUHAMMAD AYOUB
Senior Lecturer
Chemical Engineering Department
Universiti Teknologi PETRONAS

Signature of Supervisor

Name of Supervisor
Dr. Muhammad Ayoub

Date: 17-03-2022

UNIVERSITI TEKNOLOGI PETRONAS
CHEMICAL-LOOPING COMBUSTION INVESTIGATION OF COPPER METAL
OXIDE WITH PRASEODYMIUM MODIFIED GAMMA-ALUMINA SUPPORT
OXYGEN CARRIER

by
MUHAMMAD QASIM

The undersigned certify that they have read and recommend to the Postgraduate Studies Programme for acceptance this thesis for the fulfillment of the requirements for the degree stated.

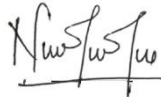


DR MUHAMMAD AYOUB
Senior Lecturer
Chemical Engineering Department
Universiti Teknologi PETRONAS

Signature:

Main Supervisor:

Dr. Muhammad Ayoub



DR. NURUL AINI AMRAN
Lecturer
Chemical Engineering Department
Universiti Teknologi PETRONAS

Signature:

Co-Supervisor:

Dr. Nurul Aini Binti Amran



Assoc. Prof. Ir Dr Abdul Halim Shah Maulud
Chair
Chemical Engineering Department
Universiti Teknologi PETRONAS

Signature:

Head of Department:

AP Ir Dr A Halim Shah B Maulud

Date:

17-03-2022

CHEMICAL-LOOPING COMBUSTION INVESTIGATION OF COPPER METAL
OXIDE WITH PRASEODYMIUM MODIFIED GAMMA-ALUMINA SUPPORT
OXYGEN CARRIER

by

MUHAMMAD QASIM

A Thesis

Submitted to the Postgraduate Studies Programme

as a Requirement for the Degree of

MASTER OF SCIENCE

DEPARTMENT OF CHEMICAL ENGINEERING

UNIVERSITI TEKNOLOGI PETRONAS

BANDAR SERI ISKANDAR,

PERAK

MARCH 2022

DECLARATION OF THESIS

Title of thesis

Chemical-looping combustion investigation of copper metal oxide with praseodymium modified gamma-alumina support oxygen carrier.

I MUHAMMAD QASIM

hereby declare that the thesis is based on my original work except for quotations and citations which have been duly acknowledged. I also declare that it has not been previously or concurrently submitted for any other degree at UTP or other institutions.



Signature of Author

Permanent address: Village Khokhar
Gharbi, Post office khas, Tehsil and
district of Gujrat, 50700, Pakistan

Date: 17-03-2022

Witnessed by



DR MUHAMMAD AYOUB
Senior Lecturer
Chemical Engineering Department
Universiti Teknologi PETRONAS

Signature of Supervisor

Name of Supervisor
Dr. Muhammad Ayoub

Date: 17-03-2022

DEDICATION

This study is wholeheartedly dedicated to my parents, Dr Shazia Shukrullah, my brother Muhammad Asim, and my colleague Nur Adibah Ghazali who had inspired me and given me strength when I was on the verge of giving up, and who continue to be moral, spiritual, emotional, and financial support.

ACKNOWLEDGEMENTS

I expressed my heartfelt gratitude to Almighty Allah, the Most Merciful and Compassionate, for providing me with the opportunity and enabling me to complete this critical research project. I had the incredible privilege of being a graduate student under the guidance of Senior Lecturer Dr Muhammad Ayoub. I want to offer my profound thanks and admiration for his excellent counsel, support, encouragement, and care throughout this project. I owe him a debt of gratitude for believing in me and allowing me to work with him, as well as for being such a fantastic mentor with his boundless energy. I am also incredibly thankful to my co-supervisors, Dr Aqsha and Dr Nurul Aini Binti Amran, for their supports.

The Postgraduate Office of Universiti Teknologi PETRONAS (UTP) provided financial assistance in the form of graduate assistantships, which is sincerely acknowledged. I would also like to thank the employees of the Postgraduate Study Programme, as well as the staff and technicians of the Chemical Engineering Department.

I engaged with a wide range of people while working on this project, including researchers, educators, and professionals. They have helped me to better understand and think about things. I want to express my heartfelt gratitude in particular. During my time at UTP, I want to convey my deep gratitude to my colleagues for their technical assistance, support, and dialogue.

ABSTRACT

The amount of CO₂ in the atmosphere is rising due to the combustion of fossil fuels to fulfill the energy demand. This study aims to synthesize a potential oxygen (OC) using wet impregnation method for chemical looping combustion (CLC) process. Two types of OCs (monometallic and bimetallic) were prepared. All the synthesized OCs were calcined at 450 °C using muffle furnace. For monometallic OCs, the oxygen transport capacities (OTCs) of 0.018 mg of O₂/mg of OC, 0.026 mg of O₂/mg of OC, and 0.026 mg of O₂/mg of OC were determined for 10FeA, 10CuA and 10CoA based OCs, respectively. The 10CuA OC was the fastest to be reduced in 1 min out of all monometallic OCs tested in CLC process. Some agglomeration was observed for all prepared OCs when characterized using FESEM analysis. EDX results confirmed that the copper (Cu) contents for both 10CuA and 10CuPA OCs after 10 redox cycles were increased from 7.5 wt% to 21.3 wt% and 7.9 wt% to 16.4 wt%, respectively. The peaks corresponding to Cu-contents for 10CuPA-based OC were retained compared to 10CuA-based OC when scanned from 10° to 90° in XRD analysis. The cyclical oxidation-reduction cycles for CLC performed using thermogravimetric analysis (TGA). The reduction reaction of OC was carried out using 5% CH₄/N₂ while oxidation reaction using air in TGA. The main criteria for the selection of the OCs for CLC include oxygen transport capacities, agglomeration, and spinel formation. TGA results confirmed that 10CuPA-based OC has high OTC (0.0267 mg of O₂/ mg of OC) as compared to 10CuA-based OC (0.0240 mg of O₂/ mg of OC) and maintained OTC of about 0.0267 mg of O₂/ mg of OC after 10 redox cycles. 20CuPA-based OC was used to optimize the process parameters such as time and temperature using RSM. The highest OTC of 0.0546 mg of O₂/ mg of OC at optimum operating conditions (3 min and 800 °C) was achieved. The prepared Cu-based Pr-modified alumina support oxygen carriers exhibited excellent results for OTC along with its phase

stability. These effective properties making them attractive choices for use in the CLC process especially applicable for energy production from power generation plants.

ABSTRAK

Jumlah CO₂ di dalam atmosfera semakin meningkat disebabkan pembakaran bahan bakar fosil untuk memenuhi permintaan tenaga. Kajian ini bertujuan untuk mensintesis pembawa oksigen (OC) yang berpotensi menggunakan kaedah impregnasi basah untuk proses pembakaran gelung kimia (CLC). Dua jenis OC (monologam dan dwilogam) telah disediakan. Semua OC yang disintesis telah dikalsin pada suhu 450°C menggunakan relau pembakar. Untuk OC monometal, kapasiti pengangkutan oksigen (OTC) sebanyak 0.018 mg O₂/mg OC, 0.026 mg O₂/mg OC dan 0.026 mg O₂/mg OC telah diperolehi untuk OC berasaskan 10FeA, 10CuA dan 10CoA. OC 10CuA ditemui paling cepat mengalami tindak balas pengurangan hanya dalam masa 1 minit berbanding OC monometal yang lain yang diuji dalam proses CLC. Beberapa aglomerasi telah dipernampak untuk semua OC yang disintesis melalui pencirian menggunakan analisis FESEM. Keputusan EDX mengesahkan bahawa kandungan kuprum (Cu) untuk kedua-dua 10CuA dan 10CuPA OC selepas 10 kitaran redoks masing-masing meningkat dari 7.5% berat kepada 21.3% berat dan 7.9% berat kepada 16.4% berat. Puncak bersepadan dengan kandungan Cu untuk OC berasaskan 10CuPA ditemui kekal berbanding OC berasaskan 10CuA apabila diimbis dari 10° to 90° dalam analisis XRD. Kitaran tindak balas pengurangan pengoksidaan untuk CLC dilakukan menggunakan analisis termogravimetrik (TGA). Tindak balas pengurangan OC dijalankan menggunakan 5% CH₄/N₂ manakala tindak balas pengoksidaan menggunakan udara dalam TGA. Kriteria utama untuk pemilihan OC untuk CLC adalah termasuk kapasiti pengangkutan oksigen, aglomerasi, dan pembentukan spinel. Keputusan TGA mengesahkan bahawa OC berasaskan 10CuPA mempunyai OTC yang tinggi (0.0267 mg O₂/ mg OC) berbanding OC berasaskan 10CuA (0.0240 mg O₂/ mg OC) dan mengekalkan OTC kira-kira 0.0267 mg O₂/mg OC selepas 10 kitaran redoks. OC berasaskan 20CuPA digunakan untuk mengoptimumkan parameter proses seperti masa dan suhu menggunakan RSM. OTC tertinggi sebanyak 0.0546 mg O₂/mg OC telah dicapai pada keadaan operasi optimum (3 min dan 800 °C). Pembawa oksigen

sokongan alumina Pr-ubah suai berasaskan Cu yang telah disediakan mempamerkan keputusan cemerlang untuk OTC disamping kestabilan fasanya. Ciri-ciri yang OC berkesan ini menjadikannya pilihan yang menarik untuk digunakan dalam proses CLC terutamanya untuk pengeluaran tenaga dari loji penjanaan kuasa.

In compliance with the terms of the Copyright Act 1987 and the IP Policy of the university, the copyright of this thesis has been reassigned by the author to the legal entity of the university,

Institute of Technology PETRONAS Sdn Bhd.

Due acknowledgement shall always be made of the use of any material contained in, or derived from, this thesis.

© Muhammad Qasim, 2021

Institute of Technology PETRONAS Sdn Bhd

All rights reserved.

TABLE OF CONTENT

ABSTRACT.....	vii
ABSTRAK.....	ix
LIST OF FIGURES	xv
LIST OF TABLES	xvii
LIST OF NOMENCLATURE.....	XVIII
CHAPTER 1 INTRODUCTION	1
1.1 Background study	1
1.2 Problem statement	3
1.3 Objectives	4
1.4 Scope of work	5
CHAPTER 2 LITERATURE REVIEW	6
2.1 Importance of chemical looping combustion for energy production.....	6
2.2 Chemical looping combustion process	7
2.2.1 Oxygen transport capacity.....	8
2.3 Types of oxygen carriers	10
2.3.1 Spinel form oxides	10
2.3.2 Perovskite form oxides.....	13
2.3.3 Waste material oxides	16
2.3.4 Natural mineral oxides	19
2.3.5 Single metal oxides	22
2.3.5.1 Nickel oxide (NiO)	22
2.3.5.2 Copper oxide (CuO).....	25
2.3.5.3 Iron oxide (FeO)	28
2.3.5.4 Manganese oxide (MnO)	31
2.3.5.5 Cobalt oxide (CoO).....	33
2.3.6 Mixed metals oxides.....	36
2.4 Optimizations of process parameters.....	40

2.4.1 Response surface methodology	41
2.4.2 Model fitting and statistical analysis	42
CHAPTER 3 METHODOLOGY	45
3.1 Materials and reagents	46
3.2 Preparation of monometallic OCs	46
3.3 Preliminary screening of monometallic OCs.....	47
3.4 Preparation of bi-metallic OC.....	48
3.5 Preliminary screening of bimetallic OCs.....	49
3.6 Characterization of oxygen carriers	51
3.6.1 Surface morphology	51
3.6.2 X-ray diffraction.....	51
3.6.3 Temperature programmed reduction.....	52
3.7 CLC experiments	52
3.8 Design of experiments and statistical analysis	53
CHAPTER 4 RESULTS AND DISCUSSION	56
4.1 Redox cycle for the preliminary screening of OCs	56
4.2 Effect of addition of promoter (Pr-oxide) on 10CuA oxygen carrier	58
4.2.1 FESEM analysis	58
4.2.2 X-Ray diffraction analysis	61
4.2.3 Temperature programmed reduction analysis	64
4.2.4 Thermogravimetric analysis for CLC process	65
4.3 Statistical analysis of process parameters.....	70
4.3.1 Effect of process parameters on response	73
4.3.2 Parametric analysis of oxygen transport capacity using 3D response surface plot.....	74
4.4 Optimization of process parameters	76
CHAPTER 5 CONCLUSION AND RECOMMENDATIONS	78
5.1 Conclusion	78

5.2 Recommendations.....	79
APPENDIX A SAMPLE CALCULATIONS.....	90
APPENDIX B TGA PROFILES AT 800 °C.....	92

LIST OF FIGURES

Figure 2.1: Diagram for chemical looping combustion (CLC) process [44].	8
Figure 3.1: Overall flow chart of research methodology.	45
Figure 3.2: Schematic diagram of OCs synthesis by using wet impregnation method.	47
Figure 3.3: The flow diagram of screening for the best monometallic and bimetallic oxygen carriers.	50
Figure 3.4: The setup for chemical looping combustion process using TGA.	53
Figure 4.1: TGA profile for 10CuA, 10 CoA and 10FeA OCs using air as an oxidizing gas and 5% CH ₄ /N ₂ at 800 °C.	57
Figure 4.2: TGA profiles for one redox cycle of Pr-oxide and La-oxide based OCs using 5% CH ₄ /N ₂ gas at 800 °C.	58
Figure 4.3: SEM images of 10CuA fresh (a) & after 10 cycles (b) and 10CuPA fresh (c) & after 10 cycles (d).	59
Figure 4.4: XRD analysis for the fresh and used with and without praseodymium OCs (10CuPA and 10CuA).	63
Figure 4.5: TPR profile 10CuA and 10CuPA fresh and used (10 cycles) oxygen carriers.	65
Figure 4.6: TGA profile for 10CuA and 10CuPA OCs during 10 redox cycles in CLC process.	66
Figure 4.7: TGA profile at 800 °C for mass-based conversion of 10CuPA-OC measured using 5% CH ₄ /N ₂ reducing gas (left) and air oxidizing gas (right).	67
Figure 4.8: TGA comparison between 10CuPA and 20CuPA-based OCs at 800 °C and 3 min reduction time using 5% CH ₄ (reducing gas) and air (oxidizing gas).	68
Figure 4.9: Predicted vs actual data for response (oxygen transport capacity).	73
Figure 4.10: Perturbation plot for oxygen transport capacity influenced by time and temperature.	74
Figure 4.11: 3D response surface plot of oxygen transport capacity for parametric analysis.	75

Figure A.5.1: TGA profile for 10CuA and 10CuPA OCs during 10 redox cycles in CLC process.....	91
Figure B.5.2: TGA profile for 10FeA-based OC (a), 10CoA-based OC (b), and 10CuA-based OC (c) during an oxidation-reduction cycle in CLC process using 5% CH ₄ /N ₂ and air at 800 °C.....	93
Figure B.5.3: TGA profile for La-oxide OC (a) and Pr-oxide OC (b) during an oxidation-reduction cycle in CLC process using 5% CH ₄ /N ₂ and air at 800 °C.....	94
Figure B.5.7: TGA profile for 10CuPA-based OC (a) and 20CuPA-based OC (b) during 10 redox cycles in CLC process using 5% CH ₄ /N ₂ and air at 800 °C.	95

LIST OF TABLES

Table 2.1: Oxygen transport capacity of pure metal oxides [41].....	9
Table 2.2: Oxygen transport capacities of spinel-based oxygen carriers in CLC process.	12
Table 2.3: Oxygen transport capacities of perovskite-based oxygen carriers in CLC process.....	15
Table 2.4: Oxygen transport capacities of waste materials-based oxygen carriers in CLC process.....	18
Table 2.5: Oxygen transport capacities of natural materials as oxygen carriers used in chemical looping combustion process.	21
Table 2.6: Oxygen transport capacities of Ni-based oxygen carriers in CLC process.	24
Table 2.7: Oxygen transport capacities of Cu-based oxygen carriers in CLC process.	27
Table 2.8: Oxygen transport capacities of Fe-based oxygen carriers in CLC process.	30
Table 2.9: Oxygen transport capacities of Mn-based oxygen carriers in CLC process.	32
Table 2.10: Oxygen transport capacities of Co-based oxygen carriers in CLC process.	35
Table 2.11: Oxygen transport capacity of mixed-based Oxygen Carriers.....	39
Table 3.1: The specifications and details of material used for the preparation of oxygen carriers.....	46
Table 3.2: The details of equipment used during characterization.	51
Table 3.3: Range for the operating parameters for designing the experiment array....	54
Table 3.4: Experimental design for actual and predicted results.	55
Table 4.1: Elemental compositions of 10CuA,10CuPA, and 20CuPA-based oxygen carriers.....	60
Table 4.2: The 2θ angles corresponding to different crystal phases of 10CuA and 10CuPA oxygen carriers.	62
Table 4.3: The oxygen transport capacity of past studies compared with present study of oxygen carrier for CLC.....	69
Table 4.4: ANOVA results for oxygen transport capacity of oxygen carrier.....	71

Table 4.5: Predicted and experimental results for the optimized process parameters. 77

LIST OF NOMENCLATURE

R_o	Oxygen transport capacity
MeO	Metal oxide
Me	Metal in reduced form
W_o	Weight of detached oxygen (mg)
$W_{o.o.c}$	Weight of fully oxidized oxygen carrier (mg)
CCS	Carbon capture and storage
m_o	Mass of oxygen carrier when full oxidized
m_r	Mass of oxygen carrier when full reduced

LIST OF ABBREVIATIONS

TGA	Thermogravimetric analyzer
OC	Oxygen carrier
CLC	Chemical looping combustion
OTC	Oxygen transport capacity
CCS	Carbon capture and storage

CHAPTER 1

INTRODUCTION

In this chapter the comprehensive introduction of the current project is provided. The background study includes the greenhouse gas emissions due to increasing demand of energy, carbon capture and storage technologies and chemical looping combustion process. The use of oxygen carrier in chemical looping combustion process, problem statement, research objectives and scope of the research are described in this chapter.

1.1 Background study

Fossil fuels have great potential to be used for the next 20 years to sustain the growing energy requirements. Renewable energy sources and nuclear energy have limitations at large scale applications in terms of cost and availability to fulfilling energy demands in the future [1, 2].

As a consequence of dependency on fossil fuels for energy generation in Asian countries, the concentration of carbon dioxide (CO₂), chlorofluorocarbons (CFCs), sulfur oxides (SO_x), nitrogen oxides (NO_x), other trace gases, and some organic particulates keep increasing, from combustion in the power plants [3]. It is expected that the global temperature expands around 0.8 °C at the start of the 20th century, where two-third rise since 1980 and hence lead to global warming [4]. The increase in the concentration of CO₂ in the atmosphere made difficult to control further climate change. It has become a significant concern of the world to control CO₂ emissions or capture instead of releasing it to the air. There are different techniques to regulate CO₂ emissions, as mentioned below [3] :

- i. Decreasing energy utilizations and growing energy efficiency.

- ii. Using negligible carbon fuels.
- iii. Utilizing renewable energy sources.
- iv. By planting trees.
- v. CO₂ segregating.

These methods can be one of the solutions to sustain the global climate. Even if all above five methods are implemented, the amount of CO₂ cannot be decreased to low levels. Carbon Capture and Storage (CCS) is the technology used to capture the CO₂ after the combustion of fossil fuels. About 90 % of CO₂ can be captured by using CCS [5]. There are three basic methods for carbon-capturing: i. Pre-combustion, ii. Post-combustion, and iii. Oxy-fuel combustion [6]. In pre-combustion, CO₂ is captured before combustion of fossil fuels by converting fossil fuels into CO₂ and H₂. In post-combustion, CO₂ is captured after the combustion process from the flue gas while in oxy-fuel combustion pure oxygen is provided for the combustion [7]. In oxy-fuel combustion the term chemical looping technology is used. This technology involves, the redox cycle of oxygen carrier (OC) is more important. Gas-solid separation as compared to gas-gas separation is easier and it decreases the energy penalty [8]. Until 1987, the word chemical looping technology was not used. Chemical looping technology further divided into sub-technologies like chemical looping combustion (CLC), chemical looping hydrogen generation (CLHG) [9, 10], chemical looping gasification (CLG) [11, 12], chemical looping reforming (CLR) and OC aided combustion (OCAC) [13-15] depends upon the source of oxygen (air and/or H₂O) and product (CO₂, H₂, syngas). In 1954, Lewis and Gilliland presented a patent with the name "Production of pure carbon dioxide" as CLC, but at that time, it was not familiar with the name of CLC [16]. Richter and Knotche proposed the CLC concept for the first time in 1983 [17]. In the last decades, the advancements in the CLC process have been improved to get high efficiency. OC is a fundamental part of all kinds of chemical looping processes. It transfers oxygen from the gaseous oxygen source to the fuel for combustion process. Several parameters need to consider for designing a productive and efficient system. Critical requirements for a successful OC are high oxidation states of metals, it must have sufficient reduction and oxidation rates, mechanical strength in fluidized beds and resistance to agglomeration.

The OCs used for the CLC technology are in the form of metal oxides derived from transition metals group in the period table. The overall performance of CLC process depends on the stability of these OCs. In previous studies, different transition metals have been commonly investigated as OCs for example Ni (nickel) [18], Cu (copper) [19], Co (cobalt) [20], Fe (iron) [21] and Mn (manganese) [22]. The activity of OCs depends on type of metal oxide used for CLC process. Unfortunately, these metal oxides have some serious drawbacks, which hinder their performance in CLC process. Ni-based and Cu-based OCs revealed exceptional performance. Nevertheless, Ni is expensive and needs suitable safety precautions to handle its waste materials owing to its toxic characteristics. Copper-based OCs function poorly at high temperatures because of their low melting point [23]. It was found that the efficiency of the CLC process was decreased due to less reactivity of Mn-based OCs [24]. Particle agglomeration is a concern when pure metal oxides are used as OCs, which affects their stability. The addition of suitable supports such as Al_2O_3 [25], TiO_2 [26, 27], SiO_2 [28] and CeO_2 [29] have been successfully employed to increase the stability and performance of the metal oxides during multiple redox cycles. However, besides using these supports, it was examined by previous research work that the particles of Cu-based OC undergo agglomeration at high temperatures. For example, the activity loss was observed for 60 wt% Cu- CeO_2 due to agglomeration during few redox cycles [30]. The interaction between Cu contents and $\gamma\text{-Al}_2\text{O}_3$ support at high temperature resulted in the formation of highly stable spinel compound [31, 32]. This spinel compound causes loss of Cu contents and hence the OTC of the OC decreases. The modification of support with a suitable promoter showed the absence of spinel compound by avoiding interaction between active metal and support [25, 33]. It has been well reported that praseodymium (Pr) oxide has good redox properties [34, 35]. As a result, developing a less expensive, more environmentally friendly, and new materials-based OC for the CLC process is highly desirable.

1.2 Problem statement

The durability and longevity of the CLC during exceptional performance, the choice of an oxygen carrier is of primary importance. High reactivity at temperatures 700-900 °C, fuel conversion and thermal stability of OC without agglomeration are

required during multiple redox cycles. Generally, single oxide-based OC more likely undergo sintering and attrition effect. These deficiencies shorten the lifetime of single metal oxide-based OC. The praseodymium modified support might reduce the attraction between active metal (CuO) and support (Al_2O_3). This low attraction between active metal and support might prevent the formation of unreactive spinel compounds. Furthermore, due to the redox properties of praseodymium oxide, the OTC of an OC can be increased. Therefore, using mixed metals-based OC could enhance its reactivity and thermal stability in redox cycles.

Among fossil fuels, the combustion of methane gas is very common in CLC process because of its huge resources. For the complete combustion of CH_4 gas in CLC units, excess amount of oxygen from OC is demanded. Low amount oxygen transferred by OC causes incomplete combustion of methane gas. Therefore, high oxygen transport capacity (OTC) of OC is required during multiple redox cycles in CLC process.

So far, very rare or no optimization using response surface methodology (RSM) reported in previous studies. The optimum conditions for metal loading, reaction temperature and time are required to achieve best performance of OC in CLC process.

1.3 Objectives

This thesis aims to identifying the optimal materials for chemical looping combustion process. Experimental studies are carried out to investigate the performance of 10CuPA-OC and to find the optimum operating conditions for CLC process. Following are the objectives of this project:

- To synthesize and characterize mixed metals oxide-based oxygen carriers for chemical looping combustion process.
- To investigate the oxygen transport capacity of as-synthesized oxygen carriers for methane combustion.
- To optimize the process parameters (time and temperature) for the chemical looping combustion of methane gas in the presence of prepared oxygen carrier.

1.4 Scope of work

The support γ -Al₂O₃ with nitrate precursors of Cu and Pr were used for the preparation of OC. The prepared OC was synthesized by wet impregnation method. The OC was calcined at 450 °C for 4 h. The surface properties such as surface morphology, crystal phase analysis and composition of OC were analyzed using Zeiss Supra55VP model field emission scanning electron microscope (FESEM), energy dispersive X-ray spectroscopy and D8 Advance Bruker XRD, respectively. TPR test was conducted using TPDRO100 equipped with a thermal conductivity detector (TCD). The performance of OC for CLC was analyzed in Thermogravimetric Analysis (TGA) using 5% CH₄/N₂ as reducing gas while air was used as an oxidizing gas. The operating parameters were optimized using design expert 12 by applying Central Composite method. Two independent variables, temperature, and time were chosen with a range of 800-950 °C and 1-3 min, respectively. However, one dependent variable, OTC, was investigated for the optimization of process parameters.

CHAPTER 2

LITERATURE REVIEW

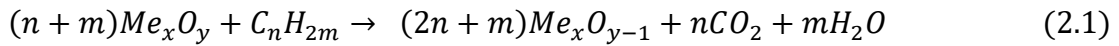
This chapter contains extensive study on all aspects of the research. A general explanation for the importance of chemical looping combustions process and chemical looping technology is described in Sections 2.1 and 2.2, respectively. Different types of oxygen carriers such as spinel form, perovskite form, waste materials, natural minerals, single oxides and mixed oxides-based OCs critically discussed in Section 2.3. Furthermore, the optimization of process parameters and their influence on oxygen transport capacity is elaborated in Section 2.4.

2.1 Importance of chemical looping combustion for energy production

Carbon capture and storage (CCS) is the process of capturing CO₂ produced by burning of fossil fuels and storing it permanently in a suitable site, such as saline aquifers or depleted oil wells. CCS might lower mitigation costs by 27.5 percent if broadly adopted in the power and energy industries [36], relative to situations where it is not utilized. There are three common methods for capturing CO₂ such as post- and pre-combustion capture, as well as oxy-fuel combustion [37, 38]. Traditional CCS methods demand the addition of process parts to conventional thermal power plants, resulting in higher capital costs and lower efficiency [39, 40]. CLC creates a stream of carbon dioxide that is ideal for sequestration due to a significant change in the mechanism of combustion compared to conventional methods. As a result, the efficiency loss is less as compared to other CCS methods. Several authors have claimed that CLC is one of the most cost-effective CO₂ capture technologies [41, 42], as well as having a lesser ecological consequence than solvent-based technologies [43].

2.2 Chemical looping combustion process

Chemical looping combustion (CLC) consists of two interconnected fluidized bed reactors, one is air reactor (AR) and other is fuel reactor (FR). Between AR and FR, metal oxide known as oxygen carrier (OC) circulates. In CLC, air and fuel are never mixed since air is introduced in the AR and fuel in the FR. The role of OC is to transfer oxygen from AR to FR. In the FR, OC particles are reduced by fuel as shown in Equation (2.1):



After reducing, OC enters to AR where in the presence of air, it oxidized to regenerate as to its original form shown in Equation (2.2):



This regenerated OC sent again to FR for reducing. In this way loop for CLC completes. Loop seals are used in between AR and FR to avoid leakage of air to FR and fuel gas to AR. After combustion of fuel, CO₂ with water vapors emitted from the exhaust of FR as shown in Fig. 2.1. By condensing water vapors, inherent CO₂ can be captured. Separation between gas-solid, is easy and less energy cost because CO₂ is separated from OC in the fuel reactor and oxygen depleted by OC from air in the AR. Heat released in conventional combustion is same in amount as total heat emitted from reduction and oxidation steps in CLC described by Hess's law, states that net enthalpy change in complete chemical reaction remains same if the reaction completes in one step or more than one. So, the reaction in CLC is same as in combustion of fossil fuel with convention air.

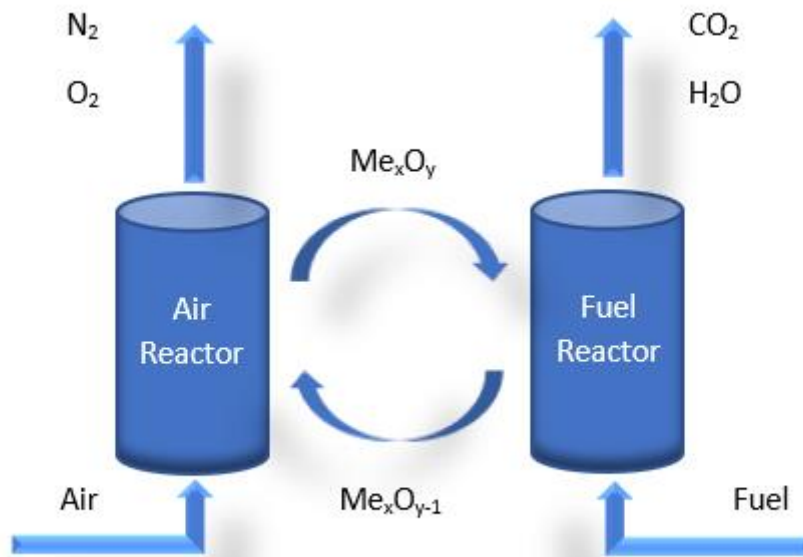


Figure 2.1: Diagram for chemical looping combustion (CLC) process [44].

Oxygen is carried by OC in the form of (O) and transferred to the fuel for its combustion in fuel reactor to produce pure CO₂ without nitrogen gas. In this way, it saves additional costs required for the separation of CO₂ from nitrogen and hence inherent CO₂ can be captured instead of releasing it in the atmosphere. In fact, it helps to prevent climate change due to CO₂ major contribution in Greenhouse gases (GHGs). For CLC process, very low or negligible NO_x emissions have been investigated. Mostly, NO_x emissions occurred at higher temperatures starting from 1200 °C [45, 46]. Overall, the performance of CLC process depends on the type of OC used.

2.2.1 Oxygen transport capacity

The OTC is also known as oxygen ratio, is defined as the ratio of gained oxygen weight to the weight of the OC. Different terms were used for OTC such as; oxygen donation capacity, oxygen releasing capacity, oxygen carrying capacity, oxygen mobility, oxygen converted, and oxygen transfer capacity. Oxygen ratio can be calculated by using this formula, $R_o = (m_o - m_r) / m_o$. Where m_o is referred to the mass of OC when it is fully oxidized and m_r is mass of OC when it is fully reduced in the redox cycle. R_o means the maximum amount of oxygen that can be delivered from air to fuel reactor for a given mass flow of recirculating particles. The R_o of metal-based

OC can be measured by using TGA where changes of weight are obtained as a function of temperature. Theoretical OTC can be calculated by dividing the weight of reduced oxygen molecules by the weight of the oxidized OC as Equation (2.3):

$$\text{Oxygen capacity} = \frac{k W_o}{W_{o.o.c}} \quad (2.3)$$

Where: W_o is the weight of detached oxygen (mg), $W_{o.o.c}$ is the weight of fully oxidized OC (mg); and k is the oxygen detachment factor (-). A higher OTC reduces the rate of recirculation of solid; thus, higher fuel conversion rates can be acquired. Oxygen ratio will affect the complexity and efficiency of the system; hence it must be considered first in the screening process of the OC. Table 2.1 gives the summary of OTC for different metal oxides (OCs). It was reported that the reduction of hematite to Fe has the highest value of OTC. Conversion of hematite to magnetite produced just 0.03 OTC, which was 10 times less than the expected value of 0.3. However, the transformation of Fe_2O_3 to Fe_3O_4 (hematite to magnetite) results in the oxidation of methane in interconnected fluidized bed reactor.

Table 2.1: Oxygen transport capacity of pure metal oxides [41].

Metal-based oxygen carriers	Oxygen Transfer Capacity (Ro)		Ref.
	Theoretical value	Experimental Data	
Fe_2O_3/Fe_3O_4	0.03	0.013-0.027	[47-50]
Fe_2O_3/FeO	0.10	0.04	[51, 52]
Mn_3O_4/MnO	0.07	0.01-0.06	[48, 53, 54]
CuO/Cu_2O	0.10	0.05	[55, 56]
CuO/Cu	0.20	0.02-0.16	[48, 49, 57]
NiO/Ni	0.21	0.02-0.16	[27, 48, 49]
Co_3O_4/Co	0.27	0.01-0.02	[55, 58]
CoO/Co	0.21	0.16-0.17	[59, 60]

OTC decreases with attrition and agglomeration of the material and with carbon deposition. The phase change of the OC during oxidation and reduction cycles may affect OTC. Low-oxygen vacancy energy OC are more likely to release lattice oxygen because of the oxygen vacancy created by the release of oxygen from the OC's surface.

2.3 Types of oxygen carriers

The following conditions should be met by the appropriate oxygen carrier: (i) high reactivity in multiple oxidation/reduction processes, (ii) high fuel conversion (iii) retardation against carbon deposition (iv) resistant to agglomeration at high temperatures, (v) fluidization capability and (vi) economic feasibility [61]. For suitable oxygen carriers, the reactivity should retain at temperatures 700-900 °C over multiple redox cycles. Overall OCs can be divided into two categories: Natural materials-based oxides and synthetic or commercial metals-based OCs. The synthetic OCs are further classified on the bases of either number of active metals present in it or on the structure of OC. Based on active metals, OCs divided into monometallic OCs (single metal oxides), mixed metal-based OCs that include bimetallic OCs (bi-metal oxides) and trimetallic OCs (tri-metal oxides). On the basis of structure, OCs can be divided into two categories: spinel-shaped and perovskite-shaped. Other than these, some waste materials are also being utilized as OCs for CLC process.

2.3.1 Spinel form oxides

Metal oxides at high temperatures react with the support to form spinel oxide, which cannot reduce further. Later, spinels of different metal oxides were tested as support for OC. Zeng et al. [62] analyzed the redox properties of ternary spinel material. The use of spinel support helped to retard sintering and enhanced stability of OC for multiple redox cycles. First, the active metal phase exsolved from the parent spinel material during reduction and dissolved again to parent spinel material during the oxidation process [63]. The OTC of 6.7 wt% was reported after a few cycles among spinel $(\text{Mn}_{0.77}\text{Fe}_{0.23})_3\text{O}_4$ and $(\text{Mn}_{0.77}\text{Fe}_{0.23})\text{O}$ [64]. NiO with different spinels has been investigated to resist coke formation. All three spinels (NiFe_2O_4 , MgFe_2O_4 , and BaFe_2O_4) successfully opposed coke generation. In the reduction process, 19 wt% oxygen was released when NiFe_2O_4 spinel in the presence of NiO, was reduced in

methane atmosphere [65]. However, BaFe_2O_4 was more stable in redox cycles. Cui et al. [63] observed that the OTC was improved from 0.78-1.07 mmol/g (for conventional FeAlO_x and Fe_2O_3) to 2.37 mmol/g (for spinel NiFeAlO_x) and was found stable during 20 cycles. The highest OTC for first cycles was achieved that was 12.16 mmol/g. However, OC, which showed high OTC, exhibited sintering of particles. Riley et al. [66] found that $\text{CuFe}_{1.5}\text{Al}_{0.5}\text{O}_4$ showed higher OTC as compared to CuFeAlO_4 . The modification of Fe and Al based OC into spinel structure, improved the porosity of pellets and increased the mechanical strength of material. The OCT of $\text{CuFe}_{1.5}\text{Al}_{0.5}\text{O}_4$ was 4.7 wt% higher than CuFeAlO_4 even after 25-cycle. Mn together with Fe supported with TiO_2 as an OC investigated with different molar ratios of metals. The highest OTC of 7.8 wt% was observed with 80 wt% of Mn and 13 wt% Fe_2O_3 and exhibited highest reactivity towards fuel gases. When Mn-Fe molar ratio of 0.66:0.34 used as OC with addition of 7 wt% TiO_2 , OTC of 9.4 wt% was achieved [67, 68]. The OTC of spinel structure-based OCs are compared in Table 2.2.

Table 2.2: Oxygen transport capacities of spinel-based oxygen carriers in CLC process.

Oxygen Carrier	Method	Fuel (Vol%)	Oxygen transport capacity (wt%)	Equipment	Cycles	Ref.
$(\text{Mn}_{0.77}\text{Fe}_{0.23})_2\text{O}_3$	Spray drier	Syngas, coal	6.7	TGA, 500 Wth CLC ^a	4	[64]
Mn ₈ 7FeTi ₇	Grinding and mixing	H ₂ , CO or CH ₄	7.8	TGA	N/A	[67]
$(\text{Mn}_{0.66}\text{Fe}_{0.34})_2\text{O}_3 \cdot (\text{TiO}_2)_{0.15}$	Spray-dried	Bituminous coal, Sub-bituminous coal	9.4	0.5 kWth CLC unit	500	[68]
CuFeAlO_4 , $\text{CuFe}_{1.5}\text{Al}_{0.5}\text{O}_4$	Mixed in rotary drum	CH ₄ /Ar	14.7	Bench scale fluidized bed reactor, TGA	25	[66]
NiFe ₂ O ₄ , MgFe ₂ O ₄ , BaFe ₂ O ₄	In-situ polymerizable complex method	CH ₄	19	TGA	30	[65]
NiFeAlO _x FeAlO _x (x = 0.25, 0.5, 0.75 and 1)	Sol-gel method	CO	19.45	TGA, Fixed bed reactor	20	[63]

^aWth = Watt-thermal

2.3.2 Perovskite form oxides

To improve OC's properties in the application of CLC, many combinations of metal oxides with various supports have been investigated. Each metal oxide has its characteristics like thermal and mechanical stability, reactivity with fuel, and OTC for CLC operation. The performance of complex structure-based and perovskite-based OCs were also studied in CLC. Metal oxides with a crystal structure similar to calcium titanium oxide (CaTiO_3) considered as perovskite. In general, perovskite can be written as ABX_3 ; both A and B refer to cations, and X is an anion. To date, perovskite-based OCs for the CLC process are being used to reduce attrition, agglomeration, and carbon deposition [69].

However, the problem related to the regeneration of perovskite materials is concerned. Abad et al. [70] studied $\text{CaMn}_{0.775}\text{Ti}_{0.125}\text{Mg}_{0.1}\text{O}_{2.9-\delta}$ (where δ indicates the oxygen contents) as an OC and observed that OTC lessens after a few time. They found that the lowering of OTC was due to incomplete reformation of perovskite. The total OTC of the earliest material decreased from 8.4–9.0 wt% to 7.9–8.6 wt%. Further, they have observed that this could be due to the generation of CaMn_2O_4 and Ca_2MnO_4 mixed oxides rather than perovskite structure. Ksepko et al. [71] examined $\text{Sr}(\text{Fe}_{1-x}\text{Cu}_x)\text{O}_{3-\delta}$ (with $x = 0, 0.1$ and 0.33) as OC. $\text{Sr}(\text{Fe}_{0.67}\text{Cu}_{0.33})\text{O}_3$ provided highest reduction of 4.86 wt% as compared to SrFeO_3 , and $\text{Sr}(\text{Fe}_{0.9}\text{Cu}_{0.1})\text{O}_3$. Furthermore, the addition of Cu^{2+} stabilized the OC during 20 redox cycles in TGA. Overall, for all measured temperatures, the stability of all three OCs against regeneration in the oxidation cycle was found to be significant. The prepared OC was tested at high temperature and results showed that OC has the ability to resist against high temperatures with crushing strength more than 1 N. SEM analysis confirm that there was no sign of agglomeration. Jiang et al. [72] reported a La-Cu-Ni-O type perovskite structured based material ($\text{LaCu}_x\text{Ni}_{1-x}\text{O}_3$) as a suitable OC that exhibited high reactivity and stability. The highest OTC of 1.7 was obtained for $\text{LaCu}_{0.1}\text{Ni}_{0.9}\text{O}_3$. The OC showed stability in 30 redox cycles. SEM images showed that the structure of OC for fresh and after 30 cycles was same and no agglomeration was observed. Furthermore, the reactivity of the OC was

same even after 30 cycles. Perovskite structure-based OCs were successfully regenerated without any carbon deposition or agglomeration that display high thermal and mechanical stability. The comparison for perovskite structured OC is given in Table 2.3.

Table 2.3: Oxygen transport capacities of perovskite-based oxygen carriers in CLC process.

Oxygen Carrier	Method	Fuel (Vol%)	Oxygen transport capacity (wt%)	Equipment	Cycles	Ref.
$\text{LaCu}_x\text{Ni}_{1-x}\text{O}_3$	Combustion synthesis	CH_4	1.7	TGA, Solar-heat driven chemical-looping combustion	30	[72]
$\text{Sr}(\text{Fe}_{1-x}\text{Cu}_x)\text{O}_{3-\delta}$	Mechanical mixing calcination	H_2/Ar	4.86	TGA	5	[71]
$\text{La}_{0.1}\text{Ca}_{0.9}\text{Cu}_{0.1}\text{Ni}_{0.9}\text{O}_3$	Combustion method	CH_4	7.8	TGA	5	[73]
$\text{CaMn}_{0.775}\text{Ti}_{0.125}\text{Mg}_{0.1}\text{O}_{2.9-\delta}$	N/A	CH_4, H_2 or CO	9.0	TGA	10	[70]

2.3.3 Waste material oxides

For CLC operations, Fe-based OCs are most favorable, owing to less cost and high reactivity. Waste materials containing iron contents can be useful as OCs for CLC. It may reduce material costs and will utilize useless waste into useful material. Metallurgical waste is a great resource that consists of a significant amount of Fe. The OTC of waste material-based OCs from the previous studies reviewed in Table 2.4. Di et al. [74] proposed that steel slag from industrial residues of metallurgical industries is suitable for OC. The elemental analysis of steel slag showed that the main elements were CaO, Fe₂O₃, SiO, and MgO with composition of 45.9, 9.36, 14.2, and 9.42 wt%, respectively. After sulfating the steel slag in SO₂ atmosphere, 39.49 wt% of sulfating slag was consisted by CaSO₄. Further, they have investigated the performance of steel slag as an OC in TGA. They reported that in the beginning, OTC was 18.35 wt%, and after a few cycles, OTC was decreased, and a steady value of 10.63 wt% for OTC was observed in the following redox cycles. The OTC was due to oxidation and reduction reactions of CaSO₄. The lowering in OTC was observed due to loss of sulfur contents during redox cycle. TGA results showed that by lowering the reaction temperature the loss of sulfur can be prevented. This reveals that CaSO₄ at high temperature losses sulfur most likely during oxidation process. Miller et al. [75] investigated the OCs based on Fe oxide, and Mn minerals with different molar ratios have been designed and prepared by using different supports, such as spent fluid catalytic cracking catalyst (FCC). The effects of temperature and molar ratio of Fe and Mn on oxygen transfer capacity were studied. From temperature 900 °C to 1100 °C, OTC was significantly increased by 27 % up to 67 %. Highest value 76 % of theoretical OTC was achieved for 0Fe100Mn/FCC. However, at 1100 °C sintering and agglomeration was occurred that resulted in decrease of reactivity of OC confirmed by SEM images.

Overall, for selecting best OCs many factors are to be considered. One of them is cost that take in account before selection of OC. Natural resources are inexpensive and are abundant to use as an OC for CLC. Natural ores of Fe and Mn and combination of these ores for the use of OC in CLC processes are getting more attention. Moreover, the OTC of Fe and Mn is high and can be used for many reduction and oxidation cycles.

Most of these ores contain other metals like; SiO_2 , TiO_2 , CeO_2 and Al_2O_3 which enhance the properties of OC. The presence of CeO_2 as promoter can reduce agglomeration and spinal formation. Furthermore, CeO_2 could enhance the OTC due to good redox properties. On the other hand, the utilization of waste materials for OC could decrease the cost of overall CLC application. Furthermore, the environment pollution due to wasting the materials could be lowered to some extent by utilizing it for CLC.

Table 2.4: Oxygen transport capacities of waste materials-based oxygen carriers in CLC process.

Oxygen Carrier		Method	Fuel (Vol%)	Oxygen transport capacity (wt%)	Equipment	Cycles	Ref.
Active site (wt%)	Support						
Fe=20	Spent alumina-silica catalyst	Incipient wetness impregnation	Char	1.9	Drop tube fixed bed reactor	5	[76]
N/A	Oxidized printed circuit board metals	Pyrolysis and gasification	Coal and rice straw	3.57	TGA	N/A	[77]
Ca	OPCB Waste manganese sand filter material	Wet ballmilling method	Coal	14.5	TGA	20	[78]
N/A	Steel slag	N/A	CO	18.35	TGA	12	[74]
N/A	LD slag	N/A	Syngas, CH ₄ /N ₂	1.16	12 MWth fluidized bed boiler	3	[79]
Mn=40	FCC	Impregnation method	CH ₄ /Ar=10	74 % of available	Lab-scale reactor	15	[75]

2.3.4 Natural mineral oxides

The use of natural minerals that are rich in metals and globally available in huge resources reduces the overall cost of CLC process [4]. Among natural minerals, ilmenite and hematite ores mostly consist of Fe. Furthermore, Fe is more suitable candidate as an environment safety concerns and economical. Because of the huge resources of hematite ores, hematite shows the most abundant Fe ore in the world and has been studied broadly for the CLC processes [41, 47]. The investigation of hematite from South Africa region was done under different operating conditions by Shen et al. [80]. Hematite mine for the combustion of lignite coal in 3 kWth CLC bubbling fluidization analyzed for 10 tests and OTC of 2.77 wt% was found. It was observed that staged fluidization in fuel reactor was an effective method to get high carbon efficiency about 81-96 %. The efficiency of the unit between 57.8 % to 80.3 % for the capturing of carbon dioxide with long lasting operation time of 300-342 h was found. This study showed that OC based on hematite could be used in a unit of 3 kWth consist of interconnected fluidized bed reactor.

Hammache et al. [81] investigated the performance of three types of OCs for the combustion of coal char using lab scale drop tube fixed bed reactor. It was observed that the OTC for hematite changed with calcination. The OTC for hematite as received was varied from 0.15-0.265 g of O₂/ g of OC as number of redox cycles were increased from 10 to 50. But for calcined hematite the value of OTC was decreased from 0.11-0.14 g of O₂/ g of OC between 1-5 cycles. On other hand the OTC of red mud-based OC as received (0.2-0.3 g of O₂/ g of OC) was lower than when OC heated (0.47-0.36 g of O₂/ g of OC) and used for CLC process. Similarly, the effect of BaAl₂O₄ addition to iron ore-based OC for the CLC of syngas was studied. The OTC of 23.9 wt% was achieved during 50 oxidation and reduction redox cycles when 10 wt% BaAl₂O₄ was added to iron ore [82]. Almost similar results were found for hematite from Tierga used as OC in 0.5 kWth CLC unit. The OTC for the fresh calcined OC was 2.5 wt% which was increased to 2.8 wt% when it was for the combustion of coal during 30 h [83]. Tierga ore as an OC in (In-situ gasification) iG-CLC process was investigated for different types of biomasses (forest residue, pine sawdust, olive stones, almond shell) combustion. The characterization results showed that Tierga ore was mainly consisted

of Fe_2O_3 , SiO_2 , Al_2O_3 , CaO , and MgO phases. For all types of biomasses, the combustion process occurred in same trend and nearly 100 % CO_2 was captured. Total oxygen demand was 25-30 %, that was increased 1 % due to the presence of tar at the outlet of fuel reactor [84].

Abad et al. [85] investigated the reactivity of Gabon manganese ore-based OC in 0.5 kWth continues CLC process and found that by increasing the residence time of solid inventory in fuel reactor and temperature of fuel reactor resulted in significant increase in carbon capture. Moldenhauer et al. [86] compared five types of manganese ores using 300 W unit circulating fluidized-bed reactor for CLC process. Biomass volatile, methane and syngas were used as reducing gases for 80-280 redox cycles. The properties of all five manganese ores (Elwaleed, Tshipi, Guizhou, Braunitz, and Morro da Mina ores) were greatly different. Among all, Guizhou ore showed highest reactivity with high mechanical strength, low attrition rate and oxygen released was 3 vol% in the dry gas. Although both Elwaleed and Tshipi presented high fuel conversion but their lifetimes in redox cycles were not good due to poor thermal and mechanical stability. The OTC for iron-based OCs along with type of fuel used is given in Table 2.5.

Table 2.5: Oxygen transport capacities of natural materials as oxygen carriers used in chemical looping combustion process.

Oxygen Carrier	Method	Fuel	Oxygen transport capacity (wt%)	Equipment	Cycles	
(a) Hematite, (b) Fe/FCCs (c) Red mud (bauxite)	N/A	Coal char, Basin char	(a) 0.265 (b) 1.72 (c) 0.47 O released/mole Fe (mol/mol)	Lab-scale drop tube fixed bed reactor	(a) 10-50 (b) 1-5 (c) 1-10	[81]
Hematite mine	N/A	Lignite coal	2.77	3 kWth CLC bubbling fluidization	N/A	[80]
Petroleum coke, Manganese ore	N/A	Preheated at 170 °C	1.7	Batch fueled bubbling fluidized bed reactor, TGA, 0.5 kWth CLC unit.	N/A	[87]
Hematite mine	Crushed	coal	2.8		N/A	[83]
Manganese ore	Crushed and thermally treatment	South African bituminous coal	7.3	0.5 kWth CLC unit	N/A	[85]
Tierga ore	Crushed	Forest residue, pine sawdust, olive stones, almond shell	2.5	Type of fluidized bed reactor	N/A	[84]

2.3.5 Single metal oxides

Single oxide means, OCs that are prepared using one metal oxide with or without one or more than one inert support. The example of single oxide OC is NiO-Al₂O₃, where NiO is active site of OC and Al₂O₃ is inert support. During Oxidation and reduction cycles in CLC process, oxygen adsorbed and released due to active site of OC. Different metals-based single oxides with their OTCs were investigated in CLC process which are discussed below:

2.3.5.1 Nickel oxide (NiO)

Ni-based OCs were early named as OC being most reactive with CH₄ and is also the most investigated OC. The concerns of Ni-based OCs are due to their significant reactivity with the fuels and reasonably complete conversions of fossil fuels are secured, these OCs show the incredible ability of operating at high temperatures in the range of 900–1100 °C. Amongst all single metal OCs, NiO has the highest OTC, which is 21 wt%. It was found that 1.84-6.0 wt% OTC can be achieved with Ni-based OCs at 700-1000 °C [88, 89]. There are some limitations which include the presence of CO and H₂ at the outlet of the FR due to thermodynamic constraints, their toxic nature due to which specific safety measures are needed for its usage, moderate reaction rate due to high porosity and they are expensive than other materials. Pure NiO as a result of their unusual porosity have low reaction rates [45, 90]. The OTC of Ni-based OCs from literature is given in Table 2.6.

Dueso et al. [91] investigated the effect of different composition of syngas on the combustion efficiency using Ni-based OC synthesized by impregnation method. It was found that the combustion efficiency of CLC process was not influenced by the composition of syngas, but lowest combustion efficiency was observed when CO gas used. This is because NiO has low reactivity towards CO gas. However, NiO showed highest reactivity with H₂ and OTC was 3.8 wt% during 50 h continues operation in CLC process. Hence the OTC of OC altered by reactivity between fuel gas and OC. In

addition, the OC to fuel ratio greatly affect the combustion efficiency resulted about 99 % efficiency when this ratio was 5. On other hand, Ni-based OC supported with CaSO_4 was used for the production of syngas. The OTC of 4.6 wt% was achieved for the combustion of lignite fuel in tubular furnace reactor. With the increasing number of redox cycles agglomeration was observed that might be due to presence of ash. Furthermore, sulfur in the reaction gas, made OC poison because NiO captured sulfur from reaction gas [92].

At high temperature, Ni support with alumina formed NiAl_2O_4 spinel compound [93]. Spinel compound has strong interaction with alumina support that cannot take part in reductive and oxidative reactions. This causes loss of Ni contents in the OC after few redox cycles. Recently Ni with zirconia/titania shell modified alumina support also has been investigated as an alternative to avoid spinel formation. The addition of core shell powder prevented the contact between Ni and support alumina, resulted in the stability of OC at high temperature. Furthermore, it prevented spinel (NiAl_2O_4) formation and decreased attrition and hence no activity loss was occurred even after 10 redox cycles. The OTC of the OC was 9.3 wt% reported for the combustion of methane gas [94]. Thus, the coating with core-shell structure promoter can stabilize the reactivity (OTC) of OC in repeating reduction and oxidation cycles. Similarly, at what was observed in the case of 35 % $\text{NiO}/\text{Al}_2\text{O}_3@\text{Zr}$ (mesoporous zirconia shell coated all over γ -Alumina) OC is considered a better choice for the combustion of coal. The OTC of about 9.7 wt% was observed during operation in CLC process [95]. Due to these reasons, Ni-based OC always mixed with different active site metals during the last decade.

In summary, it can be resulted that NiO has great potential to use it in CLC processes due to its high reactivity. The limitations that reduce the attention for the selection of Ni-based OCs can be eliminated by the use of modified supports. Coating on support with suitable promoter could be best choice for Ni-based OCs. Furthermore, the addition of one or more than one active metals to Ni-based OCs could increase the OTC.

Table 2.6: Oxygen transport capacities of Ni-based oxygen carriers in CLC process.

Oxygen Carrier		Method	Fuel (Vol%)	Oxygen transport capacity (wt%)	Equipment	Cycles	Ref.
Active site (wt%)	Support						
Ni=18	$\alpha\text{Al}_2\text{O}_3$	Hot incipient wet impregnation	Syngas	3.8	TGA, Batch fluidized bed reactor, CLC plant	N/A	[91]
Ni=27	CaSO_4	Precipitation method	Lignite	4.6	Tube furnace reactor	N/A	[92]
Ni=30	$\gamma\text{Al}_2\text{O}_3@\text{Zr}$	Core shell method	CH_4	~9.3	TGA	10	[94]
Ni=35	$\text{Al}_2\text{O}_3@\text{Zr}$	Core shell method	Coal	~9.7	TGA	1	[95]

2.3.5.2 Copper oxide (CuO)

Generally, Cu-based OCs have been shown a promising OC candidate because it possesses good reactivity and OTC at low temperature and undergo complete combustion to produce H₂O and CO₂ without suffering from thermodynamic restriction. Moreover, Cu is considered less expensive material compared to other transition elements (Co and Ni). However, the main drawback of using Cu-based OCs is the agglomeration issue because the melting point of Cu is relatively low, which is indicated at 1085 °C [96]. In order to improve the performance of Cu-based OCs, various supporting material such as CuO/SiO₂ [28], CuO/Al₂O₃ [97] and CuO/olivine [98] were tested.

It has been well-reported that the OTC of Cu-based OCs may be decreased due to the spinel type structures. For example, 0.82 ratio of Al₂O₃ to CaO in OC, exhibited around 2 wt% of OTC, which is much approximate to their theoretical values. But, when this ratio was gradually increased up to 9.44, OTC was dropped along with increasing the redox cycles. On the other hand, OTC was decreased due to the utilization of less amount of Al, which could generate CuAl₂O₄ [31]. In this respect, the use of fly ash as support for Cu-based OC exhibited high thermal and mechanical stability. The OTC of 11.2 g O₂/100 g OC was calculated. The stability of the OC was analyzed for 90 cycles, and there was no sintering and deactivation of OC, observed. XRD results confirmed that CuAl₂O₄ is not formed [99].

Another important observation for preventing spinel CuAl₂O₄ was calcium looping integrated with chemical looping combustion (CaL-CLC) process using Cu-based OC in the presence of CaO, MgO and Al₂O₃ support by Ma et al. [25]. The OC based on CaO and MgO showed highest reactivity with OTC of almost 25 wt% (0.25 g-O₂/g-Cu) and no attrition was observed as compared to OCs without CaO or MgO. The stability of OC over 30 redox cycles was considered due to the core-shell structure. MgO layer on the surface of Al₂O₃ prevented the interaction of CaO/CuO with the support and hence the structure of the OC was remains unchanged throughout 30 cycles. This shows that the structure of OC has directly association with OTC and the structure depends on the preparation method. Tian et al. [26] also admitted that OC with

hierarchical structure have excellent performance. The use of titanium dioxide (TiO_2) as support for Cu-based OCs, showed excellent mechanical stability. High OTC 15.4 wt% was achieved close to the theoretical OTC 15.5 wt%. These results revealed that in the presence of TiO_2 and Al_2O_3 , CuO almost entirely reduced to form Cu. Furthermore, the reduction rate influenced by the concentration of the gaseous fuel and operating temperature.

The use of zirconium dioxide as the support for Cu-based OC was investigated by Adánez-Rubio et al. [19]. The OTC for fresh and 30 h operation in a methane atmosphere was studied. A significant loss of OTC from 2.6 wt% to 1 wt% was noticed. The results from continues 30 h unit showed that about 62.1 % CuO contents lost and due to which combustion efficiency was diminished. This depletion of CuO contents was the result of attrition that was observed in attrition jet index profile. These authors concluded that the addition of ZrO_2 did not improve the performance of CLC process. The OTC of Cu-based OCs prepared by different methods is given in Table 2.7.

From these observations, it was concluded that in Al_2O_3 supported OC, the activity and OTC decreases as Al_2O_3 contents increase due to the formation of spinel compound. While the modified alumina support by core-shell method with promoters like MgO or CaO retards the formation of CuAl_2O_4 . CuO is suitable OC for CLC process but the loss of Cu contents due to attrition causes decrease OTC. The mechanical and thermal stability can be increased with the use of TiO_2 support.

Table 2.7: Oxygen transport capacities of Cu-based oxygen carriers in CLC process.

Oxygen Carrier		Method	Fuel (Vol%)	Oxygen transport capacity (wt%)	Equipment	Cycles	Ref.
Active site (wt%)	Support						
Cu=2-20	fuel ash, Al ₂ O ₃	Mixing	Coal	~ 2	TGA	5	[31]
Cu=13	ZrO ₂	Incipient wetness impregnation	CH ₄	2.6	TGA, 500 Wth Continuous Unit	N/A	[19]
Cu=60	Fly ash	Agglomeration	Mixture of H ₂ , CH ₄ , H ₂ O, CO ₂ & N ₂	11.2	TGA	90	[99]
Cu=77.5	@TiO ₂ -Al ₂ O ₃	Self-assembly template combustion synthesis method	H ₂ , CO, CH ₄	15.5	TGA	N/A	[26]
Cu=N/A	CaO/MgO@Al ₂ O ₃	Co-precipitation & wet impregnation	CO ₂ & CH ₄	~ 25	TGA	30	[25]

2.3.5.3 Iron oxide (*FeO*)

Though Fe-based OCs have weak redox characteristics, low OTC, and low methane conversion as compared to Ni, Cu and Co nonetheless Fe-based OCs are considered feasible candidate for the application of CLC because of its environmental friend and low cost. Subsequently, Fe-based OCs showed two important properties, which are high resistance to agglomeration and low tendency to carbon deposition. Thus the activity of OCs can be controlled and maintained for a few redox cycles [96]. Fe-based OCs showed different oxidation states such as Fe₂O₃, Fe₃O₄, FeO, and Fe. Fe₂O₃ can be reduced to Fe through overall reaction based on Equation (2.4):



However, only the transformation of Fe₂O₃ to Fe₃O₄ is applicable for methane's oxidation in an interconnected fluidized bed reactor due to the limitations of thermodynamic and selectivity of product CO₂ and H₂O. Whereas, further reduction to FeO (wustite) or metallic Fe will promote the production of syngas (CO and H₂) [100]. The reaction of oxidation and reduction of metal is calculated using Equation (2.5):

$$X = \frac{m - m_r}{m_o - m_r} \quad (2.5)$$

Where *m* is referred to mass of iron oxide, *m_r* is mass of reduced Fe and *m_o* is mass of Fe when fully oxidized. Supporting material such as Al₂O₃, CeO₂, TiO₂ and ZrO₂ have been prepared and carried out using the wetness impregnation technique for Fe-based OCs. Based on XRD analysis, Fe supported with ZrO₂ showed a complete reduction, while the formation of metal phase FeO and Fe₃O₄ was existed after the reduction of Fe-supported with CeO₂ and Fe/TiO₂ respectively [101]. Table 2.8 represents the OTC of Fe-based OCs prepared by different methods for the combustion of solid, liquid and gaseous fuels.

However, Fe-based OCs also tested with spent fluid catalytic cracking (FCC) support. The highest OTC 14.1 % was reported for Fe/FCC compared to OTC for Fe-based OCs supported with Al₂O₃ and SiO₂. When the temperature was increased from 900 °C to 1100 °C, OTC was decreased for FCC supported OC and resulted in the

formation of CO. Meanwhile compared scanning electron microscope (SEM) images of Fe/FCC at 900 °C and 1100 °C, OC particles were agglomerated for 1100 °C reaction temperature [21]. This result suggests that sintering and agglomeration cause to loss of OC activity. Ma et al. [102] claimed that the sintering of material was subjected to a decrease in surface area that was examined in Brunauer–Emmett–Teller (BET) analysis, which caused a lower in OTC from 2.89 wt% to 2.02 wt%. At high temperatures, Fe₂O₃ in the presence of Al₂O₃ lost its activity after a few redox cycles. The evaluation of gas composition analyses confirmed that there is no carbon deposition. Therefore, the activity loss of OC was due to sintering verified by SEM and EDS analysis. Huang et al. [103] compared OC based on Fe-substituted Ba-hexaaluminate with same OC prepared by traditional method. These researchers found that OTC for new method-based OC (BF_xA-H, x=1,2) was higher than OC prepared by traditional method (BF_xA-C, x=1,2) that was 0.85 mmol/g. The reactivity and recyclability tests in fixed-bed quartz tube reactor reveals that OTC for new OC was 1.3 times higher. BET analysis shows that the specific surface area of BF_xA-H was higher than BF_xA-C owing to higher reactivity. Similar trend for specific surface area was observed in their previous research work [104]. Bhui et al. [105] observed that pure iron oxide could release (O₂) 86 % of the total oxygen present in Fe₂O₃. Fe₂O₃ showed highest reactivity with volatile gases from coal in the presence of inert atmosphere and produced about 88.7 % CO₂ gas. EDX analysis evidences the absence of sintering due to active metal oxide particles.

Apart from these research works, Serrano et al. [106] reported the CLC of liquid fossil fuels using Fe-based alumina supported OC. SEM images indicated that agglomeration was not formed subjected to the consistent with the good fluidization in the cyclic process. During oxidation and reduction cycles the OTC of 2 wt% was observed. The reactivity test using TGA exhibited that the operating hours and presence of impurities like sulfur and other metals have no effect on the reactivity of OC. But the nature of chemical bond in hydrocarbon greatly affects its reactivity. It is speculated that due to sintering effect Fe-based OCs possess a low value of oxygen mobility. Another way of losing OC reactivity during CLC process is solid-solid transformation. At different temperatures and pressures conditions Fe has different crystal structures that result in a change in oxygen occupancy.

Table 2.8: Oxygen transport capacities of Fe-based oxygen carriers in CLC process.

Oxygen Carrier		Method	Fuel (Vol%)	Oxygen transport capacity (wt%)	Equipment	Cycles	Ref.
Active site (wt%)	Support						
Fe=N/A	Ba-hexaaluminate	Co-precipitation & coating	CH ₄ /He	1.36	Fixed bed quartz tubular reactor	50	[103]
Fe=40	γAl ₂ O ₃	Impregnation	Diesel, mineral & synthetic lubricant oil	2.0	TGA, 1 kWth CLC unit	N/A	[106]
Fe=42	Al ₂ O ₃	Mechanically mixing	CO/N ₂	2.89	Fixed bed reactor	20	[102]
Fe=40	FCC ^a	Impregnation & sonication	CH ₄ /Ar	14.1	Altamira AMI-300-unit flow control scheme	15	[21]
Fe=N/A	Coal	N/A	Coal	86 % of theoretical	TGA, Batch fluidized bed reactor	N/A	[105]

^a Spent fluid catalytic cracking

2.3.5.4 Manganese oxide (*MnO*)

Due to high reactivity and stability at high temperatures, manganese oxide is a suitable candidate as an OC for CLC process. Mn-based OCs meet the majority of the characteristics for usage as an OC, but when related to Fe-based OCs, they have a considerably greater reactivity, in addition to being economical and non-toxic. Mn-based OCs also have several oxidation states like Mn, MnO, MnO₂, Mn₂O₃, and Mn₃O₄. Results from the literature for the OTC of Mn-based OC are given in Table 2.9. In recent years, few research works were conducted using Mn-based with different support materials OC for CLC. When the Mn₃O₄ loading was 21.4 wt% on zirconia support, the OTC of 2.7 % was found. While, for CaAl₂O₄ support, 15.9 wt% of Mn₃O₄ showed 1.1 % OTC. Among all OCs, Mn-based zirconia (from Saint Gobain) supported OC prepared by incipient hot impregnation method showed fast reactivity in oxidation and reduction reactions during reactivity test in 100 redox cycles. SEM images showed that the shape of particles for fresh and used OC was similar that indicates particles were not agglomerated unlike when zirconia (from MELChemicals) used using incipient impregnation method [22].

Cloete et al. [107] investigated Mn-based OC for highly efficient power production. The OTC was 75 % of the theoretical value reported. For the combustion of coal, 95% of CO₂ was captured with 45.4 % efficiency of power production plant. The use of MgO as support for Mn-based OC was examined by Hwang et al. [108]. The OTC of 8.74 wt% was maintained during five redox cycles with methane as reducing gas. The XRD pattern showed that the phase and crystal structure was remained unchanged. SEM images confirmed that there is no agglomeration was observed. The stability in the OTC might be due to resistance of Mn-based OCs against agglomeration and attrition. Furthermore, the reactivity behavior with different types of fuel was different. When the fuel was CO and CH₄ significant carbon deposited on OC surface. In summary, it can be concluded that Mn-based OCs, zirconia, MgO and CaAl₂O₄ support materials are more preferable supports used instead of Al₂O₃. However, MgO could be more effective support for Mn-based OC because it reduces the agglomeration and stabilize OTC.

Table 2.9: Oxygen transport capacities of Mn-based oxygen carriers in CLC process.

Oxygen Carrier		Method	Fuel (Vol%)	Oxygen transport capacity (wt%)	Equipment	Cycles	Ref.
Active site	Support						
Mn	CaAl ₂ O ₄ , ZrO ₂	Incipient wetness impregnation	H ₂ or CH ₄ & water vapor	2.70	TGA, Batch fluidized bed reactor	100	[22]
	Ca ₂ AlMnO _{5.5} (oxidized), Ca ₂ AlMnO ₅ (reduced) & inert	N/A	Syngas	75 % of theoretical	TGA	N/A	[107]
	MgO	Solid-state reaction	H ₂ /N ₂ , CO/CO ₂ , CH ₄ /N ₂ , and CH ₄ /CO ₂	8.74	TGA	5	[108]

2.3.5.5 Cobalt oxide (CoO)

Though Cobalt oxide has environmental concerns and cost issues, it was considered the right candidate for OCs due to its high OTC. Co experiences many oxidation states in the redox reaction, which are Co_3O_4 , CoO , and Co . However, at a temperature above $900\text{ }^\circ\text{C}$, Co_3O_4 tends to convert to CoO , showing that it is easy to decompose and unstable around at that temperature. Hence, for CLC application, only phase transformation of CoO and Co is being taken into consideration. Despite that, only a few works are conducted since it is less favorable toward thermodynamics [109]. The support materials such as Al_2O_3 , TiO_2 , and MgO experience a strong interaction with metal oxide and forming unreactive compounds, CoAl_2O_4 , CoTiO_3 , and $\text{Mg}_{0.4}\text{Co}_{0.6}\text{O}$, respectively. It was reported from the previous study when CoO was impregnated on Al_2O_3 , the formation of CoAl_2O_4 was observed in XRD analysis during oxidation and reduction reaction [110]. The OTC of different Co-based OCs achieved by previous research works are given in Table 2.10.

Due to high reactivity with the fuels, good properties towards fluidization with low attrition, low carbon deposition and high stability, alumina is the most favorable support material used for Co-based OCs. Only 10 wt% Co on gamma-alumina support and pure Co-oxide were used to investigate its reactivity with methane gas using gas. For 10 min reduction test in TGA, it was noticed that pure Co was fully reduced (O_2 -released) in first 2 min while 10%Co- $\gamma\text{Al}_2\text{O}_3$ most of O_2 was released in less than 2 min and remaining O_2 was released throughout 10 min. For comparison in full redox cycle, pure Co-based OC was not fully re-oxidized, but alumina supported Co-based OC fully re-oxidized in 2 min with OTC of 2.6 wt%. These findings show that $\gamma\text{Al}_2\text{O}_3$ enhances the Co-based OC [34].

Titanium dioxide (TiO_2) is studied as the support material for a Co-based OC because it showed high reactivity and OTC. X-ray photoelectron spectroscopy (XPS) and SEM images confirmed that agglomeration was very small; even the number of cycles was increased from 1 to 10 cycles. With this negligible agglomeration the OTC amount was not affected. Furthermore, as the number of cycles was increased, the

oxygen transfer rate also increased. OTC for hydrogen and methane gases were 10.2 wt% and 10.5 wt%, respectively. For both gases, actual OTC was approximate to theoretical OTC [111]. Cimino et al. [112] investigated the effect of transition metals (Co, Mn, Cu) addition on $\text{La}_2\text{O}_2\text{SO}_4$ for the CLC of methane. Among these active metals, Co showed significant improvement in oxygen storage of OC. TG-MS-FTIR analysis revealed that Co- $\text{La}_2\text{O}_2\text{SO}_4$ is extremely reactive to CH_4 at 800 °C with significant reaction rates and high CO_2 selectivity, preventing the output degradation associated with decomposition during CLC process.

In recent years, the use of single metal oxides has been decreased due to limited reactivity during few cycles only. This might be due to poor thermal and mechanical stability of single oxides that result agglomeration and attrition which causes the depletion of metal oxides and OTC of OC. Hence, the performance of CLC could decrease due to low durability of OCs in redox cycles. Therefore, the OTC and stability of metal oxide (monometallic) OCs could increase by introducing promoters or doping with bi-metallic or tri-metallic oxides. Among single oxides, Ni and Fe are the most favorable candidates for OCs due their high OTC and economical. Their reactivity and stability during multiple redox cycles could be improved by using highly stabilized support and promoter that provide high surface area to Ni and Fe.

Table 2.10: Oxygen transport capacities of Co-based oxygen carriers in CLC process.

Oxygen Carrier		Method	Fuel (Vol%)	Oxygen transport capacity (wt%)	Equipment	Cycles	Ref.
Active site (wt%)	Support						
Co=10	$\gamma\text{Al}_2\text{O}_3$	Wet impregnation method	CH_4/N_2	2.6	TGA	1	[34]
Co=N/A	TiO_2	Sol-gel method	H_2/N_2 & CH_4/N_2	10.2	TGA	10	[111]
Co=1	$\text{La}_2\text{O}_2\text{SO}_4$	Impregnation method	CH_4/N_2	15.5	TGA	15	[112]

Generally, single oxide-based oxygen carriers more likely undergo sintering and attrition effect. These deficiencies shorten the lifetime of single metal oxide-based oxygen carriers. Luo et al. [113] investigation revealed that single metal oxide can only provide lattice oxygen (O) during redox reactivity reactions at specific partial pressure of oxygen values, which makes limited use in chemical looping applications. The use of mixed metal oxides-based oxygen carriers has resolved this constraint and oxygen in gas phase could be transferred for complete combustion.

2.3.6 Mixed metals oxides

Recently the combination of various active metal oxides has been studied in OCs with complicated form of metal oxide. The mixed metal oxide improved the stability and reactivity of OC, enhanced mechanical strength and reduced the risk of toxic substances, reduced carbon deposition and better fuel processing. In mixed metal oxides bimetallic and trimetallic based OCs were studied in CLC process. In recent scientific work on CLC processes a combination of several transition metals (Mn, Fe, Ni, Cu, Co) was assessed. The OTC of different metals based mixed oxides OCs are given in Table 2.11.

In mixed metal oxides, combination of different active metals such as CuO, Fe₂O₃ and Mn₃O₄ supported with Al₂O₃ and spinel structure prepared by different methods (incipient wetness impregnation, sol-gel, spray dry, spray granulation, and tumbling technique) were analyzed using TGA and a batch fluidized-bed reactor [27, 114, 115]. Adnan et al. [116] investigated the performance of Ni-Fe with La modified Al₂O₃ supported OC in CLC process. The method used for the preparation of OC was sequence incipient wetness impregnation. During reactivity in redox cycles, the OTC of 0.055 g O₂/g OC was achieved for the combustion of H₂ gas.

The addition of Cu to Fe-based OC has been investigated in 50-kWth CLC. Spray drying and tumbling method have been used to examine the performance of OC. Siriwardane et al. [114] found that with both methods no agglomeration was observed even though 30 % of Cu was used to prepare CuO-Fe₂O₃/alumina. The OTC changed from 0.9 to 6.4 % depends on the reduction of reaction occurred for Cu and Fe. In

addition, these researchers showed that OC prepared via granulation and spray drying showed excellent performance during the 25-cycle fluidized bed testing conducted at 800°C. However, a significant particle loss was observed in spray drying compared to the tumbling method during the 50 kWth test. Benincosa et al. [117] studied the effect of Cu addition to Fe-Mn based OC. The reactivity of the trimetallic based OC was improved. The actual OTC of 18.2 % during the redox cycles was higher than theoretical OTC of 17.9 %. Similar results were found when the performance of same OC was tested using CO fuel gas. The OTC was higher for Cu-Fe-Mn based OC than bimetallic and monometallic based OCs [118].

Over the last few years, wide range of materials have been investigated as OCs for CLC. Instead of single metal oxides, mixed metal oxides were more preferred. Every metal improves the properties of OC in terms of OTC, stability in several redox cycles, retardation of metal sintering and coke resistance. However, for CLC, OCs need to be considered for synthetic approach and their chemical composition and metal loading. NiO and CuO exhibit highest oxygen transport capacities with 21 wt% and 20 wt% respectively, among all single metal oxide-based oxygen carriers. The investigation of CLC process for the combustion of natural gas was carried out in 10-140 kWth plants using Ni and Cu-based OCs [119-122]. In the process of methane reforming, NiO was considered an excellent material, but for the chemical looping combustion of methane, NiO exhibited poor performance due to carbon deposition [123]. However, the reactivity of Cu-based OCs in the oxidation and reduction cycles is high [51]. Furthermore, Cu-based OCs can release O₂ during the combustion of solid fuels at temperature greater than 700 °C [124]. In addition, Cu-based OCs are environment friendly and less expensive as compared to Ni and Co. The low Tammann temperature (the Tammann temperature determines the commencement of sintering of the bulk material) of the CuO/Cu (or CuO/Cu₂O) redox pair is the main obstacle concerned with the use of CuO-based carriers, despite their promising properties. This results in the sintering and agglomeration of OC particles at high temperatures. Additionally, during the circulation of OC particles in fluidized bed reactors, the structure of OC significantly changed by agglomeration that ensures the deactivation of fluidized bed. The Cu-based OCs using different support materials such as; γ -Al₂O₃ [34, 125], TiO₂ [26] and ZrO₂ [19] have been studied to prevent agglomeration. Among these support

materials, γ - Al_2O_3 was most studied material due to its very low attrition rate and provides high surface area and stability to active metal [126]. However, beside using these supports, it was examined by previous research works that the particles of Cu-based OC undergo agglomeration at high temperatures. For example, the activity loss was observed for 60 wt% Cu-CeO₂ due to agglomeration during few redox cycles [30]. The interaction between Cu contents and γ - Al_2O_3 support at high temperature resulted in the formation of highly stable spinel compound [31, 32]. This spinel compound causes loss of Cu contents and hence the OTC of the OC decreases. The modification of support with a suitable promoter showed the absence of spinel compound by avoiding interaction between active metal and support [25, 33]. It has been well reported that praseodymium (Pr) oxide has good redox properties when exposed with CH₄ and air using TGA [34]. Several preparation methods have been proposed for the synthesis of Cu-based OC [25, 127]. However, wet impregnation method was considered more efficient for Cu-based OCs [128].

In praseodymium-doped materials, Pr shows a mixed valence state, making it an intriguing candidate (Pr^{4+} and Pr^{3+}). Furthermore, praseodymium has a substantially greater reducibility and fast oxygen exchange activity, making it an attractive candidate for oxygen storage [35, 129]. To date the interaction of Cu with Pr-modified γ - Al_2O_3 and the importance of these interactions in CLC process have not been examined in previous literature, thus highlighting the novelty of current research work. This data gap opens the door to misinterpretation and inconsistencies in experimental measurements, especially those collected by wide ranging CLC process. The present study focused on synthesizing and investigating Cu-Pr- γ - Al_2O_3 OC using wet impregnation method. The effect of Pr on Cu- γ - Al_2O_3 based OC was studied.

Table 2.11: Oxygen transport capacity of mixed-based Oxygen Carriers.

Oxygen Carrier		Method	Fuel (Vol%)	Oxygen transport capacity (wt%)	Equipment	Cycles	Ref.
Active site (wt%)	Support/Promoter						
Ni=2.5, Fe=15	La ₂ O ₃ =2, γ -Al ₂ O ₃	Sequenced incipient wetness technique	H ₂ /Ar	5.5	Fluidized CREC riser simulator	N/A	[116]
CuO=30, Fe ₂ O ₃ =30	Alumina	Solid-state mixing/tumbling	CH ₄	6.4	Bench-scale fluidized bed reactor, NETL 50-kWth CLC	25	[114]
Cu=80, Mn=20	N/A	Sol-gel	CO/N ₂ , Shenhua bituminous coal	~9	TGA, Fixed bed reactor	22	[130]
CuO=50	Power River Basin coal fly ash, γ -Al ₂ O ₃	Mechanical mixing and wet impregnation	CH ₄ /N ₂	~11	TGA, Fixed bed reactor,	10	[115]
Fe, Co, Ni, Cu	TiO _x	Conventional sol-gel process	CH ₄ (or H ₂)/CO ₂ (or N ₂)	11.95	TGA	10	[131]
MnO ₂ , CuO	iron ore	N/A	CO/Ar	25.6	TGA	N/A	[118]

2.4 Optimizations of process parameters

The optimization of process is a method or technique that is used to optimize a whole process or process parameters to achieve maximum efficiency. This approach involves the investigation of conditions at which response can be in its best stage [132]. A conventional optimization approach known as one-factor-at-a-time that was used to investigate the effect of one parameter on the dependent parameter (by varying/adjusting one variable and keeping other parameters constant) for the optimization of a process. However, the main drawback of conventional approach is that complete influence of input parameter on output parameters cannot be addressed [133]. Moreover, the number of experiments, time for optimizing the process, cost for the research project and lack of interpretation increase for examining the interaction among several factors [134]. To overcome these shortcomings of conventional optimization approach, RSM technique can be used which applies inferential statistics [135]. RSM technique can be utilized for developing correlation among number of input and output variables. Statistical experimental design facilitates for designing first degree polynomial model [133]. RSM was introduced by Box and collaborators in the 1950s. RSM is a set of statistical and mathematical methodologies for developing, improving, and optimizing processes within predefined parameter boundaries. While numerous parameters influence the process output reaction, the goal is to optimize this response for the greatest overall performance. It describes the impact of several independent variables on the process output response over 85 percent of the time. It determines the regression model and operational settings using quantitative data gathered from well-designed trials [136, 137]. RSM may also be used to create factorial tests in terms of creating a statistical equation that can be used to evaluate the impacts of independent variables on the expected output. This methodology is the most suited for multi-factor studies, as it looks for a general relationship among numerous parameters in order to find the process's most favorable circumstances [138]. Taguchi Design, Three Level Factorial Design, BBD, and CCD are some well-known DOE designs. The most often used optimization techniques are CCD and RSM.

The temperature of the reaction is considered to be one of the most critical parameters influencing the efficiency with which fuel is employed in chemical looping combustion (CLC). The molecular perspective revealed that raising the reaction temperature was relatively useful in promoting the optimal usage of LZ coal during the reaction between LZ coal and CuFe_2O_4 in order to enhance the efficient exploitation of LZ coal [139]. Another interesting observation is that the maximal rate of oxygen production increases with increasing operational temperature. Because of the relationship between operational temperature and the amount of time the oxygen carrier was subjected to N_2 , it was possible to predict how much CuO would decompose [140]. Furthermore, it was found that the increase in residence time of OC in the fuel reactor, enhances the conversion of fuel [141]. In addition to the effects of time and temperature on the reaction rates of redox cycles, Garca-Labiano et al. [142] investigated the effect of pressure on the reaction rates of redox cycles. Increased total pressure is reported to have a detrimental influence on the reaction rates of all oxygen carriers, according to the results of the study. Taking into consideration the previously stated findings, it can be concluded that time and temperature are the most important factors influencing the responsiveness and performance of OCs during the CLC process. As a result, using RSM, it is necessary to determine the optimal process conditions (time and temperature) for the CLC process.

2.4.1 Response surface methodology

RSM is a tried-and-true approach that has been used in optimization research over the past decade. It is a method for creating experimental matrices and analyzing the data using analysis of variance (ANOVA). It established a link between the investigated operating parameters and the desired outcome [138]. RSM is the most prominent feature is that it generates 3D-plots that show the interaction of variables and their impact on the response. It is a great way to improve the efficiency of CLC process because it has the ability to change multiple process factors at the same time. Furthermore, 3D graphs facilitate in the identification of previously experimentally untested intermediate points. The following are a few procedures in the RSM application: (i) A wide range of independent parameters have significant

influence on the process, as evidenced by the literature, the experimental region's limitations, the study's aims, and the experience of researchers. (ii) choosing an experimental design and carrying out the tests according to the design experimental matrix. (iii) mathematical and statistical analysis of the experimental data, as well as model fitting (iv) the model's fitness is analyzed. (v) evaluating the optimum values for each examined variable and (vi) verifying or confirming a fitted model for the best values.

2.4.2 Model fitting and statistical analysis

To assess the fitness of the proposed RSM model and the significance of operating parameters, the statistical tool ANOVA was used. Valuable terms, lack of fitness test, and regression model are three types of statistical tests used in the evaluation [135]. The coefficients of the terms and model suggested by the proposed model are known as P-values. The significance of model can be observed by lower P-values and higher F-values (Fisher distribution). The terms of the model become significant and closer to experimental data if the P-values are ≤ 0.05 , which may happen due to the noise in the experimental results [143]. Because of the noise in the data, the P-values show that model terms are unsatisfactory. F-values are used to examine parameters within and across models. A smaller P-value and a greater F-value indicate the order of input parameters over the output. Lack of fit, on the other hand, is the discrepancy between the measured and projected value, and it can be random or predictable. The precision of the experimental results is measured by the regression model (R^2). Its value in the proposed model ranges from 0 to 1. A figure closer to 1 indicates accurate data reliability, which has a strong influence on the response. When the value is more than 0.90, the model predicts that the answer will be acceptable. The adjusted R^2 value represents the variation in data projected by the model. The non-significance model terms account for the larger gap between R^2 and adjusted R^2 . The difference between adjusted R^2 and predicted R^2 values is the model quality referee, which should be less than 0.20. The influence of process factors on response variables can be evaluated using lack of fit model analysis. In order to assess whether the model is good at relating and predicting data, the lack of fit should be non-significant [133]. The formation of 3D-

plots that illustrate the relationship of operating parameters and their effect on the response is a key component of ANOVA analysis. In addition, 3D-graphs assist in obtaining intermediate points that have not been tested experimentally. The optimization of process parameters is the most essential component of RSM. Based on the evaluated experimental data, it predicts the optimal parameters and response yield [135].

The literature review highlighted the potential of mixed oxide-based OCs for controlling CO₂ emissions using CLC technology. The stability of OCs during multiple redox cycles with high OTC is highly important to minimize overall cost of the CLC process along with high efficiency. The advantages and limitations of several OCs against different factors such as economic and environmental perspective, agglomeration, attrition, carbon deposition, oxygen vacancy, oxygen transport capacity and stability at high temperatures during number of oxidation and reduction cycles have been discussed for complete combustion of fossil fuels with inherent CO₂ capture in CLC process. Cu-based OCs have gained lot of attention among other OCs because of their high reactivity in oxidation and reduction reactions, non-toxicity, and reasonable cost. The basic idea of OCs reactivity with oxidizing and reducing environments is critically reviewed, as well as the effects of time, metal loading, and temperature on the OTC have been described. CuO is examined as an OC with distinct features and phases, as well as its limitations. The thermal stability of CuO at high temperature is one of the key challenges in the field of chemical looping combustion technology because of its low melting point. Various methods have been proposed in the literature for the preparation of Cu-based OCs such as wet impregnation method, sol gel method, coprecipitation method, self-assembly template combustion synthesis method and mechanical mixing. The wet impregnation method has been widely used due to its simplicity, reasonable cost, and environmental friendliness for large-scale production of Cu-based OC, as well as its ability to control morphology and phase composition by adjusting key synthesis parameters for improving CuO content properties. Furthermore, the use of different types of support materials such as Al₂O₃, TiO₂, SiO₂ and CeO₂ and effect of different promoters on the performance of Cu-based OC have been reviewed. It has been proved that the Pr-oxides have strong ability to modify γ -Al₂O₃ support and can be used for Cu-based OCs to prevent CuAl₂O₄ formation.

Several research gaps have been found as a result of the literature review. First, the problem is related to agglomeration due to relatively low melting point of Cu. Second, at high temperature the tendency of Cu to react with Al_2O_3 to form highly stable compound CuAl_2O_4 (do not take part in oxidation and reduction reaction) is very high. Third, to date the phase interaction in the combination of Cu with Pr-modified $\gamma\text{-Al}_2\text{O}_3$ and significance of these interactions in CLC have not been discussed in previous studies thus highlighting the novelty of current research. Furthermore, the influence of process parameters such as time and temperature on the oxygen transport capacity of OC was not studied significantly using design expert RSM in the literature. Therefore, it is necessary to synthesize a novel and promising OC for CLC process.

3.1 Materials and reagents

The nitrate precursors of copper (Cu), cobalt (Co), iron (Fe), and praseodymium (Pr) were used for the preparation of OCs. For each type of OC, gamma alumina (γ - Al_2O_3) was used support material. The details of all the material used for the synthesis of OC are given in Table 3.1.

Table 3.1: The specifications and details of material used for the preparation of oxygen carriers.

Material name	Purity	CAS No	Company
Gamma alumina γ - Al_2O_3	98 %	1344-28-1	Merck
Copper (II) nitrate trihydrate ($\text{Cu}(\text{NO}_3)_2 \cdot 3\text{H}_2\text{O}$)	≥ 99.5 %	10031-43-3	Merck
Cobalt (II) nitrate hexahydrate ($\text{Co}(\text{NO}_3)_2 \cdot 6\text{H}_2\text{O}$)	≥ 99 %	10026-22-9	Merck
Iron (III) nitrate nonahydrate ($\text{Fe}(\text{NO}_3)_3 \cdot 9\text{H}_2\text{O}$)	99 %	7782-61-8	Merck
Praseodymium (III) nitrate hexahydrate ($\text{Pr}(\text{NO}_3)_3 \cdot 6\text{H}_2\text{O}$)	99.9 %	15878-77-0	Sigma Aldrich
Lanthanum (III) nitrate hexahydrate ($\text{Ce}(\text{NO}_3)_3 \cdot 6\text{H}_2\text{O}$)	≥ 98 %	10277-43-7	Across

3.2 Preparation of monometallic OCs

The purpose of monometallic OCs is to determine the highest performance of OC based on iron-, cobalt-, and copper oxides. Three types of OCs such as 10 wt% Cu- γ - Al_2O_3 (10CuA), 10 wt% Co- γ - Al_2O_3 (10CoA) and 10 wt% Fe- γ - Al_2O_3 (10FeA) were prepared using wet impregnation method. For 10 g of OC, the first 3.80 g Cu nitrate was measured in a 500 mL size beaker for 10 wt% Cu loading. Then Cu nitrate solution was prepared by adding 100 mL of deionized (DI) water in Cu nitrate and mixed for 10

min. Similarly, the 9 g of support $\gamma\text{-Al}_2\text{O}_3$ was measured in a 500 mL size beaker and dissolved in 100 mL of DI water under continuous mixing for 10 min. After that the Cu nitrate precursor solution was added dropwise to $\gamma\text{-Al}_2\text{O}_3$ support under continuous stirring. The sample was allowed to mix for 4 h with stirring. The sample was dried in oven for 48 h at 100 °C. The dried sample was ground using porcelain mortar to make it granulate form. The sample was poured in crucible and calcined in the muffle furnace at 450 °C for 4 h to yield metal oxide (OC). All the steps were repeated for Co and Fe-based OCs to prepare 10CoA and 10FeA, respectively. For the preparation of promoters, the nitrate precursor of lanthanum and praseodymium were calcined for 4 h at 450 °C in muffle furnace. After calcination the samples were labeled as La-oxide and Pr-oxide. The schematic flow diagram for OCs preparation is shown in Fig. 3.2.

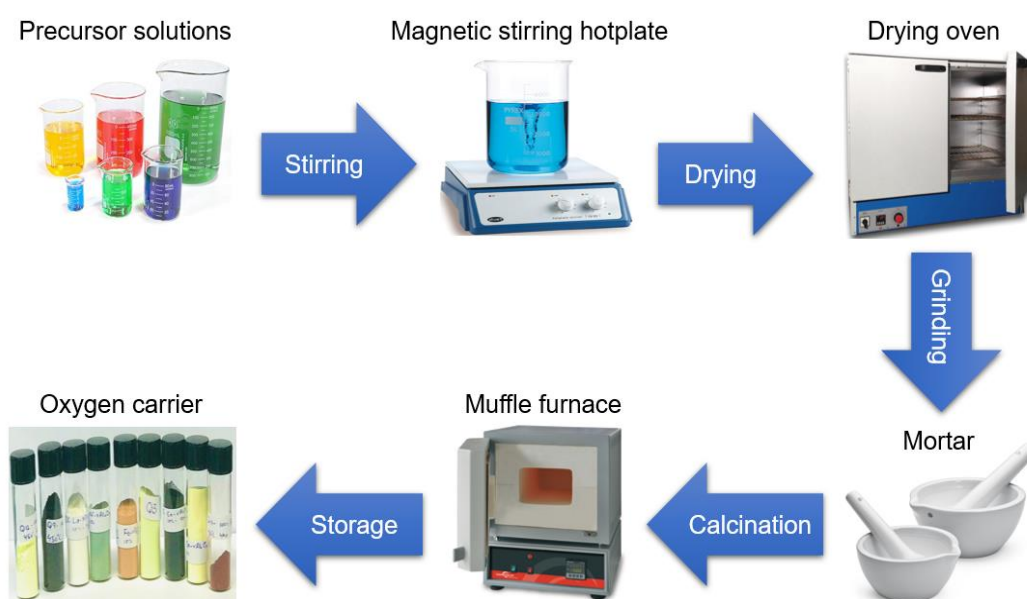


Figure 3.2: Schematic diagram of OCs synthesis by using wet impregnation method.

3.3 Preliminary screening of monometallic OCs

All monometallic OCs were tested for one redox cycle of the CLC process to identify the best single metal-based OC. For this purpose, thermogravimetric analysis (TGA) was used, and each OC (15 mg) was loaded onto a TGA pan that was heated in the furnace. First, the OC was heated from room temperature to 800 °C in the presence of N_2 gas with a heating rate of 50 °C/min. The N_2 gas valve was then closed, and the

sample (OC) was subjected to 5%CH₄/N₂ for 3 min with 80 mL/min flow rate to complete the reduction process. The oxidation reaction was carried out in the presence of air with a flow rate of 80 mL/min for 10 min. Between oxidation and reduction processes, the N₂ gas was purged for 3 min to prevent mixing of methane gas and air. For each monometallic OC, one complete redox cycle was obtained. The redox cycles of all monometallic OCs were analyzed, to choose the best candidate based on OTC and the time it took for the OC to reduce and oxidize. Based on this comparison, Cu-based monometallic was selected for bimetallic OC. The purpose of bimetallic OC is to enhance the OC properties such as OTC, reactivity and stability using an efficient promoter.

3.4 Preparation of bi-metallic OC

Cu-based OCs and praseodymium metal (promoter) were chosen after the preliminary screening of monometallic OCs. The bimetallic OC called 10 wt% Cu-5 wt% Pr- γ -Al₂O₃ (10CuPA) was synthesized using the wet impregnation method. The total amount of 10 g for the OC was prepared. First of all, the support γ -Al₂O₃ was modified with praseodymium (Pr). In a 500 mL beaker, the first 5 wt% of the known quantity of Pr nitrate was utilized for 10 g of OC. Then Pr-nitrate precursor solution was prepared by adding 100 mL of DI water in Pr nitrate and mixed for 10 min. Similarly, the 8.5 g of support γ -Al₂O₃ was measured in 500 mL beaker and dissolved in 100 mL of DI water with continues mixing for 10 min. After that the Pr nitrate precursor solution was added drop by drop to γ -Al₂O₃ support under continues stirring. The sample was allowed to mix for 4 h with stirring. The sample was dried in oven for 48 h at 100 °C. The dried sample was grinded using porcelain mortar to make it granulate form. The granulate sample was poured in crucible and calcined in the muffle furnace at 450 °C for 4 h to get 5 wt% Pr- γ -Al₂O₃. The required amount (10 wt%) of Cu nitrate was measured in 500 mL beaker and 100 mL of DI water was added to prepare Cu nitrate precursor solution. This solution was added in 5wt%Pr- γ -Al₂O₃ drop by drop to for 10 wt% Cu-5 wt% Pr- γ -Al₂O₃. The initial volume of the precursor solution was 200 mL and mixed continuously for 4 h. Then same steps were repeated for drying and calcination. Finally, the sample was labeled as (10CuPA) OC. The same

synthesis steps were repeated for the preparation of 20 wt% Cu-5 wt% Pr- γ -Al₂O₃ and the OC was labeled as 20CuPA OC. The Cu-metal loading was maximized to 20 wt% Cu. It was well reported in the literature that the maximum OTC of Cu-based OC can be achieved with increase in Cu loading but more than 20 wt% of Cu caused agglomeration [32].

3.5 Preliminary screening of bimetallic OCs

TGA was used to test and compare both types of OCs, such as 10CuPA and 20CuPA during 10 redox cycles. Based on the OTCs of both OCs, the OC with the greater OTC was chosen for the process of optimization. 15 mg of each OC sample was used in TGA, and both the oxidation and reduction reactions were carried out at 800 °C temperature. The reduction process of the OC was occurred in the presence of 5% CH₄/N₂ (3 min) while oxidation reaction was carried out in the presence of air (10 min). To avoid mixing of methane and air gases, nitrogen gas was purged for 3 min in each redox cycle. The flow chart for the screening of OCs is shown in Fig. 3.3.

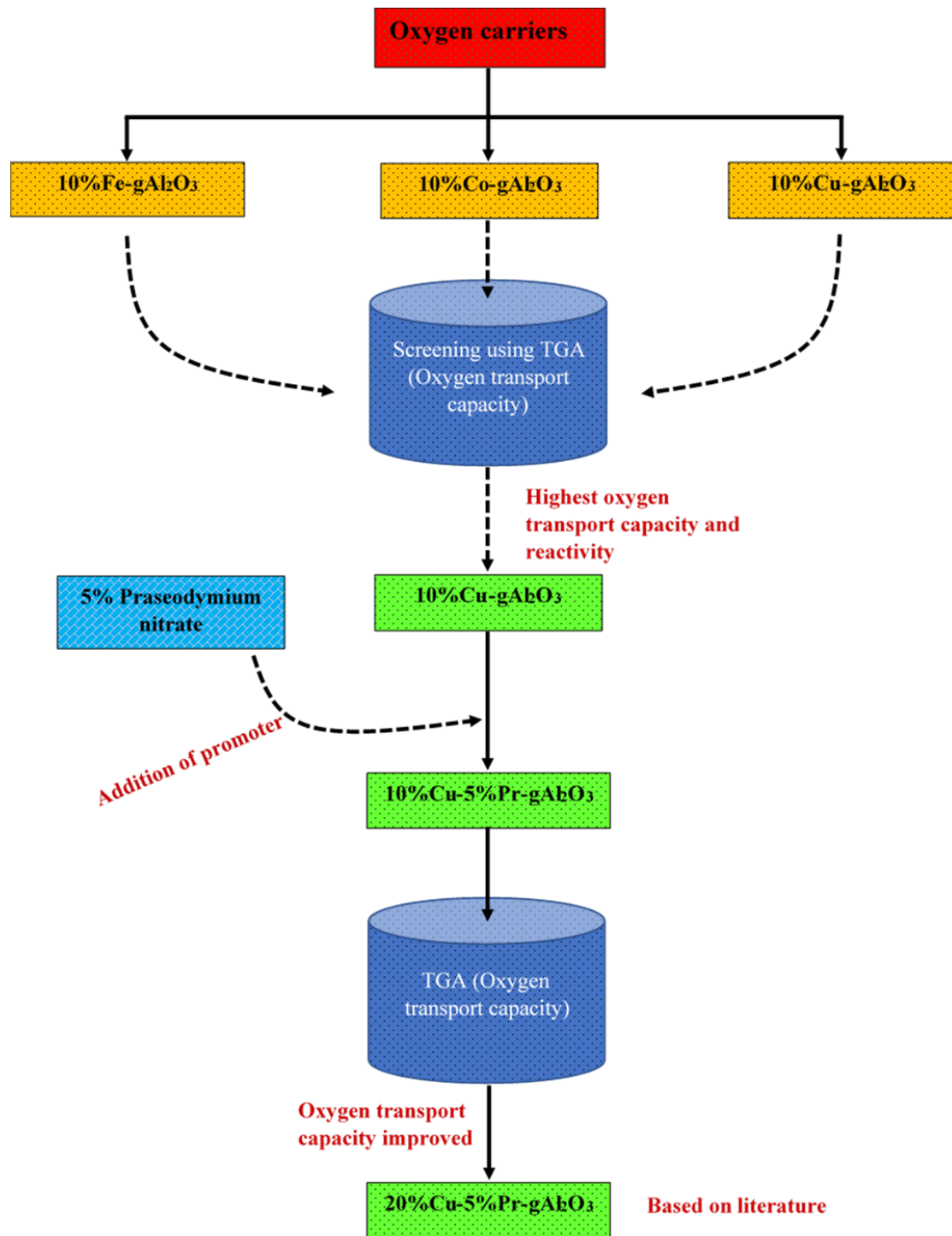


Figure 3.3: The flow diagram of screening for the best monometallic and bimetallic oxygen carriers.

3.6 Characterization of oxygen carriers

Due to the importance of the chemical, physical and morphological properties of OCs, the characterization of synthesized OCs are required for the best efficiency in CLC process. The bulk and surface properties of OCs have significant effect on the OTC of OCs during multiple redox properties. The information from different types of characterizations will help to improve the performance of OCs in CLC process. In the present study, the synthesized OCs were characterized by Field Emission Scanning Electron Microscope (FESEM), Energy Dispersive X-Ray Analysis (EDX), X-ray Diffraction (XRD) and Temperature Programmed Reduction (TPR) analysis. The description of equipment name and model used for the characterization is given in Table 3.2.

Table 3.2: The details of equipment used during characterization.

Equipment	Model	Function
Field Emission Scanning Electron Microscope (FESEM) FESEM	Zeiss Supra 55 VP	To study the surface morphology.
Energy Dispersive X-ray (EDX) Spectroscopy	Zeiss Supra 55 VP	To examine the chemical composition.
X-ray Diffraction (XRD)	Bruker D8 Advanced Diffractometer	To analyze the crystal phases
Temperature Programmed Reduction (TPR)	TPDRO100	To investigate the reduction properties of OCs

3.6.1 Surface morphology

The surface morphology of the calcined OCs was analyzed using Zeiss Supra 55 VP model field emission scanning electron microscope (FESEM). The elemental analysis or chemical composition of OCs were investigated using energy dispersive X-ray spectroscopy (EDX) with mapping. The samples of OC were spread over the copper stub along with 2 min gold film coating.

3.6.2 X-ray diffraction

The crystalline phases of synthesized OCs were examined with XRD (Bruker D8 Advance) by using Cu K α radiations over the range of with 40 kV voltage, 40 mA current and scanned from 10° to 100° for 2 θ angular domain with step size of 2°/min. The identification of generated diffraction patterns for CuO, CuAl₂O₄, and CuAlO₂ was examined using Diffraction (MAUD) software.

3.6.3 Temperature programmed reduction

TPR test was conducted using TPDRO100 equipped with a thermal conductivity detector (TCD). For TPR analysis, approximately 0.10 g sample was loaded into a reactor situated inside furnace and processed with nitrogen gas for 60 min at 200 °C. After degassing, the gas flow was switched to 5% H₂/N₂ at a rate of 30 mL/min and pre-treated at 200 °C for 1 h.

3.7 CLC experiments

The performance of prepared OCs was examined using Thermogravimetric Analysis (TGA-TA model Q50). The oxygen carriers were screened using the identical CLC setup, but the operating parameters, such as gas flowrate and the number of cycles, were distinct from those used to determine the final oxygen carrier CLC results. For each type of OC, 15 mg of sample was placed in the platinum pan. Platinum pan was hanged in the furnace of TGA by the hang down wire. The furnace of TGA was closed and the furnace was heated with heating rate of 50 °C/min up to 800 °C temperature value. The heating of sample was done in the presence of nitrogen gas with flowrate of 20 mL/min. The temperature in the furnace was equilibrated at 800 °C. Then, methane gas (5% CH₄/N₂) was streamed with flowrate of 80 mL/min for 3 min at same temperature (800 °C). Air was used as an oxidizing gas with flowrate of 80 mL/min for 10 min at 800 °C. Between methane gas and air, nitrogen gas was purged for 3 min to avoid mixing between methane and air. Total 10 number of redox cycles were performed for the selection of best metal-based OC. The schematic diagram for the CLC process using TGA is shown in Fig. 3.4.

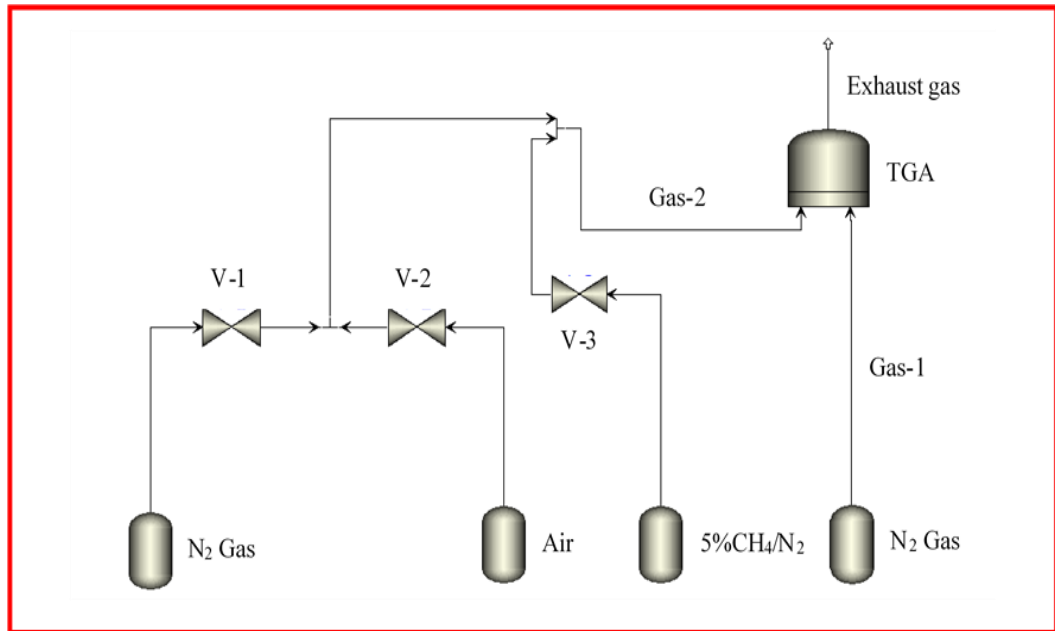


Figure 3.4: The setup for chemical looping combustion process using TGA.

Oxygen ratio can be calculated by using this formula, $R_o = (m_o - m_r) / m_o$. Where m_o is referred to the mass of OC when it is fully oxidized and m_r is mass of OC when it is fully reduced in the redox cycle. R_o means the maximum amount of oxygen that can be delivered from air to fuel reactor for a given mass flow of recirculating particles. The R_o of metal-based OC can be measured by using TGA where changes of weight are obtained as a function of temperature. The mass conversion formula ($\omega = m/m_o$, where m is mass of OC at any time and m_o is mass of OC when it is fully oxidized) can be used to evaluate the rate of oxidation and reduction over several redox cycles.

3.8 Design of experiments and statistical analysis

A statistical approach was carried out for the design of experiment with the help of Response Surface Methodology (RSM) using Central Composite Design (CCD) and Design-Expert Version 12[®] software for CLC of methane gas. RSM is a well-known approach for analyzing a number of tests and then interpreting the results using ANOVA analysis. ANOVA analysis can be used to determine if single or combined influences of process variables have a greater or lesser impact on one or more than one

response. A polynomial model equation presents a statistical correlation between variables and responses such as follow:

$$y = \beta_0 + \beta_1x_1 + \beta_2x_2 + \beta_{12}x_1x_2 + \beta_1x_1^2 + \beta_2x_2^2$$

where y is the predicted response, β_0 is an intercept, β_1x_1 and β_2x_2 values are the linear effects, $\beta_{12}x_1x_2$ value is the interaction effect, $\beta_1x_1^2$ and $\beta_2x_2^2$ values are the quadratic effects, x_1 and x_2 refer to time and temperature, respectively [144]. The relationship between the input variables and output variables can be developed using this methodology. The generated surface facilitates in the drawing of desired information with fewer or more experiments [145]. In the present study, two operating variables, time (A) and temperature (B) are selected to investigate their influences on response variable OTC. The ranges of 1-3 min and 800-900 °C for time and temperature were used, respectively. These ranges were taken on the basis of previous reported research work and experimental results [19, 25, 26, 31, 99, 114, 146, 147]. Table 3.3 gives the ranges, parameters, factors and levels for time and temperature.

Table 3.3: Range for the operating parameters for designing the experiment array.

Code	Factor	- α	-1	0	+1	+ α
A	Time, min	0.58	1	2	3	3.41
B	Temperature, °C	768.93	800	875	950	981.06

By using CCD, quadratic relations between the process parameters are generated. Total 13 experiment runs were generated by CCD. The total number of experimental runs for the two process variables with actual predicted OTC (response) is given in Table 3.4. The effect of process variables on the response either higher or lower impact was studied with the help of ANOVA analysis. Three types of tests were executed to examine the importance and validity of designed model: a) F and P values of process variables or by perturbation graph, b) R^2 value (adjusted and predicted), c) lack of fit value.

Table 3.4: Experimental design for actual and predicted results.

Run	Process parameters		Response	
	Time (A), min	Temperature (B), °C	Actual	Predicted
1	2	875	0.0540	0.0537
2	0.58	875	0.0360	0.0368
3	3.41	875	0.0523	0.0518
4	2	875	0.0539	0.0537
5	3	950	0.0518	0.0525
6	2	768.93	0.0543	0.0522
7	2	875	0.0535	0.0537
8	1	950	0.0390	0.0388
9	2	981.06	0.0490	0.0484
10	2	875	0.0530	0.0537
11	2	875	0.0543	0.0537
12	3	800	0.0546	0.0542
13	1	800	0.0480	0.0467

CHAPTER 4

RESULTS AND DISCUSSION

The overall investigations and findings of the current study are addressed in this chapter. The selection for the best metal oxide-based OC using redox cycles in TGA were analyzed in section 4.1. The effect of addition of promoter on the properties such as surface morphology, crystal phase, reduction behavior and OTC of Cu-based OC was studied in section 4.2. Furthermore, the effect and optimization of process parameters such as, time and temperature on OTC using perturbation graph and 3D response surface plot have been discussed in section 4.3 and section 4.4.

4.1 Redox cycle for the preliminary screening of OCs

The screening for the best type of OCs was conducted using TGA. All three types of OCs i.e 10CuA, 10CoA and 10FeA were investigated in one redox cycle of CLC process. The selection for the best performance-based OC was achieved based on the OTC and time was taken by OCs to release and adsorb oxygen. The comparison among the 1st redox cycles of all three types of OCs is shown in Fig. 4.1. The change in weight of OCs against time was observed. During first 40 min, the weight of OCs was decreased uniformly to some extent when temperature was increased from 0 °C to 800 °C under nitrogen atmosphere. This change in weight was occurred due to the removal of water vapors from the samples.

At 800 °C when the sample was exposed to 5% CH₄/N₂ gas for 3 min, the weight of OC was decreased due to the removal of oxygen from OC for the combustion of fuel gas (Fig. 4.1). When nitrogen gas was purged to clean the furnace of TGA from fuel gas, the weight of OCs was remained constant except for 10CoA sample. When air was introduced for 10 min, all the OCs were started oxidizing and hence the weight was increased due to oxygen adsorption. All the three types of OCs were completely regenerated. The OTCs of both 10CoA and 10CuA were 0.026 mg of O₂/mg of OC and for 10FeA it was 0.018 mg of O₂/mg of OC. The time taken by 10FeA based OC for

the complete reduction process was 5.42 min, while for 10CoA and 10CuA OCs were 5.1 min and 1 min, respectively. Therefore, both the reaction rate and OTC value for 10FeA-based OC were lower. Although the OTCs for 10CoA and 10CuA are similar but the oxidation and reduction processes for 10CuA-based OC were rapid. Therefore, 10CuA-OC was selected for further investigations. There are graphs in that show how the weight of OCs changes with temperature in TGA profiles (Appendix A).

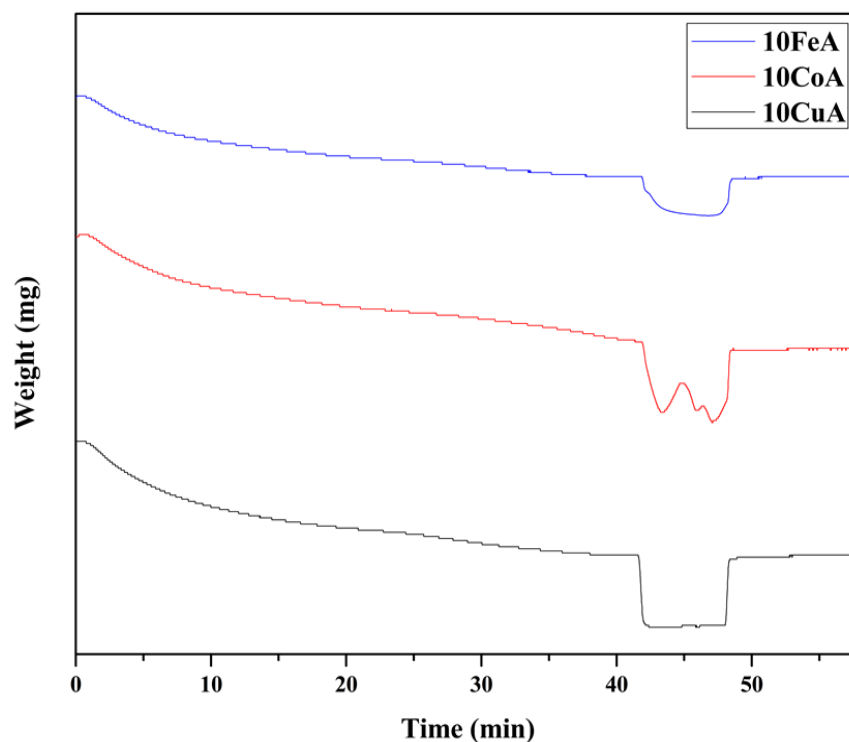


Figure 4.1: TGA profile for 10CuA, 10 CoA and 10FeA OCs using air as an oxidizing gas and 5% CH₄/N₂ at 800 °C.

Fig. 4.2 shows the comparison between Pr-oxide and La-oxide OCs during 1st redox cycles. The reactivity of La-oxide OC with methane gas for the reduction process and with air for the oxidation process was 0.002 mg of O₂/mg of OC. However, Pr-oxide showed high reactivity (completely reduced in 1 min as shown in Fig. 4.2) and OTC of 0.021 mg of O₂/mg of OC in complete redox cycle during CLC process. The Pr-oxide successfully regenerated after completion of one cycle and hence can be used as promoter for Cu-based OC as compared to La-oxide.

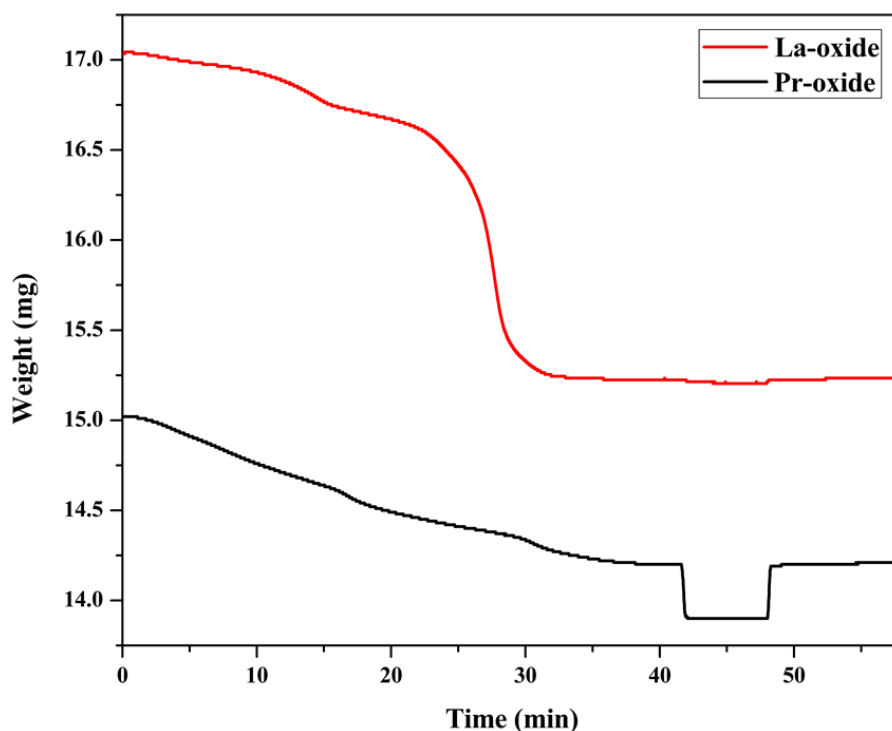


Figure 4.2: TGA profiles for one redox cycle of Pr-oxide and La-oxide based OCs using 5% CH₄/N₂ gas at 800 °C.

4.2 Effect of addition of promoter (Pr-oxide) on 10CuA oxygen carrier

For the comparison purpose, the physiochemical properties of 10CuA based OC was compared with 10CuPA based OC.

4.2.1 FESEM analysis

The surface morphologies of fresh and used OCs based on 10CuA and 10CuPA were examined using FESEM analysis. Fig. 4.3(a and b) shows the FESEM images of 10CuA-fresh (calcined) and used (in 10 oxidation reduction cycles) OCs, respectively. For both fresh and used 10CuA-based OCs, irregular shapes of the particles were observed. It can be noticed that the particle size of 10CuA after usage in 10 redox cycles was increased as shown in Fig. 4.3(b). The FESEM images of 10CuPA-fresh (calcined) and after 10 cycles, are shown in Fig. 4.3(c and d). However, after use in CLC redox

cycles, the average particle size of 10CuPA-based OC was decreased. Furthermore, an irregular shape of 10CuPA-based OC particles was examined.

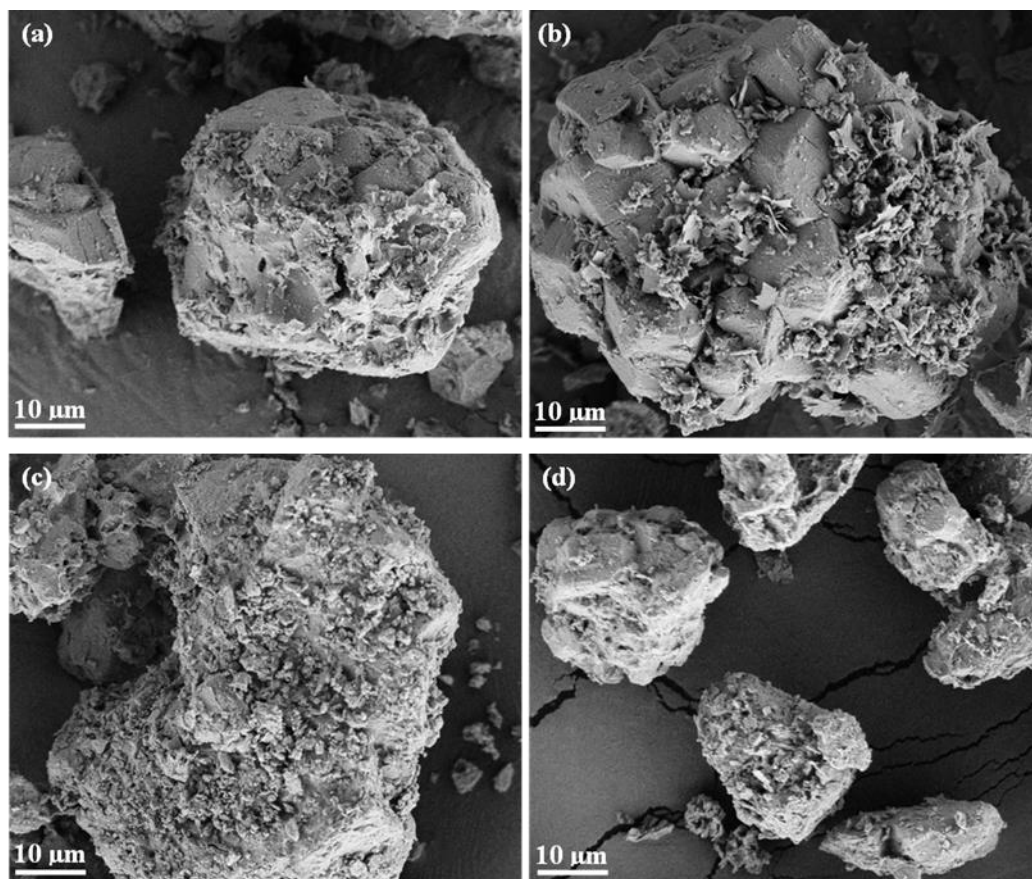


Figure 4.3: SEM images of 10CuA fresh (a) & after 10 cycles (b) and 10CuPA fresh (c) & after 10 cycles (d).

Overall, no significant difference in the surface morphologies of 10CuA and 10CuPA-based OCs was observed. Furthermore, some agglomeration was detected in the morphology of both types of OCs. The energy dispersive X-ray spectroscopy results for the composition of 10CuA, 10CuPA, and 20CuPA-based OCs are shown in Table 4.1.

Table 4.1: Elemental compositions of 10CuA,10CuPA, and 20CuPA-based oxygen carriers.

Oxygen carriers	Cu-contents (wt%)		Pr-contents (wt%)		$\gamma\text{Al}_2\text{O}_3$ (wt%)	
	Theoretical	Actual	Theoretical	Actual	Theoretical	Actual
10CuA -Fresh	10	7.5	-	-	90	92.5
10CuA-used	10	21.3	-	-	90	78.6
10CuPA-fresh)	10	7.9	5	4.3	85	87.7
10CuPA-used	10	16.4	5	6.7	85	76.7
20CuPA-fresh	20	19.9	5	9.8	75	70.2
20CuPA-used	20	26.1	5	7.3	75	66.7

The energy dispersive X-ray spectroscopy analyses showed that the Cu-contents were increased from 7.5 wt% to 21.3 wt% for 10CuA-fresh and 10CuA-used, respectively. Which indicated, the accumulation of copper contents in a specific particle associated with presence of agglomeration. However, the copper contents were increased from 7.9 wt% to 16.4 wt% for 10CuPA-fresh and 10CuPA-used, respectively. These results showed that the copper contents for 10CuPA-used are more stable as compared to the copper contents for 10CuA-used.

4.2.2 X-Ray diffraction analysis

For the crystal structure determination, XRD analysis was executed as shown in Table 4.2. The XRD findings of 10CuA and 10CuPA-based OCs for fresh (after calcination) and used (after 10 complete redox cycles) are shown in Fig. 4.4. The diffraction peaks associated to CuO at 2θ angle of 32° , 35° , 39° , 46° , 49° , 53° , 58° , 61° , 66° , 72° and 75° were observed [146]. Surprisingly, the peaks corresponding to CuAl_2O_4 at 2θ angle of 31° , 37° and 45° were also observed [148]. The peak at 2θ angle of 31° also referred to CuAlO_2 [146, 148]. For both 10CuA-fresh and 10CuPA-fresh OCs, only peaks corresponding to CuO crystal phase were observed. However, the peaks related to CuAl_2O_4 were not detected. Similar XRD results were reported in the previous studies for Cu-based OC when calcination temperature of lower than 600°C was used [148]. However, the peaks intensity of the CuO crystal phase for 10CuA-fresh were higher compared to 10CuPA-fresh. In contrast to this, the peaks intensity referred to CuO at 2θ angles of 35° , 39° , 46° and 66° for 10CuA-used OC were decreased compared to 10CuPA-used OC. Similarly, peaks for 10CuA-used associated with the CuO phase at 2θ angles of 32° , 49° , 53° , 58° , 61° , 72° and 75° were completely disappeared in comparison to 10CuPA-used. This might be due to the modification of gamma-alumina support with praseodymium metal oxide in 10CuPA-used OC stabilized the CuO contents.

Table 4.2: The 2θ angles corresponding to different crystal phases of 10CuA and 10CuPA oxygen carriers.

Oxygen carrier	Crystal phase	2θ angles
10CuA-Fresh	CuO	$32^\circ, 35^\circ, 39^\circ, 46^\circ, 49^\circ, 53^\circ, 58^\circ, 61^\circ, 66^\circ, 72^\circ$ and 75°
	CuAl ₂ O ₄	NA
	CuAlO ₂	NA
10CuA-Used	CuO	$35^\circ, 39^\circ, 46^\circ$ and 66°
	CuAl ₂ O ₄	$31^\circ, 37^\circ$ and 45°
	CuAlO ₂	31°
10CuPA-Fresh	CuO	$32^\circ, 35^\circ, 39^\circ, 46^\circ, 49^\circ, 53^\circ, 58^\circ, 61^\circ, 66^\circ, 72^\circ$ and 75°
	CuAl ₂ O ₄	NA
	CuAlO ₂	NA
10CuPA-Used	CuO	$32^\circ, 35^\circ, 39^\circ, 46^\circ, 49^\circ, 53^\circ, 58^\circ, 61^\circ, 66^\circ, 72^\circ$ and 75°
	CuAl ₂ O ₄	$31^\circ, 37^\circ$ and 45°
	CuAlO ₂	31°

For both 10CuA-used and 10CuPA-used OCs, CuAl_2O_4 and CuAlO_2 crystal phases were detected because the temperature throughout oxidation-reduction cycles was greater than $600\text{ }^\circ\text{C}$. However, the peak intensity corresponding to CuAl_2O_4 at a 2θ angle of 37° for 10CuPA-used was lower than 10CuA-used OC. For both types of OCs i.e 10CuA-used and 10CuPA-used, the peak related to CuAlO_2 was relatively small and existed at same 2θ angle (31°) for CuAl_2O_4 . This indicated that the formation of CuAlO_2 was relatively low or negligible.

This strongly suggests that the presence of praseodymium metal oxide reduced the formation of spinel compounds and enhanced the stability of active metal oxide (CuO). A similar effect was noticed in previous research work; when the contact of active metal with support was minimized, the XRD peaks corresponding to spinel compound were also decreased [149]. Hence, the addition of praseodymium to Cu-based OC significantly increased the stability of OC in terms of uniform distribution of CuO and by lowering the formation of spinel compound (CuAl_2O_4).

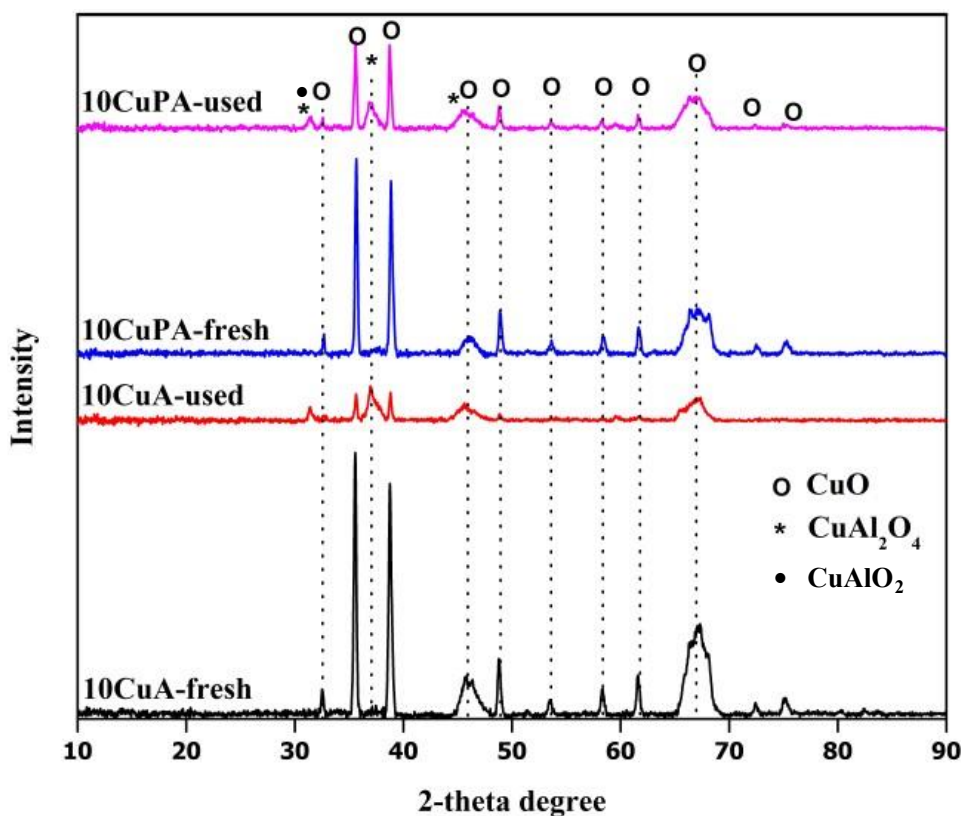


Figure 4.4: XRD analysis for the fresh and used with and without praseodymium OCs (10CuPA and 10CuA).

4.2.3 Temperature programmed reduction analysis

The reduction properties of with or without praseodymium promoted Cu-based OCs, TPR analysis was performed as shown in Fig. 4.5. The TPR profiles could be decomposed into four different curves at $\alpha = 270-300$ °C, $\beta = 390-410$ °C, $\gamma = 450-460$ °C and $\delta = 800-830$ °C. Usually, it is known that the peaks at α and β attributed to the reduction of well dispersed CuO and bulk CuO which are reduced through $\text{CuO} \rightarrow \text{Cu}$, respectively [146, 148]. However, the peaks in the range γ contributed to CuAl_2O_4 due to $\text{CuO} + \text{Al}_2\text{O}_3 \rightarrow \text{CuAl}_2\text{O}_4$ and peaks at δ associated with the reduction of CuAlO_2 [146]. At high temperature heating of CuAl_2O_4 results to the formation of CuAlO_2 [150]. The reduction reaction for the spinel compound is very slow as compared to the CuO. There are two possible redox reactions could be resulted for the formation of CuAlO_2 at temperature near to 900 °C. The first one is $4\text{CuAl}_2\text{O}_4(\text{s}) \rightarrow 4\text{CuAlO}_2(\text{s}) + 2\text{Al}_2\text{O}_3(\text{s}) + \text{O}_2(\text{g})$ and second due to the presence of excess contents of CuO i.e. $2\text{CuAl}_2\text{O}_4(\text{s}) + 2\text{CuO}(\text{s}) \rightarrow 4\text{CuAlO}_2(\text{s}) + \text{O}_2(\text{g})$ [151]. However, there is no other peaks were found above 410 °C for both 10CuA-fresh and 10CuPA-fresh owing to absence of any spinel formation. From XRD results, it is obvious that CuAl_2O_4 was not formed after calcination, perhaps due to the low calcination temperature. The peaks intensity corresponding to γ and δ for 10CuPA-used OC were lower than as compared to peaks for 10CuA-used OC. This shows that higher consumption of H_2 in 10CuA-used OC due to significant formation of spinel compound as compared to Pr-promoted, Cu-based OC. Similar results were found in XRD analysis, the addition of praseodymium reduced the formation of spinel compound.

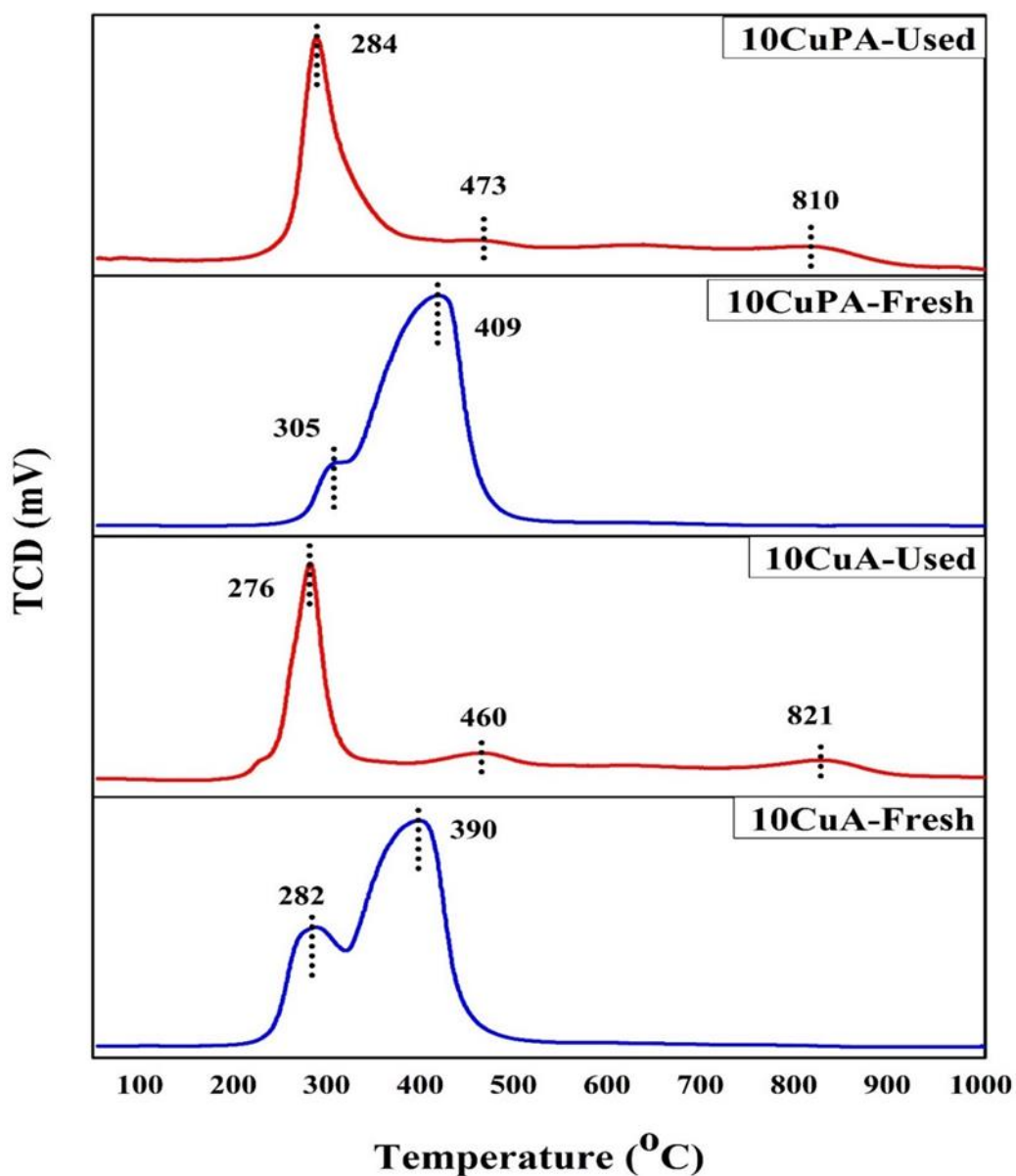


Figure 4.5: TPR profile 10CuA and 10CuPA fresh and used (10 cycles) oxygen carriers.

4.2.4 Thermogravimetric analysis for CLC process

The performance of 10CuA and 10CuPA OCs in CLC process was investigated using TGA. The TGA profiles for 10 continuous oxidation and reduction cycles using air and 5% CH_4/N_2 are shown in Fig. 4.6. The oxygen transport capacity of 0.024 (mg of O_2 / mg of OC) was achieved for 10CuA-based OC after 10 redox cycles. In contrast, the oxygen transport capacity of 0.026 (mg of O_2 / mg of OC) was attained for 10CuPA-

based OC during 10 redox cycles. It was concluded that due to the addition of praseodymium oxide in 10CuA oxygen carrier, the oxygen transport capacity was increased by 0.2 wt%. The OTC, 0.026 mg of O₂/mg of OC of 10CuPA in this study is remarkably improved compared with OTC of 10wt%Cu- γ -Al₂O₃ [142, 146, 152]. Furthermore, the reactivity of 10CuPA in oxidation and reduction reactions was uniform and smooth compared to 10CuA.

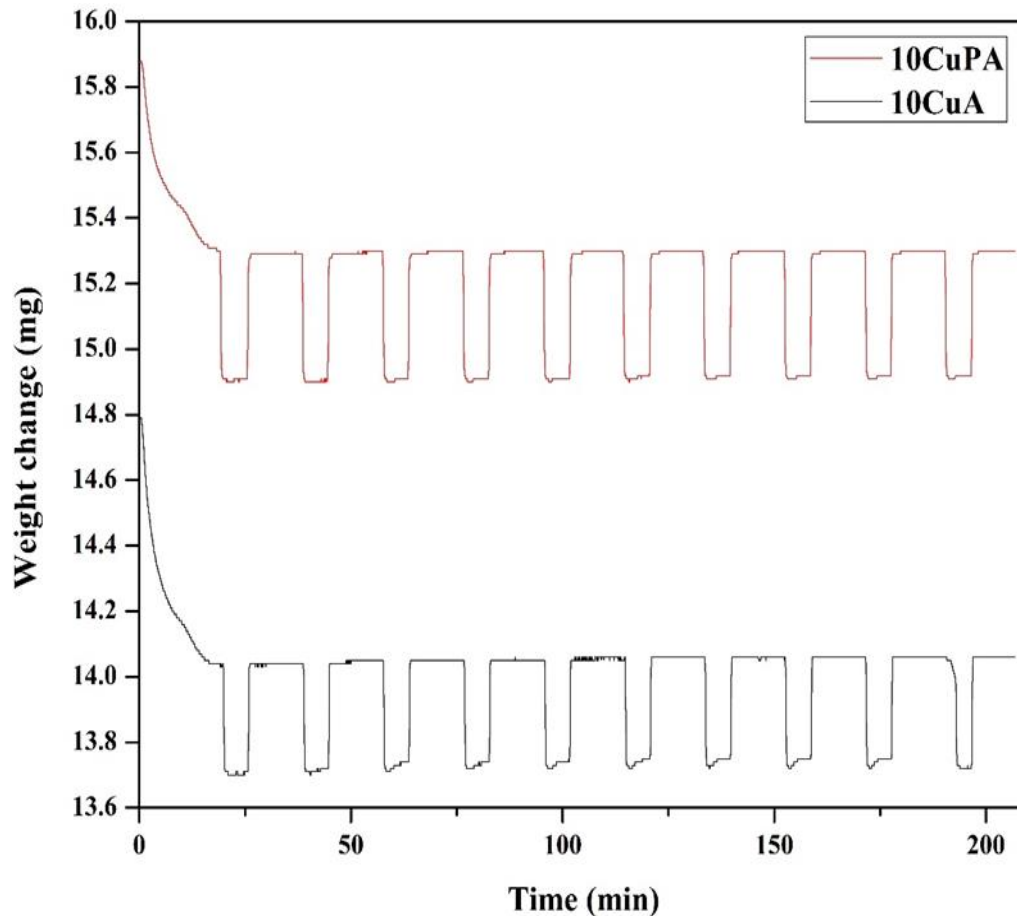


Figure 4.6: TGA profile for 10CuA and 10CuPA OCs during 10 redox cycles in CLC process.

The mass-based conversion profile of 10CuPA-OC during 10 redox cycles in CLC process using TGA in the presence of 5% CH₄/N₂ (reducing gas) and air (oxidizing gas) is presented in Fig. 4.7. As a result of the reduction in the first cycle, a relatively rapid shift in mass reduction was seen for the first 0.38 minutes, followed by a nearly linear mass loss for the next 0.21 minutes. The complete reduction achieved in 1.5 min. In the beginning the fast decrease of weight could be attributed to reduction reaction activated.

In the second cycle, the slope at the beginning of the reduction process developed in the same way as in the first cycle. The mass decrease for the third cycle during first 0.38 min was the slowest but in next 0.67 min the fastest mass decrease as was observed compared to first and second cycles. As the cycles progressed, the linear slope between 0.38 and 0.21 minutes remained nearly constant but slowing after the 10th cycle relative to the first. Overall time taken for the complete reduction process was about 0.8 min over all cycles. Despite with increasing number of redox cycles no significant change in OTC was observed. During oxidation process using air as an oxidizing gas, the mass of the OC was considerably increased in 0.5 min for all cycles. The slowest rate of oxidizing was noticed in second cycle. However, the time needed to achieve full oxidation was almost 0.65 min, which was substantially faster than reduction and remained constant as the number of cycles increased.

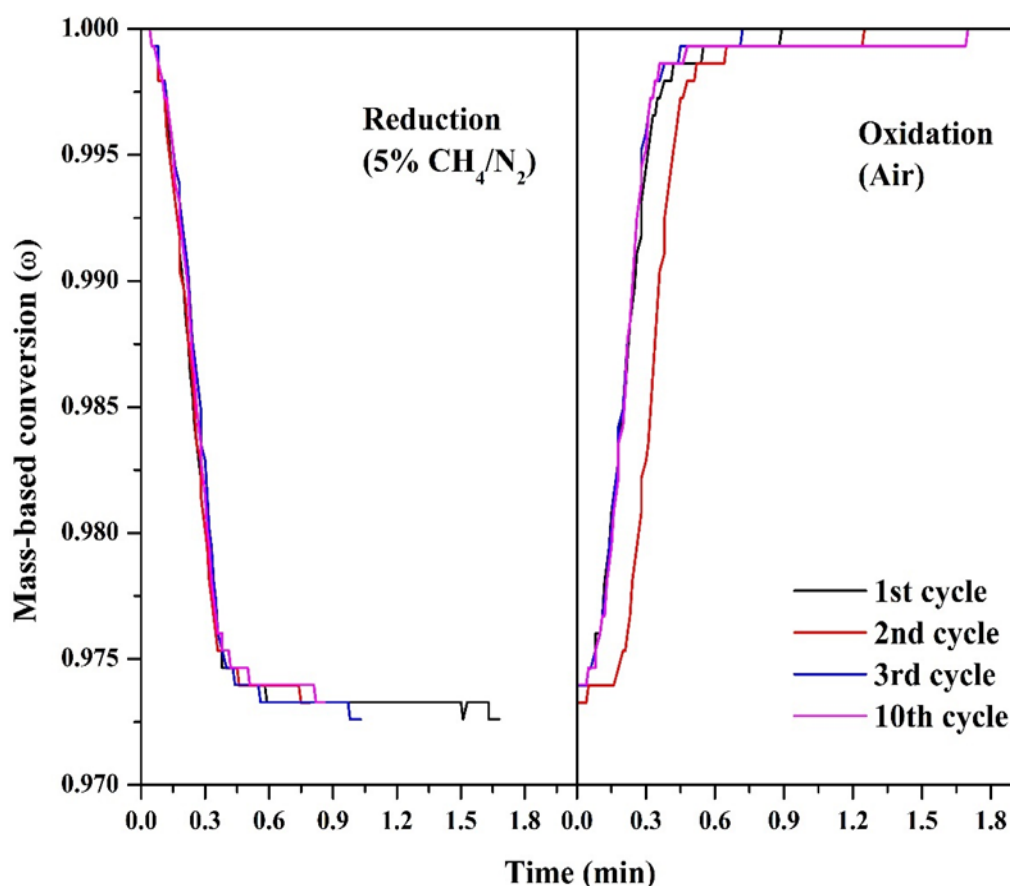


Figure 4.7: TGA profile at 800 °C for mass-based conversion of 10CuPA-OC measured using 5% CH₄/N₂ reducing gas (left) and air oxidizing gas (right).

In conclusion, 10CuPA-based OC showed better results as compared to 10CuA-based OC confirmed by XRD, TPR and TGA findings.

The TGA profile comparison for 10 redox cycles of 10CuPA and 20CuPA based OCs is shown in Fig. 4.8. The OTCs for 10CuPA and 20CuPA was 0.026 mg of O₂/mg of OC and 0.054 mg of O₂/mg of OC, respectively. It can be assumed that with increasing Cu-loading the OTC of the OC also increased. Similar findings have been reported in prior investigations, which found that as Cu contents increased, the fuel's conversion rate increased as well [153].

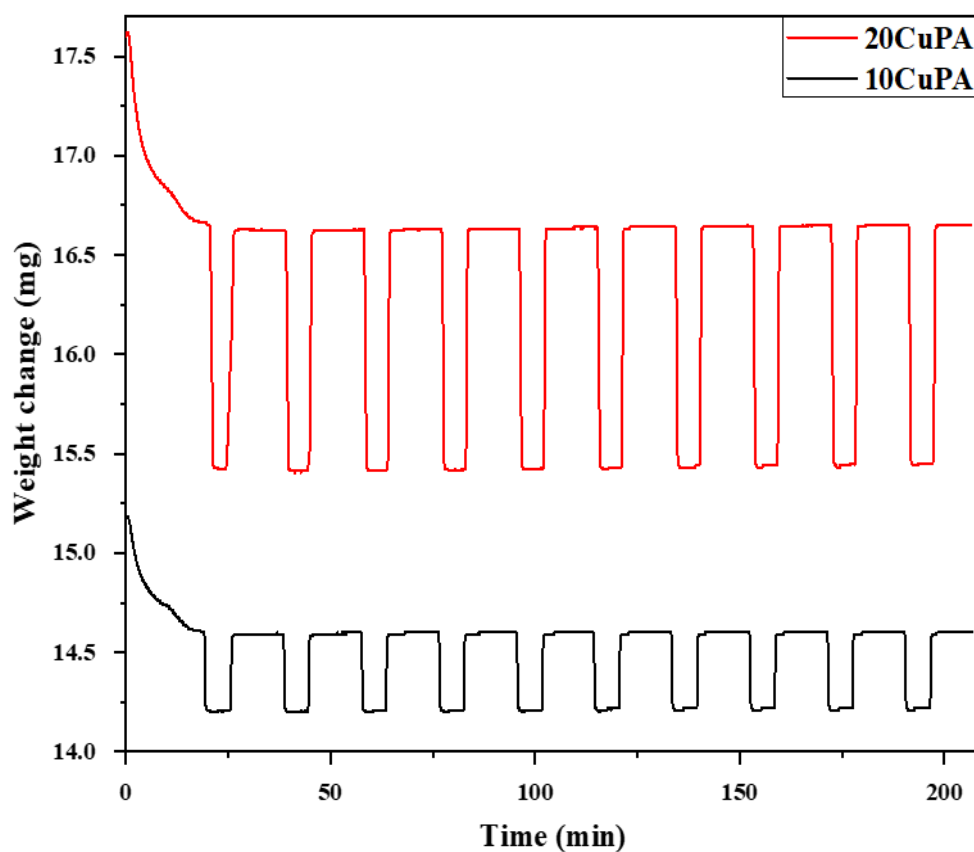


Figure 4.8: TGA comparison between 10CuPA and 20CuPA-based OCs at 800 °C and 3 min reduction time using 5% CH₄ (reducing gas) and air (oxidizing gas).

In Table 4.3, the study's contribution has been highlighted by contrasting the OTC of the OC synthesized in the current study with the OC developed in the literature.

Table 4.3: The oxygen transport capacity of past studies compared with present study of oxygen carrier for CLC.

Type of oxygen carrier	Copper loading (wt%)	Promoter (wt%)	Support	Oxygen transport capacity (wt%)	Reference
Cu-MgAl	12.0	27	MgAl ₂ O ₄	2.4	[146]
Cu-NiAl	12.8	3	Al ₂ O ₃	2.5	[146]
Cu10Al	10.0	-	Al ₂ O ₃	2.0	[142]
Fe45Al	45.0	-	Al ₂ O ₃	1.3	[142]
10CuPA	7.9	4.3	Al ₂ O ₃	2.6	Present study
20CuPA	19.9	9.8	Al ₂ O ₃	5.4	Present study

Therefore, for the optimization of oxygen transport capacity, praseodymium modified support-based (20CuPA) OC was selected as a potential candidate. The OTC of an OC highly depends on the metal loading from active site, time, and temperature. The maximum Cu-metal loading was selected based on previous literature. Several studies have been conducted on Cu-based OC for CLC process. The researchers found that OCs with Cu-contents greater than 20 wt% always agglomerated [32, 154]. Based on previous reported studies, the optimum copper metal loading for the OC was determined to be 20 wt%. Therefore, 20CuPA-based OC was used to optimize the process parameters such as time and temperature using RSM.

4.3 Statistical analysis of process parameters

For the statistical analysis, the effect of process parameters (time and temperature) on the output variable (OTC) was investigated using regression analysis. The ANOVA results was used to generate coded quadratic equation that describes the effect of independent variables (process parameters) on the dependent variable (OTC), as presented in Equation (4.1):

$$\text{Oxygen transport capacity} = 0.0537 + 0.0053A - 0.0024B - 0.0016AB - 0.0047A^2 - 0.0009B^2 \quad (4.1)$$

Where, A= Time and B= Temperature.

For given levels of each element, the equation in terms of coded factors can be used to make predictions about the OTC. The high levels of the factors are coded as +1 and the low levels of the factors are coded as -1 by design. By analyzing the factor coefficients, the coded equation can be used to determine the relative impact of the components. As indicated in Table 4.4, an ANOVA was used to assess the relevance of the model and variables for OTC.

Table 4.4: ANOVA results for oxygen transport capacity of oxygen carrier.

Source	Sum of Squares	df	Mean Square	F-value	p-value	
Model	0.0004	5	0.0001	112.69	< 0.0001	significant
A-Time	0.0002	1	0.0002	292.01	< 0.0001	
B-Temperature	0.0000	1	0.0000	60.33	0.0001	
AB	9.61×10^{-6}	1	9.6×10^{-6}	12.46	0.0096	
A ²	0.0002	1	0.0002	197.72	< 0.0001	
B ²	6.04×10^{-6}	1	6.04×10^{-6}	7.84	0.0265	
Residual	5.4×10^{-6}	7	7.71×10^{-7}			
Lack of Fit	4.38×10^{-6}	3	1.46×10^{-6}	5.78	0.0616	not significant
Pure Error	1.01×10^{-6}	4	2.53×10^{-7}			
Cor Total	0.0004	12				

$R^2 = 0.9877$; Adjusted $R^2 = 0.9790$; Predicted $R^2 = 0.9255$; Adequate Precision = 30.86

The ANOVA results showed that the predicted and experimental data for OTC were extremely close. Different design criteria like p values, R^2 , adjusted R^2 , and F values were used to ensure the effectiveness and validity of the proposed model. The predicted model's p values were less than 0.0001, indicating that the model is valid. The model terms were noteworthy if the p values were less than 0.0500, while they were non-significant if the p values were greater than 0.0500 [155]. Throughout the entire technique, all the model terms namely A, B, AB, A^2 and B^2 are significant. The R^2 coefficient of determination, which offers the proportion of total variation in the response, was used to analyze the performance of the fitted model, and a high value of R^2 (near to 1) is preferable. The accuracy of the design model depends on the value of R^2 and closer to 1 considered higher the accuracy. According to this model, R^2 of 0.9877 was obtained which presents that 98.77 % OTC variations are describable by the process parameters and only 1.33 % of experimental data could not be demonstrated by the model. The adjusted R^2 (0.9790) values are extremely close to R^2 , and the difference in R^2 and adjusted R^2 is less than 0.2 that indicates the model fitting is satisfactory, however various independent variables will make this more practical. It can change the R^2 by increasing or decreasing the number of predictions or covariates in the required design. Moreover, adequate precision was 30.86 that means this model can be used to navigate the design space. Adequate precision measures the signal to noise ratio and ratio greater than 4 is desirable. The lack of fit of F-value of 5.78 with p-value 0.061 imply that lack of fit is not significant that is required. The experimental results and predicted by RSM for OTC due to process parameters are shown in Fig. 4.9.

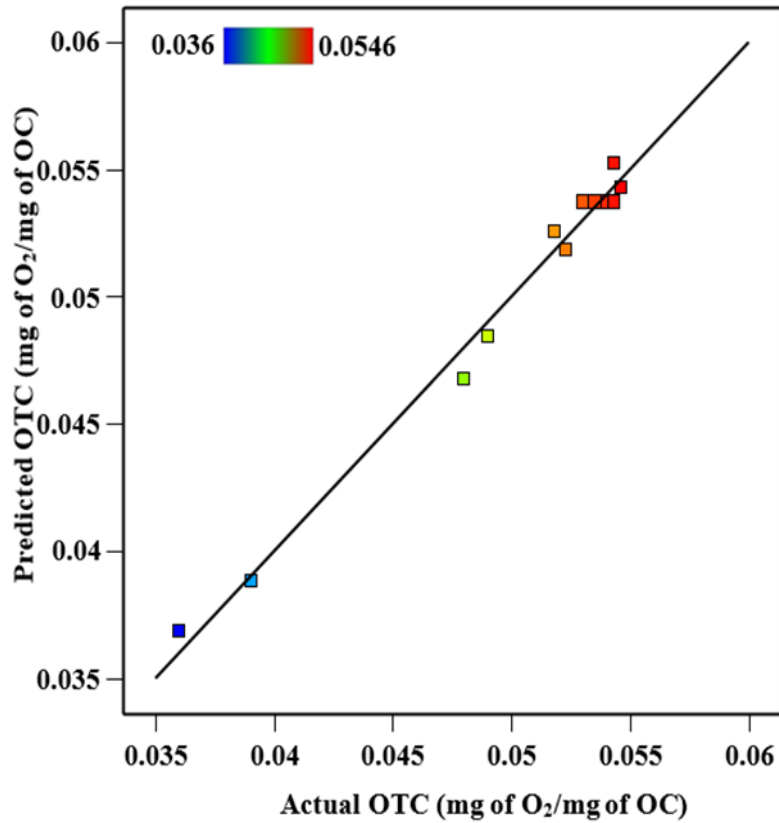


Figure 4.9: Predicted vs actual data for response (oxygen transport capacity).

4.3.1 Effect of process parameters on response

The effect of process parameter on the oxygen transport capacity in linear term was analyzed by perturbation graph as shown in Fig. 4.10. Two curved lines were found because of two process parameters (time and temperature) for the influence on the OTC. The curvature of the line is directly proportional to the influence effect on OTC [155]. Therefore, it can be revealed that time is the most influencing independent variable for the OTC owing to higher curvature.

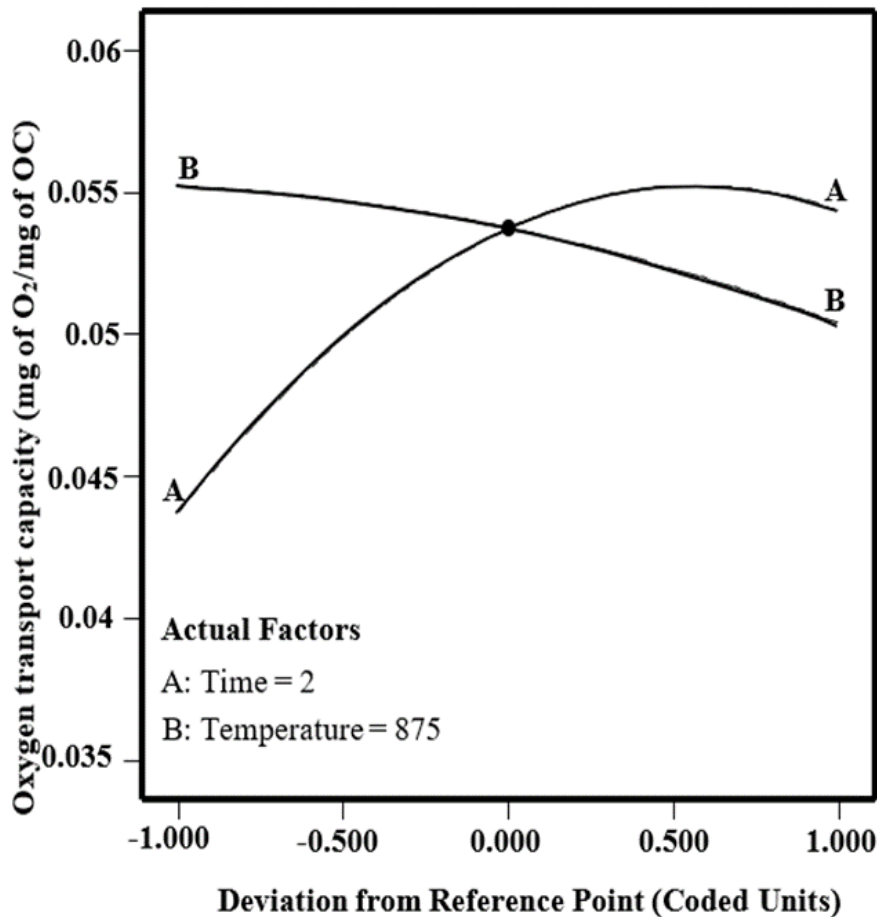


Figure 4.10: Perturbation plot for oxygen transport capacity influenced by time and temperature.

4.3.2 Parametric analysis of oxygen transport capacity using 3D response surface plot

At different process parameters, different types of OCs show different behaviors, which can either increase or decrease OTC or have no effect on it at all. As a result, the most important process parameters that have a substantial impact on the OTC of OCs during continuous redox cycles in the CLC process are time and temperature. Response surface patterns are representations of regression equation frameworks that are used to resolve the optimal level of parameters and gain a better understanding of their interactions, which can then be used to optimize the efficiency of the process. Response surface patterns are used to resolve the optimal level of parameters and gain a better understanding of their interactions. Counter plots in two dimensions (2D) and response surface plots in three dimensions (3D) are graphical representations of the regression

equation that can be used to analyze the relationship between input and output variables. The combined effect of time and temperature on the OTC of OC in 3D response surface plot is shown in Fig. 4.11. It can be observed that by increasing temperature from 800 °C to 950 °C during 1 min reduction reaction time, the OTC of OC was gradually decreased from 0.048 to 0.039 mg of O₂/ mg. However, when the reduction reaction time for OC was slightly increased, the OTC was drastically increased. Hence, at 800 °C with the increase in time from 1 min to 3 min, the OTC was significantly increased from 0.048 to 0.0546 mg of O₂/ mg of OC. It can be concluded that change reaction temperature slightly changes the amount of OTC. Similar to perturbation analysis, 3D response surface analysis reveals that among two process parameters, time has the highest effect on the OTC of Cu-based praseodymium modified alumina OC as compared to temperature.

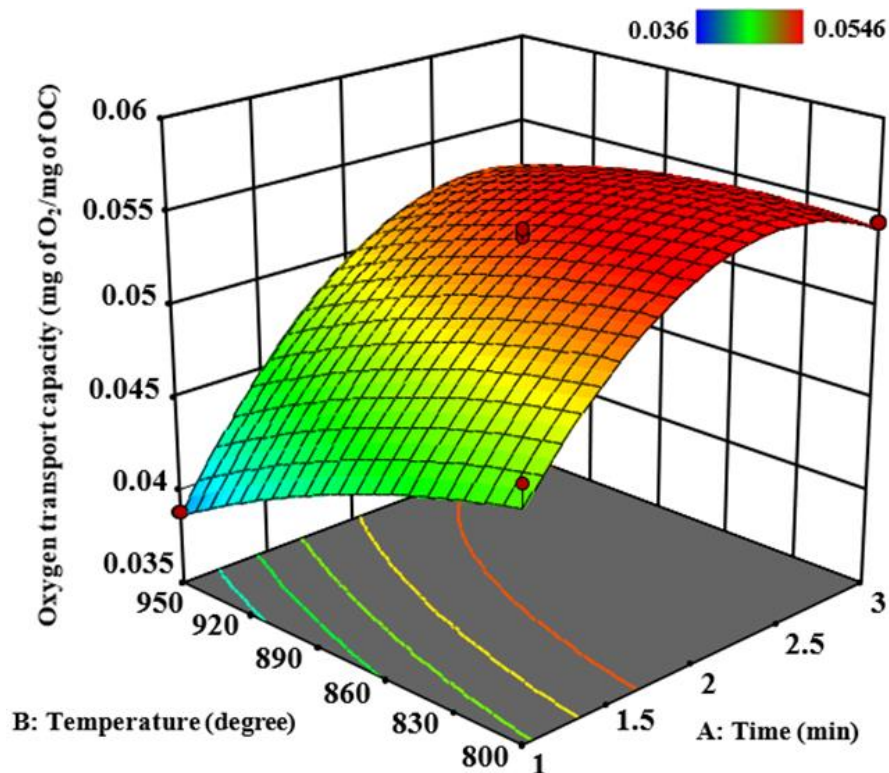


Figure 4.11: 3D response surface plot of oxygen transport capacity for parametric analysis.

4.4 Optimization of process parameters

It is necessary to do numerical optimization in order to maximize OTC using a tool that has been implemented for experimental findings of the CLC process using TGA for operating conditions. The experiment was performed three times as shown in Table 4.5 for confirmation of the predicted oxygen transport capacity against 800 °C and a three-minute reduction reaction to confirm the predicted oxygen transport capacity. This allowed for a comparison of the actual oxygen transport capacity with the expected oxygen transport capacity based on the first phase of testing. The model's predictions and confirmation tests were revealed to be in excellent concordance, proving the efficiency and reliability of the model. The optimal variables were determined to be a time of 3 min and a temperature of 800 °C, which resulted in a predicted oxygen transfer capacity of 0.054 mg of O₂/ mg of OC. The standard deviation for OTC was determined to be 0.0004, indicating a high degree of conformity between experimental and predicted findings.

Table 4.5: Predicted and experimental results for the optimized process parameters.

Confirmation runs	Time (min)	Temperature (°C)	OTC (mg of O ₂ / mg of OC)		Percentage error (%)
			Predicted	Experimental	
Run 1	3	800	0.054	0.0541	0.18
Run 2	3	800	0.054	0.0546	1.11
Run 3	3	800	0.054	0.0551	2.03
Standard deviation	-	-	-	0.0004	-

CHAPTER 5

CONCLUSION AND RECOMMENDATIONS

5.1 Conclusion

The major goal of this research was to develop chemically and thermally stable oxygen carriers for the chemical looping combustion process that could generate clean energy without releasing CO₂ into the atmosphere. The study was categorized into three sections in order to pursue this objective. The first section involved the preparation of single metal oxide and bimetallic based oxygen carriers. Three types of single metal-based OCs such as 10CoA, 10FeA, and 10CuA were synthesized and compared using CLC process. In second section a thermogravimetric analyzer was used to investigate the performance of synthesized OCs for reactivity test using 5% CH₄/N₂ as reducing gas and air as an oxidizing gas for CLC process. The oxygen transport capacity (OTC) of 0.018 mg of O₂/mg of OC, 0.026 mg of O₂/mg of OC, and 0.026 mg of O₂/mg of OC was determined for 10FeA, 10CuA and 10CoA based OCs, respectively. Although the 10CuA and 10CoA OTCs were determined to be equivalent, the reduction time for 10CuA was 1 min and the reduction time for 10CoA-based OC was 5.1 min. OC based on 10CuA has been used for the preparation of bimetallic oxides because of its faster reduction process, higher OTC, and less expensive cost perspective among single metal-based OCs. Between two types of promoters (Pr-oxide and La-oxide), Pr-oxide showed higher OTC of 0.021 mg of O₂/mg of OC compared to La-oxide (0.002 mg of O₂/mg of OC) and successfully regenerated after completion of redox cycles. The aim of this work was to analyze whether a bimetallic CuPr- γ -Al₂O₃ based oxygen carrier could be used as an OC in chemical looping combustion. The OTC of a CuPr-based OC was 0.0267 mg of O₂/ mg of OC, which was higher than previous reported results without Pr-modified, Cu-based OCs. Furthermore, it exhibited high stability in terms of maintaining high OTC as the cycle progressed. Both TPR and XRD results revealed that addition of Pr to Cu-based OC displayed phase stability even after 10 redox cycles as compared to OC without Pr. The FE-SEM analysis showed that the

surface morphology of CuPr-based OC was irregular, and some agglomeration was observed. Although, agglomeration was confirmed, but it did not affect the OTC of OC. Hence, these results indicate that a CuPr-based oxygen carrier could be a promising material for use as an oxygen carrier in CLC process.

5.2 Recommendations

In light of the findings of the current study, the following recommendations could be put in place for future knowledge and investigation:

- In this study, CH₄ was employed to investigate the CLC process. Instead of using CH₄, natural gas might be used to explore the effects of other gases present. There are many ways to study the inactivation of oxygen carriers in natural gas because most natural gas sources have a low Sulphur content.
- The primary purpose of chemical looping combustion with carbon capture is to convert CH₄ to full products during reduction, namely CO₂ and H₂O. Therefore, it is essential to evaluate the CH₄ reduction kinetics with copper oxide. Using CH₄ as a fuel with praseodymium-based OCs implies several additional difficult reaction steps. Identifying each elementary step and plotting the entire reaction framework requires significantly more effort to explain the role of each single reaction mechanism.
- Cu catalyzing the CH₄ cracking reaction, hence accelerating the reduction kinetics. The enhanced kinetics of the Cu-based composite perovskites oxygen carriers efficiently reduces the working temperature, resulting in increased unit performance. Additionally, materials are exposed to fewer brutal environments at lower temperatures, resulting in increased stability and longevity.
- A series of bench-scale tests should be carried out to identify potential problems, such as pressure fluctuations and problem areas.
- To estimate and measure the rate of gas evolution during the CLC redox process, a gas analyzer device and a thermogravimetric analyzer (TGA) can be

employed together. This can assist in determining the rate at which intermediates, and ultimate products of gases are consumed or produced.

- Finding out how bi- and tri-support combinations affect the redox process, carbon production, and stability of synthetic oxygen carriers would be intriguing.

REFERENCES

- [1] J. Yang, L. Ma, J. Yang, Z. Guo, H. Liu, and W. Zhang, "Chemical looping gasification of phosphogypsum as an oxygen carrier: The Ca and S migration mechanism using the DFT method," (in eng), *Sci Total Environ*, vol. 689, pp. 854-864, Jul 1 2019.
- [2] J. Ma *et al.*, "Fate of Mercury in Volatiles and Char during in Situ Gasification Chemical-Looping Combustion of Coal," (in eng), *Environ Sci Technol*, vol. 53, no. 13, pp. 7887-7892, Jul 2 2019.
- [3] S. P. Raghuvanshi, A. Chandra, A. K. J. E. C. Raghav, and Management, "Carbon dioxide emissions from coal based power generation in India," vol. 47, no. 4, pp. 427-441, 2006.
- [4] M. Matzen, J. Pinkerton, X. Wang, and Y. Demirel, "Use of natural ores as oxygen carriers in chemical looping combustion: A review," *International Journal of Greenhouse Gas Control*, vol. 65, pp. 1-14, 2017.
- [5] G. J. I. E. A. P. Energy, France, "CO2 Status Report 2017," 2018.
- [6] M. M. Hossain and H. I. J. C. E. S. de Lasa, "Chemical-looping combustion (CLC) for inherent CO2 separations—a review," vol. 63, no. 18, pp. 4433-4451, 2008.
- [7] M. B. Toftegaard, J. Brix, P. A. Jensen, P. Glarborg, A. D. J. P. i. e. Jensen, and c. science, "Oxy-fuel combustion of solid fuels," vol. 36, no. 5, pp. 581-625, 2010.
- [8] M. Ishida, D. Zheng, and T. J. E. Akehata, "Evaluation of a chemical-looping-combustion power-generation system by graphic exergy analysis," vol. 12, no. 2, pp. 147-154, 1987.
- [9] L.-l. Wang, L.-h. Shen, W. Liu, S. J. E. Jiang, and Fuels, "Chemical Looping Hydrogen Generation Using Synthesized Hematite-Based Oxygen Carrier Comodified by Potassium and Copper," vol. 31, no. 8, pp. 8423-8433, 2017.
- [10] T. Liu *et al.*, "Research of coal-direct chemical looping hydrogen generation with iron-based oxygen carrier modified by potassium," vol. 42, no. 16, pp. 11038-11046, 2017.
- [11] M. Sarafraz, M. Jafarian, M. Arjomandi, and G. J. I. J. o. H. E. Nathan, "The thermo-chemical potential liquid chemical looping gasification with bismuth oxide," vol. 44, no. 16, pp. 8038-8050, 2019.
- [12] W. Qin *et al.*, "Methanol solution promoting cotton fiber chemical looping gasification for high H2/CO ratio syngas," vol. 44, no. 14, pp. 7149-7157, 2019.
- [13] H. Thunman, F. Lind, C. Breitholtz, N. Berguerand, and M. J. F. Seemann, "Using an oxygen-carrier as bed material for combustion of biomass in a 12-MWth circulating fluidized-bed boiler," vol. 113, pp. 300-309, 2013.
- [14] P. Wang, H. Leion, H. J. E. Yang, and Fuels, "Oxygen-Carrier-Aided Combustion in a bench-scale fluidized bed," vol. 31, no. 6, pp. 6463-6471, 2017.
- [15] M. Rydén, M. Hanning, A. Corcoran, and F. J. A. S. Lind, "Oxygen carrier aided combustion (OCAC) of wood chips in a semi-commercial circulating fluidized bed boiler using manganese ore as bed material," vol. 6, no. 11, p. 347, 2016.
- [16] E. R. G. Warren K Lewis, "Production of pure carbon dioxide," 1954. Available: <https://patents.google.com/patent/US2665972A/en#patentCitations>.
- [17] H. J. Richter and K. F. Knoche, "Reversibility of Combustion Processes," in *Efficiency and Costing*, vol. 235(ACS Symposium Series, no. 235): AMERICAN CHEMICAL SOCIETY, 1983, pp. 71-85.
- [18] J.-I. Baek *et al.*, "The effects of using structurally less-stable raw materials for the support of a spray-dried oxygen carrier with high NiO content," *Fuel*, vol. 102, pp. 106-114, 2012.
- [19] I. Adánez-Rubio *et al.*, "Performance Evaluation of a Cu-Based Oxygen Carrier Impregnated onto ZrO2 for Chemical-Looping Combustion (CLC)," *Industrial & Engineering Chemistry Research*, vol. 59, no. 15, pp. 7255-7266, 2020.
- [20] J. H. Hwang *et al.*, "A thermogravimetric study of CoTiO3 as oxygen carrier for chemical looping combustion," *Catalysis Today*, vol. 303, pp. 13-18, 2018/04/01/ 2018.
- [21] D. D. Miller, M. Smith, and D. Shekhawat, "Development of Fe-based oxygen carrier using spent FCC catalyst as support for high temperature chemical looping combustion," *Fuel*, vol. 259, p. 116239, 2020.
- [22] T. Costa *et al.*, "Mn-based oxygen carriers prepared by impregnation for Chemical Looping Combustion with diverse fuels," *Fuel Processing Technology*, vol. 178, pp. 236-250, 2018.

- [23] A. Nandy, C. Loha, S. Gu, P. Sarkar, M. K. Karmakar, and P. K. Chatterjee, "Present status and overview of Chemical Looping Combustion technology," *Renewable and Sustainable Energy Reviews*, vol. 59, pp. 597-619, 2016.
- [24] N. M. Afandi, A. N. A. Manap, F. H. Mansor, M. F. A. Ghani, N. Kadir, and W. Liu, "Characterization of Fe₂O₃/Mn₂O₃ oxygen carrier for chemical looping combustion prepared by dry impregnation method," *International Journal of Engineering and Technology (UAE)*, vol. 7, no. 4, pp. 674-677, 2018.
- [25] J. Ma, D. Mei, W. Peng, X. Tian, D. Ren, and H. Zhao, "On the high performance of a core-shell structured CaO-CuO/MgO@ Al₂O₃ material in calcium looping integrated with chemical looping combustion (CaL-CLC)," *Chemical Engineering Journal*, vol. 368, pp. 504-512, 2019.
- [26] X. Tian, M. Su, and H. Zhao, "Kinetics of redox reactions of CuO@ TiO₂-Al₂O₃ for chemical looping combustion and chemical looping with oxygen uncoupling," *Combustion and Flame*, vol. 213, pp. 255-267, 2020.
- [27] M. M. Tijani, A. Aqsha, and N. Mahinpey, "Synthesis and study of metal-based oxygen carriers (Cu, Co, Fe, Ni) and their interaction with supported metal oxides (Al₂O₃, CeO₂, TiO₂, ZrO₂) in a chemical looping combustion system," *Energy*, vol. 138, pp. 873-882, 2017/11/01/ 2017.
- [28] M. San Pio, M. Martini, F. Gallucci, I. Roghair, and M. van Sint Annaland, "Kinetics of CuO/SiO₂ and CuO/Al₂O₃ oxygen carriers for chemical looping combustion," *Chemical Engineering Science*, vol. 175, pp. 56-71, 2018.
- [29] N. C. Means, S. Hammache, W. A. Burgess, B. H. Howard, and M. W. Smith, "Evaluation of the Redox Performance and Characterization of Fe₂O₃/CeO₂/ZrO₂ Oxygen Carriers under High Temperature in Situ Gasification Chemical-Looping Combustion Conditions," *Energy & Fuels*, vol. 34, no. 1, pp. 871-878, 2020/01/16 2020.
- [30] Q. Imtiaz, A. Kurlov, J. L. M. Rupp, and C. R. Müller, "Highly Efficient Oxygen-Storage Material with Intrinsic Coke Resistance for Chemical Looping Combustion-Based CO₂ Capture," *ChemSusChem*, vol. 8, no. 12, pp. 2055-2065, 2015.
- [31] J. Dai, L. Hughey, and K. J. Whitty, "Influence of fuel ash on the recoverability of copper from the spent material of chemical looping combustion," *Fuel Processing Technology*, vol. 201, p. 106358, 2020.
- [32] L. F. de Diego, P. Gayán, F. García-Labiano, J. Celaya, A. Abad, and J. Adánez, "Impregnated CuO/Al₂O₃ Oxygen Carriers for Chemical-Looping Combustion: Avoiding Fluidized Bed Agglomeration," *Energy & Fuels*, vol. 19, no. 5, pp. 1850-1856, 2005/09/01 2005.
- [33] M. Qasim, M. Ayoub, A. Aqsha, and M. Zulficar, "Preparation of Metal Oxide-based Oxygen Carriers Supported with CeO₂ and γ -Al₂O₃ for Chemical Looping Combustion," *Chemical Engineering & Technology*, vol. 44, no. 4, pp. 782-787, 2021.
- [34] M. Qasim, M. Ayoub, A. Aqsha, and N. A. Ghazali, "Investigation and Comparison for the Redox Behavior of Different Metal Oxides (Ni, Fe, Co, Cu, Ce, La, Pr) with and without Gamma-Alumina Support for the Chemical Looping Combustion," *Solid State Technology*, vol. 63, no. 6, pp. 19450-19460, 2020.
- [35] G. Zhou and R. J. Gorte, "Thermodynamic Investigation of the Redox Properties for Ceria-Hafnia, Ceria-Terbium, and Ceria-Praseodymium Solid Solutions," *The Journal of Physical Chemistry B*, vol. 112, no. 32, pp. 9869-9875, 2008/08/01 2008.
- [36] O. Edenhofer, *Climate change 2014: mitigation of climate change*. Cambridge University Press, 2015.
- [37] M. E. Boot-Handford *et al.*, "Carbon capture and storage update," *Energy & Environmental Science*, vol. 7, no. 1, pp. 130-189, 2014.
- [38] N. MacDowell *et al.*, "An overview of CO₂ capture technologies," *Energy & Environmental Science*, vol. 3, no. 11, pp. 1645-1669, 2010.
- [39] L. Zhu, P. Jiang, and J. Fan, "Comparison of carbon capture IGCC with chemical-looping combustion and with calcium-looping process driven by coal for power generation," *Chemical Engineering Research and Design*, vol. 104, pp. 110-124, 2015/12/01/ 2015.
- [40] D. Keairns, N. Kuehn, R. Newby, and V. Shah, "Guidance for NETL's Oxycombustion R&D Program: Chemical Looping Combustion Reference Plant Designs and Sensitivity Studies," NETL2014.
- [41] J. Adanez, A. Abad, F. Garcia-Labiano, P. Gayan, and L. F. de Diego, "Progress in Chemical-Looping Combustion and Reforming technologies," *Progress in Energy and Combustion Science*, vol. 38, no. 2, pp. 215-282, 2012/04/01/ 2012.

- [42] A. Bhawe *et al.*, "Screening and techno-economic assessment of biomass-based power generation with CCS technologies to meet 2050 CO₂ targets," *Applied Energy*, vol. 190, pp. 481-489, 2017/03/15/ 2017.
- [43] F. Petrakopoulou, G. Tsatsaronis, A. Boyano, and T. Morosuk, "Exergoeconomic and exergoenvironmental evaluation of power plants including CO₂ capture," *Chemical Engineering Research and Design*, vol. 89, no. 9, pp. 1461-1469, 2011/09/01/ 2011.
- [44] J. Yan, L. Shen, Z. Ou, J. Wu, S. Jiang, and H. Gu, "Enhancing the performance of iron ore by introducing K and Na ions from biomass ashes in a CLC process," *Energy*, vol. 167, pp. 168-180, 2019/01/15/ 2019.
- [45] M. Ishida, H. J. I. Jin, and E. C. Research, "A novel chemical-looping combustor without NO_x formation," vol. 35, no. 7, pp. 2469-2472, 1996.
- [46] H.-J. Ryu, G.-T. Jin, and C.-K. Yi, "Demonstration of inherent CO₂ separation and no NO_x emission in a 50kW chemical-looping combustor: continuous reduction and oxidation experiment," in *Greenhouse Gas Control Technologies 7*: Elsevier, 2005, pp. 1907-1910.
- [47] Z. Yu *et al.*, "Iron-based oxygen carriers in chemical looping conversions: A review," *Carbon Resources Conversion*, vol. 2, no. 1, pp. 23-34, 2019.
- [48] P. Cho, T. Mattisson, and A. Lyngfelt, "Comparison of iron-, nickel-, copper-and manganese-based oxygen carriers for chemical-looping combustion," *Fuel*, vol. 83, no. 9, pp. 1215-1225, 2004.
- [49] A. Abad, J. Adánez, F. García-Labiano, L. F. de Diego, P. Gayán, and J. Celaya, "Mapping of the range of operational conditions for Cu-, Fe-, and Ni-based oxygen carriers in chemical-looping combustion," *Chemical Engineering Science*, vol. 62, no. 1, pp. 533-549, 2007/01/01/ 2007.
- [50] M. Johansson, T. Mattisson, and A. Lyngfelt, "Investigation of Fe₂O₃ with MgAl₂O₄ for Chemical-Looping Combustion," *Industrial & Engineering Chemistry Research*, vol. 43, no. 22, pp. 6978-6987, 2004/10/01 2004.
- [51] J. Adánez, L. F. de Diego, F. García-Labiano, P. Gayán, A. Abad, and J. M. Palacios, "Selection of Oxygen Carriers for Chemical-Looping Combustion," *Energy & Fuels*, vol. 18, no. 2, pp. 371-377, 2004/03/01 2004.
- [52] E. R. Monazam, R. W. Breault, and R. Siriwardane, "Reduction of hematite (Fe₂O₃) to wüstite (FeO) by carbon monoxide (CO) for chemical looping combustion," *Chemical Engineering Journal*, vol. 242, pp. 204-210, 2014/04/15/ 2014.
- [53] T. R. Costa *et al.*, "Mn-based oxygen carriers prepared by impregnation for Chemical Looping Combustion with diverse fuels," *Fuel Processing Technology*, vol. 178, pp. 236-250, 2018.
- [54] D. Mei *et al.*, "Manganese Minerals as Oxygen Carriers for Chemical Looping Combustion of Coal," *Industrial & Engineering Chemistry Research*, vol. 55, no. 22, pp. 6539-6546, 2016/06/08 2016.
- [55] H. Song, K. Shah, E. Doroodchi, T. Wall, and B. Moghtaderi, "Reactivity of Al₂O₃- or SiO₂-Supported Cu-, Mn-, and Co-Based Oxygen Carriers for Chemical Looping Air Separation," *Energy & Fuels*, vol. 28, no. 2, pp. 1284-1294, 2014.
- [56] X. Tian, M. Su, and H. Zhao, "Kinetics of redox reactions of CuO@TiO₂-Al₂O₃ for chemical looping combustion and chemical looping with oxygen uncoupling," *Combustion and Flame*, vol. 213, pp. 255-267, 2020/03/01/ 2020.
- [57] Y. Zhang, E. Doroodchi, and B. Moghtaderi, "Chemical looping combustion of ultra low concentration of methane with Fe₂O₃/Al₂O₃ and CuO/SiO₂," *Applied energy*, vol. 113, pp. 1916-1923, 2014.
- [58] H. A. Alalwan, D. M. Cwiertny, and V. H. Grassian, "Co₃O₄ nanoparticles as oxygen carriers for chemical looping combustion: A materials characterization approach to understanding oxygen carrier performance," *Chemical Engineering Journal*, vol. 319, pp. 279-287, 2017/07/01/ 2017.
- [59] E. N. Son *et al.*, "Study on the redox characteristics of CaCo based oxygen carrier for Chemical Looping Combustion," *Chemical Engineering Journal*, vol. 377, 2019.
- [60] F. García-Labiano, L. F. de Diego, J. Adánez, A. Abad, and P. Gayán, "Temperature variations in the oxygen carrier particles during their reduction and oxidation in a chemical-looping combustion system," *Chemical Engineering Science*, vol. 60, no. 3, pp. 851-862, 2005/02/01/ 2005.

- [61] M. M. Hossain, D. Lopez, J. Herrera, and H. I. de Lasa, "Nickel on lanthanum-modified γ -Al₂O₃ oxygen carrier for CLC: Reactivity and stability," *Catalysis Today*, vol. 143, no. 1, pp. 179-186, 2009/05/15/ 2009.
- [62] D. Zeng *et al.*, "Enhanced hydrogen production performance through controllable redox exsolution within CoFeAlO_x spinel oxygen carrier materials," *Journal of Materials Chemistry A*, vol. 6, no. 24, pp. 11306-11316, 2018.
- [63] D. Cui *et al.*, "A high-performance oxygen carrier with high oxygen transport capacity and redox stability for chemical looping combustion," *Energy Conversion and Management*, vol. 202, p. 112209, 2019.
- [64] R. Pérez-Vega *et al.*, "Chemical Looping Combustion of gaseous and solid fuels with manganese-iron mixed oxide as oxygen carrier," *Energy Conversion and Management*, vol. 159, pp. 221-231, 2018.
- [65] A. Mishra, R. Dudek, A. Gaffney, D. Ding, and F. Li, "Spinel oxides as coke-resistant supports for NiO-based oxygen carriers in chemical looping combustion of methane," *Catalysis Today*, 2019.
- [66] J. Riley, R. Siriwardane, and J. Poston, "Bench scale analysis of the physical attrition properties for copper-ferri-aluminate oxygen carriers during chemical looping combustion," *Powder Technology*, vol. 366, pp. 891-905, 2020.
- [67] M. Abián *et al.*, "Titanium substituted manganese-ferrite as an oxygen carrier with permanent magnetic properties for chemical looping combustion of solid fuels," *Fuel*, vol. 195, pp. 38-48, 2017.
- [68] R. Pérez-Vega *et al.*, "Coal combustion via Chemical Looping assisted by Oxygen Uncoupling with a manganese-iron mixed oxide doped with titanium," *Fuel Processing Technology*, vol. 197, 2020.
- [69] A. Nandy *et al.*, "Present status and overview of Chemical Looping Combustion technology," vol. 59, pp. 597-619, 2016.
- [70] A. Abad *et al.*, "Kinetics of CaMn_{0.775}Ti_{0.125}Mg_{0.102} 9- δ perovskite prepared at industrial scale and its implication on the performance of chemical looping combustion of methane," *Chemical Engineering Journal*, p. 124863, 2020.
- [71] E. Ksepko, "Perovskite Sr (Fe_{1-x}Cu_x) O_{3- δ} materials for chemical looping combustion applications," *International Journal of Hydrogen Energy*, vol. 43, no. 20, pp. 9622-9634, 2018.
- [72] Q. Jiang, H. Zhang, Q. Kang, H. Hong, and H. Jin, "Properties and reactivity of LaCuxNi_{1-x}O₃ perovskites in chemical-looping combustion for mid-temperature solar-thermal energy storage," *Applied Energy*, vol. 228, pp. 1506-1514, 2018.
- [73] Q. Jiang, Y. Cao, X. Liu, H. Zhang, H. Hong, and H. Jin, "Chemical Looping Combustion over a Lanthanum Nickel Perovskite-Type Oxygen Carrier with Facilitated O₂- Transport," *Energy & Fuels*, vol. 34, no. 7, pp. 8732-8739, 2020/07/16 2020.
- [74] Z. Di, Y. Cao, F. Yang, F. Cheng, and K. Zhang, "Studies on steel slag as an oxygen carrier for chemical looping combustion," *Fuel*, vol. 226, pp. 618-626, 2018/08/15/ 2018.
- [75] D. D. Miller, M. Smith, and D. Shekhawat, "Interaction of manganese with aluminosilicate support during high temperature (1100 °C) chemical looping combustion of the Fe-Mn-based oxygen carrier," *Fuel*, vol. 263, 2020.
- [76] S. Hammache, N. Means, W. Burgess, B. Howard, and M. Smith, "Investigation of low-cost oxygen carriers for chemical looping combustion at high temperature," *Fuel*, vol. 273, p. 117746, 2020/08/01/ 2020.
- [77] B. Bhui and V. Prabu, "Techno-economic evaluation of electronic waste based oxygen carriers for co-chemical looping combustion of coal and biomass integrated combined cycle power generating systems," *Energy Conversion and Management*, vol. 236, p. 114075, 2021/05/15/ 2021.
- [78] T. Ren, M. An, X. Hu, J. Ma, and Q. Guo, "Development of inexpensive perovskite Mn-based oxygen carriers using the waste manganese sand for chemical looping gasification," *International Journal of Energy Research*, vol. 45, no. 2, pp. 2416-2431, 2021.
- [79] F. Hildor, T. Mattisson, H. Leion, C. Linderholm, and M. Rydén, "Steel converter slag as an oxygen carrier in a 12 MWth CFB boiler – Ash interaction and material evolution," *International Journal of Greenhouse Gas Control*, vol. 88, pp. 321-331, 2019/09/01/ 2019.
- [80] T. Shen, S. Wang, J. Yan, L. Shen, and H. Tian, "Performance improvement of chemical looping combustion with coal by optimizing operational strategies in a 3 kWth interconnected fluidized bed," *International Journal of Greenhouse Gas Control*, vol. 98, 2020.

- [81] S. Hammache, N. Means, W. Burgess, B. Howard, and M. Smith, "Investigation of low-cost oxygen carriers for chemical looping combustion at high temperature," *Fuel*, vol. 273, 2020.
- [82] H. Wang *et al.*, "Barium aluminate improved iron ore for the chemical looping combustion of syngas," *Applied Energy*, vol. 272, p. 115236, 2020/08/15/ 2020.
- [83] T. Mendiara, A. Abad, L. F. de Diego, F. García-Labiano, P. Gayán, and J. Adánez, "Reduction and oxidation kinetics of Tierga iron ore for Chemical Looping Combustion with diverse fuels," *Chemical Engineering Journal*, vol. 359, pp. 37-46, 2019.
- [84] T. Mendiara *et al.*, "Chemical Looping Combustion of different types of biomass in a 0.5 kWth unit," *Fuel*, vol. 211, pp. 868-875, 2018.
- [85] A. Abad *et al.*, "Assessment of the improvement of chemical looping combustion of coal by using a manganese ore as oxygen carrier," *Fuel Processing Technology*, vol. 176, pp. 107-118, 2018.
- [86] P. Moldenhauer, S. Sundqvist, T. Mattisson, and C. Linderholm, "Chemical-looping combustion of synthetic biomass-volatiles with manganese-ore oxygen carriers," *International Journal of Greenhouse Gas Control*, vol. 71, pp. 239-252, 2018.
- [87] X. Liu *et al.*, "[CLCG] Petroleum coke conversion behavior in catalyst-assisted chemical looping combustion," *Chinese Journal of Chemical Engineering*, 2020.
- [88] C. Dueso, F. García-Labiano, J. Adánez, F. Luis, P. Gayán, and A. J. F. Abad, "Syngas combustion in a chemical-looping combustion system using an impregnated Ni-based oxygen carrier," vol. 88, no. 12, pp. 2357-2364, 2009.
- [89] P. Erri, A. J. I. Varma, and E. C. Research, "Spinel-supported oxygen carriers for inherent CO₂ separation during power generation," vol. 46, no. 25, pp. 8597-8601, 2007.
- [90] M. Ishida and H. J. J. o. c. e. o. J. Jin, "A novel combustor based on chemical-looping reactions and its reaction kinetics," vol. 27, no. 3, pp. 296-301, 1994.
- [91] C. Dueso, F. García-Labiano, J. Adánez, F. Luis, P. Gayán, and A. Abad, "Syngas combustion in a chemical-looping combustion system using an impregnated Ni-based oxygen carrier," *Fuel*, vol. 88, no. 12, pp. 2357-2364, 2009.
- [92] J. Yang *et al.*, "Syngas preparation by NiO–CaSO₄-based oxygen carrier from chemical looping gasification technology," *Journal of the Energy Institute*, vol. 94, pp. 191-198, 2021/02/01/ 2021.
- [93] L. Blas, P. Dutournié, S. Dorge, L. Josien, D. Kehrli, and A. Lambert, "Thermal stability study of NiAl₂O₄ binders for Chemical Looping Combustion application," *Fuel*, vol. 182, pp. 50-56, 2016/10/15/ 2016.
- [94] D. Karami, A. H. Soleimansalim, M. H. Sedghkerdar, and N. Mahinpey, "Preparation of Novel Oxygen Carriers Supported by Ti, Zr-Shelled γ -Alumina for Chemical Looping Combustion of Methane," *Industrial & Engineering Chemistry Research*, vol. 59, no. 7, pp. 3221-3228, 2020/02/19 2020.
- [95] M. H. Sedghkerdar, D. Karami, and N. Mahinpey, "Reduction and oxidation kinetics of solid fuel chemical looping combustion over a core-shell structured nickel-based oxygen carrier: Application of a developed grain size distribution model," *Fuel*, vol. 274, p. 117838, 2020/08/15/ 2020.
- [96] J. Adanez, A. Abad, F. Garcia-Labiano, P. Gayan, and F. Luis, "Progress in chemical-looping combustion and reforming technologies," *Progress in energy and combustion science*, vol. 38, no. 2, pp. 215-282, 2012.
- [97] M. M. Tijani, A. Aqsha, N. Yu, and N. Mahinpey, "Determination of redox pathways of supported bimetallic oxygen carriers in a methane fuelled chemical looping combustion system," *Fuel*, vol. 233, pp. 133-145, 2018.
- [98] X. Wang *et al.*, "CuO supported on olivine as an oxygen carrier in chemical looping processes with pine sawdust used as fuel," *Chemical Engineering Journal*, vol. 330, pp. 480-490, 2017.
- [99] A. Skulimowska *et al.*, "Chemical looping with oxygen uncoupling (CLOU) and chemical looping combustion (CLC) using copper-enriched oxygen carriers supported on fly ash," *Fuel Processing Technology*, vol. 168, pp. 123-130, 2017.
- [100] T. Mattisson, A. Lyngfelt, and P. Cho, "The use of iron oxide as an oxygen carrier in chemical-looping combustion of methane with inherent separation of CO₂," *Fuel*, vol. 80, no. 13, pp. 1953-1962, 2001.
- [101] M. M. Tijani, A. Aqsha, and N. Mahinpey, "X-ray diffraction and TGA kinetic analyses for chemical looping combustion applications," *Data in brief*, vol. 17, pp. 200-209, 2018.

- [102] Z. Ma, S. Zhang, and R. Xiao, "Insights into the relationship between microstructural evolution and deactivation of Al₂O₃ supported Fe₂O₃ oxygen carrier in chemical looping combustion," *Energy Conversion and Management*, vol. 188, pp. 429-437, 2019.
- [103] F. Huang *et al.*, "Fe-substituted Ba-hexaaluminate with enhanced oxygen mobility for CO₂ capture by chemical looping combustion of methane," *Journal of Energy Chemistry*, vol. 29, pp. 50-57, 2019.
- [104] F. Huang, X. Wang, A. Wang, J. Xu, and T. Zhang, "A two-step synthesis of Fe-substituted hexaaluminates with enhanced surface area and activity in methane catalytic combustion," *Catalysis Science & Technology*, vol. 6, no. 13, pp. 4962-4969, 2016.
- [105] B. Bhui and P. Vairakannu, "Experimental and kinetic studies on in-situ CO₂ gasification based chemical looping combustion of low ash coal using Fe₂O₃ as the oxygen carrier," *Journal of CO₂ Utilization*, vol. 29, pp. 103-116, 2019.
- [106] A. Serrano, F. García-Labiano, L. de Diego, P. Gayán, A. Abad, and J. Adánez, "Chemical Looping Combustion of liquid fossil fuels in a 1 kWth unit using a Fe-based oxygen carrier," *Fuel Processing Technology*, vol. 160, pp. 47-54, 2017.
- [107] S. Cloete, A. Giuffrida, M. Romano, P. Chiesa, M. Pishahang, and Y. Larring, "Integration of chemical looping oxygen production and chemical looping combustion in integrated gasification combined cycles," *Fuel*, vol. 220, pp. 725-743, 2018.
- [108] J. H. Hwang, J. I. Baek, H. J. Ryu, J. M. Sohn, and K.-T. Lee, "Development of MgMnO_{3-δ} as an oxygen carrier material for chemical looping combustion," *Fuel*, vol. 231, pp. 290-296, 2018.
- [109] J. Adanez, A. Abad, F. Garcia-Labiano, P. Gayan, F. J. P. i. e. Luis, and c. science, "Progress in chemical-looping combustion and reforming technologies," vol. 38, no. 2, pp. 215-282, 2012.
- [110] T. Mattisson, A. Järnäs, and A. Lyngfelt, "Reactivity of some metal oxides supported on alumina with alternating methane and oxygen application for chemical-looping combustion," *Energy & Fuels*, vol. 17, no. 3, pp. 643-651, 2003.
- [111] J. H. Hwang *et al.*, "A thermogravimetric study of CoTiO₃ as oxygen carrier for chemical looping combustion," vol. 303, pp. 13-18, 2018.
- [112] S. Cimino, G. Mancino, and L. Lisi, "Performance and Stability of Metal (Co, Mn, Cu)-Promoted La₂O₂SO₄ Oxygen Carrier for Chemical Looping Combustion of Methane," *Catalysts*, vol. 9, no. 2, 2019.
- [113] S. Luo, L. Zeng, and L.-S. Fan, "Chemical looping technology: oxygen carrier characteristics," *Annual review of chemical and biomolecular engineering*, vol. 6, pp. 53-75, 2015.
- [114] R. Siriwardane *et al.*, "50-kWth methane/air chemical looping combustion tests with commercially prepared CuO-Fe₂O₃-alumina oxygen carrier with two different techniques," *Applied Energy*, vol. 213, pp. 92-99, 2018/03/01/ 2018.
- [115] X. Huang, M. Fan, X. Wang, Y. Wang, M. D. Argyle, and Y. Zhu, "A cost-effective approach to realization of the efficient methane chemical-looping combustion by using coal fly ash as a support for oxygen carrier," *Applied Energy*, vol. 230, pp. 393-402, 2018.
- [116] M. A. Adnan, A. A. A. Mohammed, H. Binous, S. A. Razzak, and M. M. Hossain, "Ni-Fe bimetallic oxides on La modified Al₂O₃ as an oxygen carrier for liquid fuel based chemical looping combustion," *Fuel*, vol. 263, 2020.
- [117] W. Benincosa, R. Siriwardane, H. Tian, and J. Riley, "Unique phase identification of trimetallic copper iron manganese oxygen carrier using simultaneous differential scanning calorimetry/thermogravimetric analysis during chemical looping combustion reactions with methane," *Applied Energy*, vol. 203, pp. 522-534, 2017.
- [118] W. Benincosa, R. Siriwardane, H. Tian, J. Riley, and J. Poston, "A particle-scale reduction model of copper iron manganese oxide with CO for chemical looping combustion," *Applied Energy*, vol. 262, 2020.
- [119] C. Linderholm, A. Abad, T. Mattisson, and A. Lyngfelt, "160 h of chemical-looping combustion in a 10 kW reactor system with a NiO-based oxygen carrier," *International Journal of Greenhouse Gas Control*, vol. 2, no. 4, pp. 520-530, 2008.
- [120] P. Kolbitsch, J. Bolhar-Nordenkampf, T. Pröll, and H. Hofbauer, "Comparison of two Ni-based oxygen carriers for chemical looping combustion of natural gas in 140 kW continuous looping operation," *Industrial & engineering chemistry research*, vol. 48, no. 11, pp. 5542-5547, 2009.
- [121] J. Adánez, P. Gayán, J. Celaya, L. F. de Diego, F. García-Labiano, and A. Abad, "Chemical Looping Combustion in a 10 kWth Prototype Using a CuO/Al₂O₃ Oxygen Carrier: Effect of Operating Conditions on Methane Combustion," *Industrial & Engineering Chemistry Research*, vol. 45, no. 17, pp. 6075-6080, 2006/08/01 2006.

- [122] H.-J. Ryu, G.-T. Jin, and C.-K. Yi, "- Demonstration of inherent CO₂ separation and no NO_x emission in a 50kW chemical-looping combustor: Continuous reduction and oxidation experiment," in *Greenhouse Gas Control Technologies 7*, E. S. Rubin *et al.*, Eds. Oxford: Elsevier Science Ltd, 2005, pp. 1907-1910.
- [123] P. Cho, T. Mattisson, and A. Lyngfelt, "Carbon Formation on Nickel and Iron Oxide-Containing Oxygen Carriers for Chemical-Looping Combustion," *Industrial & Engineering Chemistry Research*, vol. 44, no. 4, pp. 668-676, 2005/02/01 2005.
- [124] Q. Intiaz, A. Armutlulu, F. Donat, M. A. Naeem, and C. R. Müller, "Preventing Agglomeration of CuO-Based Oxygen Carriers for Chemical Looping Applications," *ACS Sustainable Chemistry & Engineering*, vol. 9, no. 17, pp. 5972-5980, 2021/05/03 2021.
- [125] M. T. Izquierdo *et al.*, "On the optimization of physical and chemical stability of a Cu/Al₂O₃ impregnated oxygen carrier for chemical looping combustion," *Fuel Processing Technology*, vol. 215, p. 106740, 2021/05/01/ 2021.
- [126] A. Cabello, P. Gayán, F. García-Labiano, L. F. de Diego, A. Abad, and J. Adánez, "On the attrition evaluation of oxygen carriers in Chemical Looping Combustion," *Fuel Processing Technology*, vol. 148, pp. 188-197, 2016/07/01/ 2016.
- [127] C. Kuang, S. Wang, M. Luo, and J. Zhao, "Reactivity study and kinetic evaluation of CuO-based oxygen carriers modified by three different ores in Chemical looping with oxygen uncoupling (CLOU) process," *Chinese Journal of Chemical Engineering*, 2021/04/20/ 2021.
- [128] L. F. De Diego *et al.*, "Development of Cu-based oxygen carriers for chemical-looping combustion," *Fuel*, vol. 83, no. 13, pp. 1749-1757, 2004.
- [129] W. Chun, G. Graham, J. Lupescu, R. McCabe, M. Koranne, and R. J. C. I. Brezny, "Reducibility of catalyzed cerium–praseodymium mixed oxides," vol. 106, no. 3, pp. 95-100, 2006.
- [130] J. Yan *et al.*, "Preparation and performance of Cu-based bimetallic oxygen carriers in chemical looping combustion with gaseous and solid fuels," *Fuel Processing Technology*, vol. 205, 2020.
- [131] B. S. Kwak, N.-K. Park, S. O. Ryu, J.-I. Baek, H.-J. Ryu, and M. Kang, "Improved reversible redox cycles on MTiO_x (M = Fe, Co, Ni, and Cu) particles afforded by rapid and stable oxygen carrier capacity for use in chemical looping combustion of methane," *Chemical Engineering Journal*, vol. 309, pp. 617-627, 2017.
- [132] Z. Rouhani, J. Karimi-Sabet, M. Mehdipourghazi, A. Hadi, and A. Dastbaz, "Response surface optimization of hydrothermal synthesis of Bismuth ferrite nanoparticles under supercritical water conditions: Application for photocatalytic degradation of Tetracycline," *Environmental Nanotechnology, Monitoring & Management*, vol. 11, p. 100198, 2019/05/01/ 2019.
- [133] S. Ray, J. A. Lalman, and N. Biswas, "Using the Box-Benkhen technique to statistically model phenol photocatalytic degradation by titanium dioxide nanoparticles," *Chemical Engineering Journal*, vol. 150, no. 1, pp. 15-24, 2009/07/15/ 2009.
- [134] S. Chowdhury, F. Yusof, M. O. Faruck, and N. Sulaiman, "Process Optimization of Silver Nanoparticle Synthesis Using Response Surface Methodology," *Procedia Engineering*, vol. 148, pp. 992-999, 2016/01/01/ 2016.
- [135] J.-C. Sin, S.-M. Lam, and A. R. Mohamed, "Optimizing photocatalytic degradation of phenol by TiO₂/GAC using response surface methodology," *Korean Journal of Chemical Engineering*, vol. 28, no. 1, pp. 84-92, 2011.
- [136] R. K, R. S, K. S, and B. K, "Application of response surface methodology to optimize the process variables for Reactive Red and Acid Brown dye removal using a novel adsorbent," *Dyes and Pigments*, vol. 70, no. 1, pp. 18-26, 2006/07/01/ 2006.
- [137] M. M. Nasef, A. A. Aly, H. Saidi, and A. Ahmad, "Optimization of reaction parameters of radiation induced grafting of 1-vinylimidazole onto poly(ethylene-co-tetrafluoroethene) using response surface method," *Radiation Physics and Chemistry*, vol. 80, no. 11, pp. 1222-1227, 2011/11/01/ 2011.
- [138] M. Mirzaei, B. Dabir, M. Dadvar, and M. Jafarikojour, "Photocatalysis of Phenol Using a Spinning Disc Photoreactor Immobilized with TiO₂ Nanoparticles: Hydrodynamic Modeling and Reactor Optimization," *Industrial & Engineering Chemistry Research*, vol. 56, no. 7, pp. 1739-1749, 2017/02/22 2017.
- [139] B. Wang *et al.*, "Effect of Reaction Temperature on the Chemical Looping Combustion of Coal with CuFe₂O₄ Combined Oxygen Carrier," *Energy & Fuels*, vol. 31, no. 5, pp. 5233-5245, 2017/05/18 2017.

- [140] S. Y. Chuang, J. S. Dennis, A. N. Hayhurst, and S. A. Scott, "Development and performance of Cu-based oxygen carriers for chemical-looping combustion," *Combustion and Flame*, vol. 154, no. 1, pp. 109-121, 2008/07/01/ 2008.
- [141] A. Cuadrat, A. Abad, F. García-Labiano, P. Gayán, L. F. de Diego, and J. Adánez, "Effect of operating conditions in Chemical-Looping Combustion of coal in a 500Wth unit," *International Journal of Greenhouse Gas Control*, vol. 6, pp. 153-163, 2012/01/01/ 2012.
- [142] F. García-Labiano, J. Adánez, L. F. de Diego, P. Gayán, and A. Abad, "Effect of Pressure on the Behavior of Copper-, Iron-, and Nickel-Based Oxygen Carriers for Chemical-Looping Combustion," *Energy & Fuels*, vol. 20, no. 1, pp. 26-33, 2006/01/01 2006.
- [143] R. K. Singh, A. Sarkar, and J. P. Chakraborty, "Effect of torrefaction on the physicochemical properties of eucalyptus derived biofuels: estimation of kinetic parameters and optimizing torrefaction using response surface methodology (RSM)," *Energy*, vol. 198, p. 117369, 2020/05/01/ 2020.
- [144] M. Inayat, S. A. Sulaiman, A. Inayat, N. B. Shaik, A. R. Gilal, and M. Shahbaz, "Modeling and parametric optimization of air catalytic co-gasification of wood-oil palm fronds blend for clean syngas (H₂+CO) production," *International Journal of Hydrogen Energy*, 2020/11/26/ 2020.
- [145] S. Yusup, Z. Khan, M. M. Ahmad, and N. A. Rashidi, "Optimization of hydrogen production in in-situ catalytic adsorption (ICA) steam gasification based on Response Surface Methodology," *Biomass and Bioenergy*, vol. 60, pp. 98-107, 2014/01/01/ 2014.
- [146] P. Gayán, C. R. Forero, A. Abad, L. F. de Diego, F. García-Labiano, and J. Adánez, "Effect of Support on the Behavior of Cu-Based Oxygen Carriers during Long-Term CLC Operation at Temperatures above 1073 K," *Energy & Fuels*, vol. 25, no. 3, pp. 1316-1326, 2011/03/17 2011.
- [147] J. Huang, W. Liu, W. Hu, I. Metcalfe, Y. Yang, and B. J. A. e. Liu, "Phase interactions in Ni-Cu-Al₂O₃ mixed oxide oxygen carriers for chemical looping applications," vol. 236, pp. 635-647, 2019.
- [148] M.-F. Luo, P. Fang, M. He, and Y.-L. Xie, "In situ XRD, Raman, and TPR studies of CuO/Al₂O₃ catalysts for CO oxidation," *Journal of Molecular Catalysis A: Chemical*, vol. 239, no. 1, pp. 243-248, 2005/09/14/ 2005.
- [149] I. Ahmed and H. de Lasa, "Syngas chemical looping combustion using a highly performing fluidizable oxygen carrier," *Catalysis Today*, vol. 343, pp. 63-71, 2020/03/01/ 2020.
- [150] P. Artizzu, E. Garbowski, M. Primet, Y. Brulle, and J. Saint-Just, "Catalytic combustion of methane on aluminate-supported copper oxide," *Catalysis Today*, vol. 47, no. 1, pp. 83-93, 1999/01/01/ 1999.
- [151] W. Hu, F. Donat, S. Scott, and J. Dennis, "The interaction between CuO and Al₂O₃ and the reactivity of copper aluminates below 1000° C and their implication on the use of the Cu-Al-O system for oxygen storage and production," *RSC advances*, vol. 6, no. 114, pp. 113016-113024, 2016.
- [152] A. Abad, F. García-Labiano, L. F. de Diego, P. Gayán, and J. Adánez, "Reduction Kinetics of Cu-, Ni-, and Fe-Based Oxygen Carriers Using Syngas (CO + H₂) for Chemical-Looping Combustion," *Energy & Fuels*, vol. 21, no. 4, pp. 1843-1853, 2007/07/01 2007.
- [153] S. K. Haider *et al.*, "Copper-based oxygen carriers supported with alumina/lime for the chemical looping conversion of gaseous fuels," *Journal of Energy Chemistry*, vol. 26, no. 5, pp. 891-901, 2017/09/01/ 2017.
- [154] I. Adánez-Rubio *et al.*, "Performance Evaluation of a Cu-Based Oxygen Carrier Impregnated onto ZrO₂ for Chemical-Looping Combustion (CLC)," *Industrial & Engineering Chemistry Research*, vol. 59, no. 15, pp. 7255-7266, 2020/04/15 2020.
- [155] M. Inayat, S. A. Sulaiman, and J. C. Kurnia, "Catalytic co-gasification of coconut shells and oil palm fronds blends in the presence of cement, dolomite, and limestone: Parametric optimization via Box Behnken Design," *Journal of the Energy Institute*, vol. 92, no. 4, pp. 871-882, 2019/08/01/ 2019.

LIST OF PUBLICATIONS

1. **Muhammad Qasim**, Muhammad Ayoub, Nur Adibah Ghazali, Aqsha Aqsha and Mariyam Ameen “Recent Advances and Development of Various Oxygen Carriers for the Chemical Looping Combustion Process: A Review”, *Industrial and Engineering Chemistry Research (ACS)*, Vol. 384 (2021), Pages 112039, (IF = 3.720).
2. **Muhammad Qasim**, Muhammad Ayoub, Aqsha Aqsha, Muhammad Zulfiqar “Preparation of Metal Oxide-based Oxygen Carriers Supported with CeO₂ and gamma-Al₂O₃ for Chemical Looping Combustion”, *Chemical Engineering and Technology (WILEY-VCH VERLAG GMBH)*, Vol. 44, (2021), Pages 782-787, (IF = 1.728).
3. **Muhammad Qasim**, Muhammad Ayoub, Aqsha Aqsha, Nur Adibah Ghazali “Investigation and Comparison for the Redox Behavior of Different Metal Oxides (Ni, Fe, Co, Cu, Ce, La, Pr) with and without Gamma-Alumina Support for the Chemical Looping Combustion”, *Solid State Technology* Vol 63, (2020).
4. Nur Adibah Ghazali, Aqsha Aqsha, Masaharu Komiyama, **Muhammad Qasim**, Mohd Hizami Mohd Yusoff, Muhammad Ayoub, Mariam Ameen, Mansour Mohammedramadan Tijani, “Comparative Study on Ni/ γ -Al₂O₃ Prepared via Ultrasonic Irradiation and Impregnation Approaches as an Oxygen Carrier in Chemical Looping Combustion”. *Industrial & Engineering Chemistry Research*, 2021, 60 (37), 13542-13552, (IF = 3.720).
5. Nur Adibah Ghazali, Mohd Hizami Mohd Yusoff, Masaharu Komiyama, Aqsha Aqsha, Mariam Ameen, **Muhammad Qasim**, “The effect of Niobium oxide as a promoter on γ -Al₂O₃ based oxygen carrier for chemical looping combustion”. *Turkish Journal of Computer and Mathematics Education*, Vol.12 No.3 (2021), 3833-3839.

APPENDIX A

SAMPLE CALCULATIONS

The oxygen transport capacity was calculated using the following formula:

$$R_o = (m_o - m_r) / m_o.$$

Where m_o is referred to the mass of OC when it is fully oxidized and m_r is mass of OC when it is fully reduced in the redox cycle. Fig. A1 shows the TGA results for 10CuA-based and 10CuPA-based oxygen carriers during 10 redox cycles. The oxygen transport capacity of 10CuA-based during 1st redox cycle was calculated as:

$$m_o = 14.04 \text{ mg}$$

$$m_r = 13.70 \text{ mg}$$

$$R_o = (14.04 - 13.70) / 13.70 = 0.024 \text{ mg of O}_2 / \text{mg of OC}$$

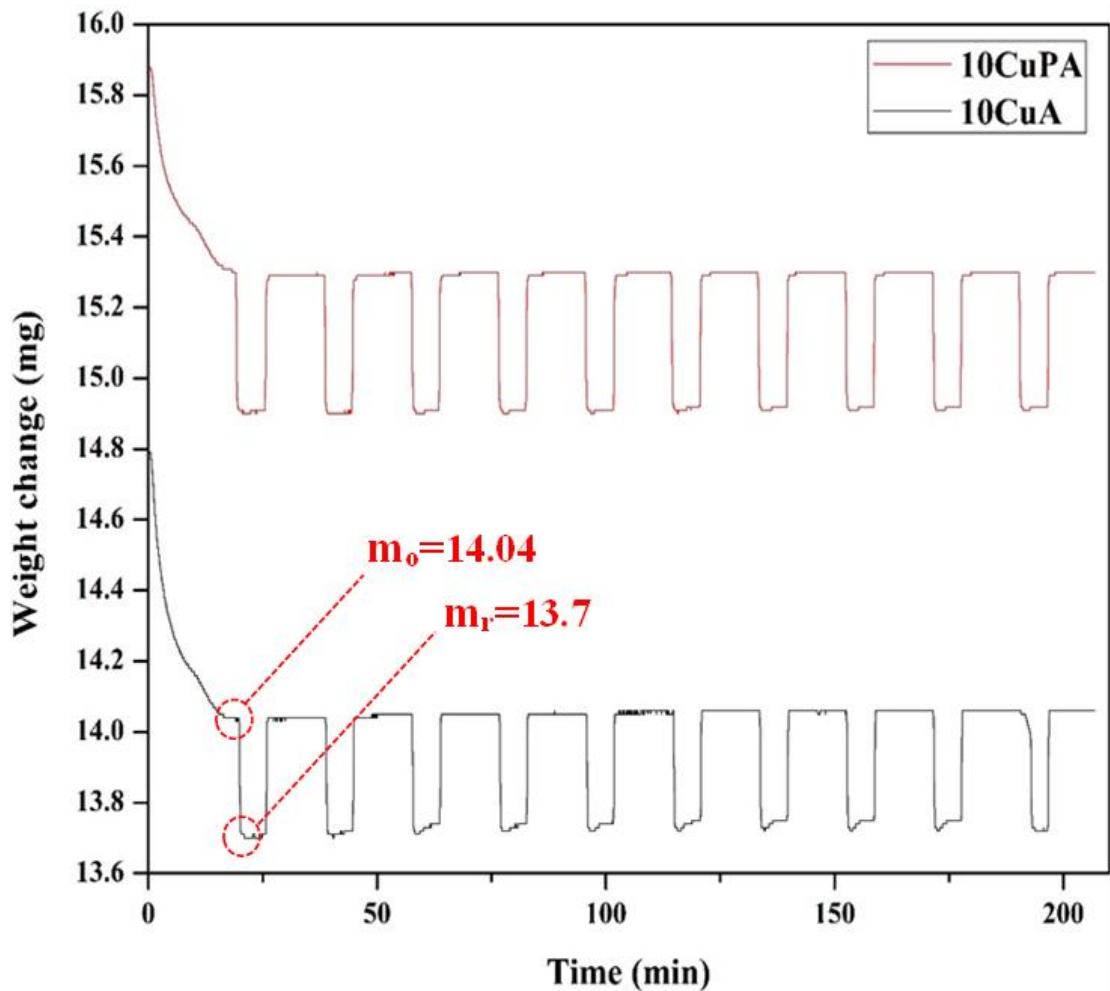


Figure A.5.1: TGA profile for 10CuA and 10CuPA OCs during 10 redox cycles in CLC process.

APPENDIX B

TGA PROFILES AT 800 °C

TGA profiles for 10FeA, 10CoA, and 10CuA based OCs

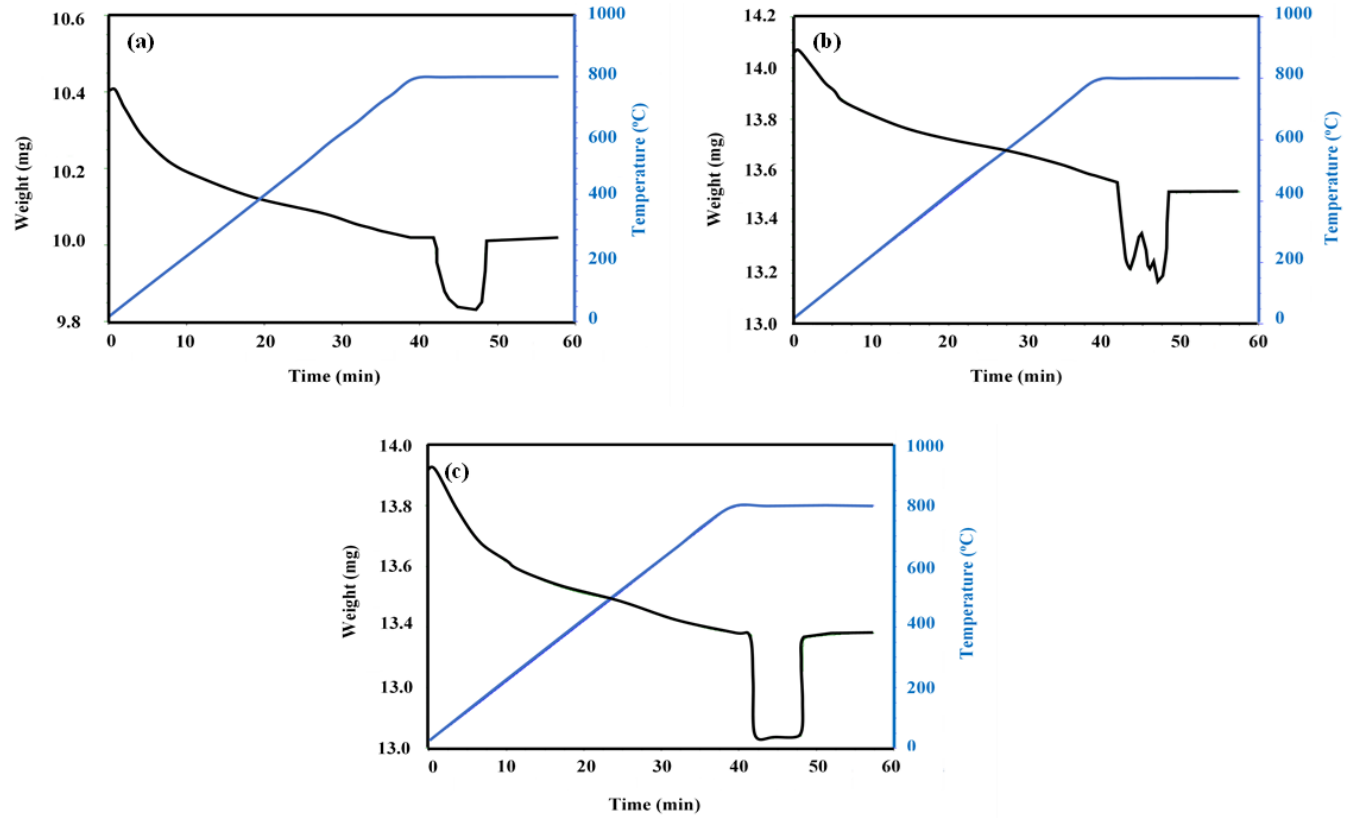


Figure B.5.2: TGA profile for 10FeA-based OC (a), 10CoA-based OC (b), and 10CuA-based OC (c) during an oxidation-reduction cycle in CLC process using 5% CH₄/N₂ and air at 800 °C.

TGA profile for La-oxide and Pr-oxide

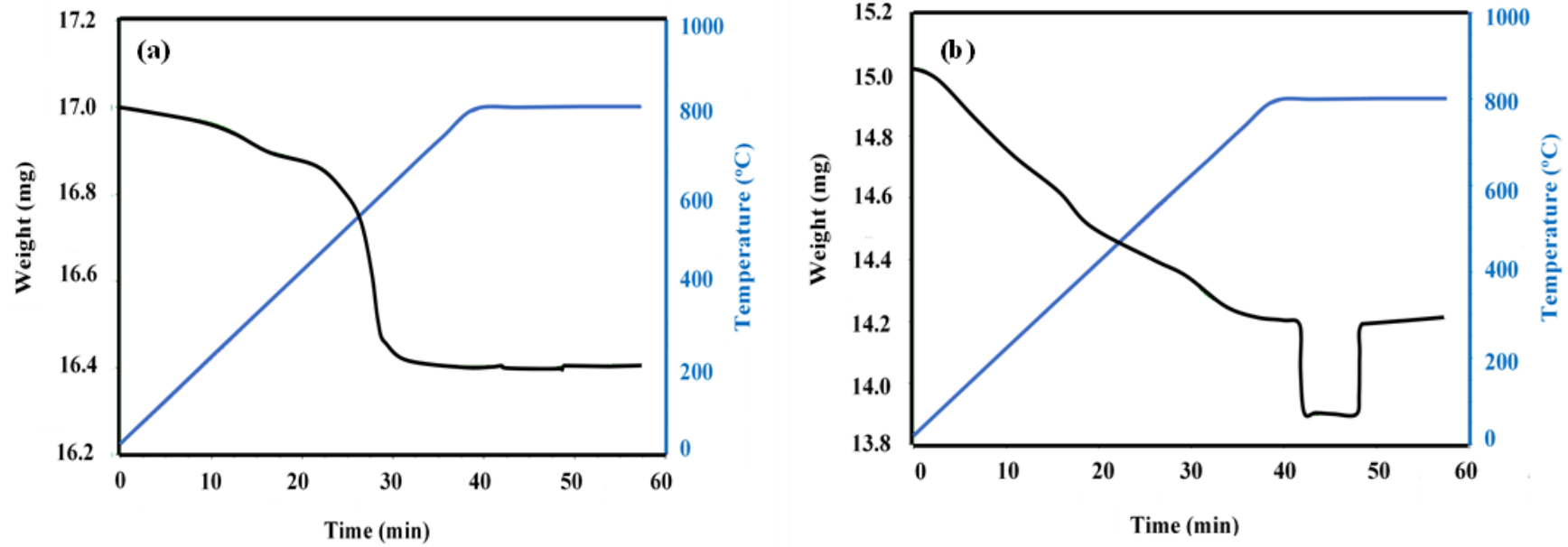


Figure B.5.3: TGA profile for La-oxide OC (a) and Pr-oxide OC (b) during an oxidation-reduction cycle in CLC process using 5% CH₄/N₂ and air at 800 °C.

TGA profile for 10CuPA-OC

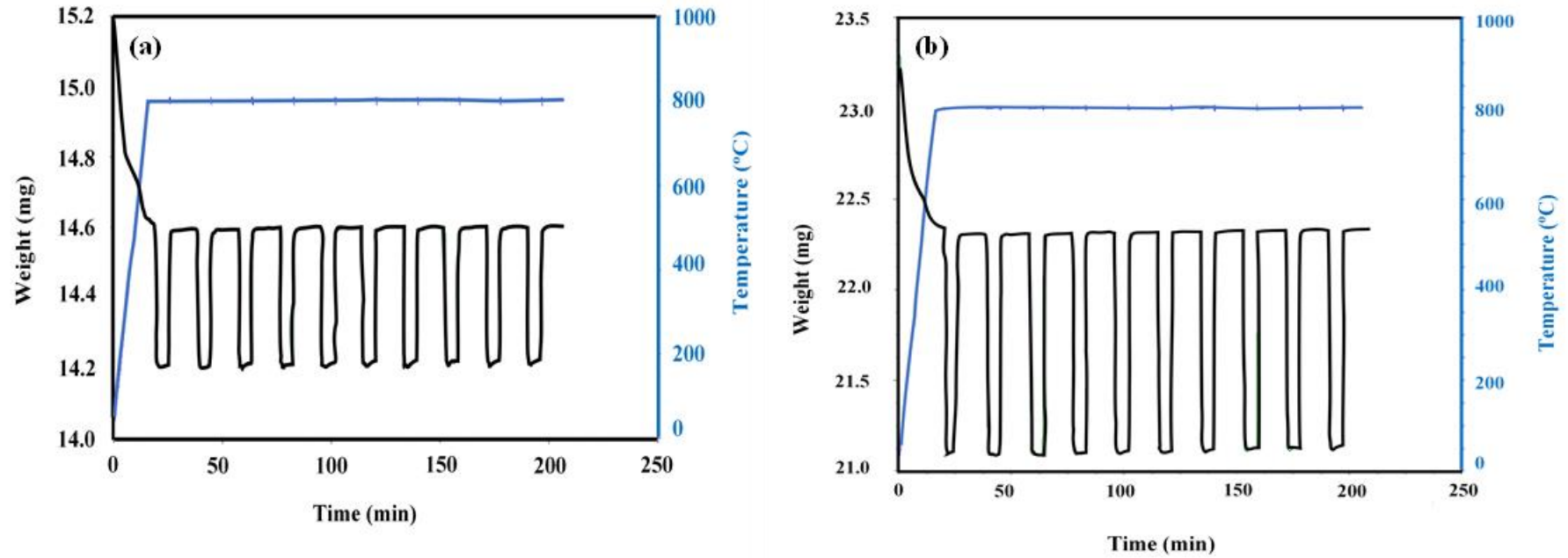


Figure B.5.4: TGA profile for 10CuPA-based OC (a) and 20CuPA-based OC (b) during 10 redox cycles in CLC process using 5% CH₄/N₂ and air at 800 °C.